Investigation of Phase Separation Kinetics in Sustainable Mixed Solvent Polymer Solutions for Hollow Fiber Membrane Fabrication

Untersuchung der Phasenseparationskinetik in Polymerlösungen mit nachhaltigen Lösungsmittelmischungen für das Spinnen von Hohlfasermembranen

Von der Fakultät für Maschinenwesen der
Rheinisch-Westfälischen Technischen Hochschule Aachen
zur Erlangung des akademischen Grades einer Doktorin
der Ingenieurwissenschaften genehmigte Dissertation

vorgelegt von

Lea Greie

Berichter/in:
Univ.-Prof. Dr.-Ing. Matthias Wessling
Prof. Dr.-Ir. Ivo Vankelecom

Tag der mündlichen Prüfung: 09.04.2026

Diese Dissertation ist auf den Internetseiten der Universitätsbibliothek online verfügbar.

Impressum

Titel: Investigation of Phase Separation Kinetics in Sustainable Mixed Solvent Polymer Solutions for Hollow Fiber Membrane Fabrication
Untersuchung der Phasenseparationskinetik in Polymerlösungen mit nachhaltigen Lösungsmittelmischungen für das Spinnen von Hohlfasermembranen

Autor: Lea Greie

Reihe: Aachener Verfahrenstechnik Series
AVT.CVT - Chemical Process Engineering
Volume: 65 (2026)

Herausgeber: Aachener Verfahrenstechnik
Forckenbeckstraße 51
52074 Aachen
Tel.: +49 (0)241 8095470
Fax.: +49 (0)241 8092252
E-Mail: secretary.cvt@avt.rwth-aachen.de
http://www.avt.rwth-aachen.de/AVT

Volltext verfügbar: 10.18154/RWTH-2026-06859

Nutzungsbedingungen: Die Universitätsbibliothek der RWTH Aachen University räumt das unentgeltliche, räumlich unbeschränkte und zeitlich auf die Dauer des Schutzrechtes beschränkte einfache Recht ein, das Werk im Rahmen der in der Policy des Dokumentenservers „RWTH Publications“ beschriebenen Nutzungsbedingungen zu vervielfältigen.

Universitätsbibliothek
RWTH Aachen University
Templergraben 61
52062 Aachen
http://www.ub.rwth-aachen.de

Acknowledgement

Ich möchte mich bei all denjenigen bedanken, die mich auf dem Weg zur Promotion begleitet, unterstützt und manchmal auch einfach davon abgehalten haben, den Verstand zu verlieren. Ich kann nicht alle namentlich nennen, hoffe aber, dass ihr wisst, wie viel ihr mir bedeutet.

Mein erster Dank gilt meinem Betreuer und Erstprüfer Univ.-Prof. Dr.-Ing. Matthias Wessling für das Vertrauen, das er mir entgegengebracht hat, sowie für die Betreuung und die Ressourcen, die diese Arbeit erst ermöglicht haben. Ebenso danke ich Prof. Dr.-Ir. Ivo Vankelecom für die Übernahme des Zweitgutachtens und die spannende sowie anregende Diskussion während der Prüfung.

Danke an Sartorius Stedim Biotech GmbH für die Möglichkeit, an diesem Forschungsprojekt zu arbeiten. Ein ganz besonderer Dank geht an Lara E. Grünig. Danke für deine fantastische Betreuung, deinen mentalen Support, jeden Quatsch zwischendurch und dafür, dass ich mich immer auf dich verlassen konnte! Den Holys danke ich dafür, dass die Arbeit mit euch nicht nur produktiv ist, sondern vor allem unglaublich viel Spaß macht. Danke, dass ihr mir stets den Rücken freigehalten habt. Ich freue mich auf alles, was noch vor uns liegt.

Danke an alle CVTler, dass ihr mich so herzlich aufgenommen habt. Besonderer Dank gilt dem MemS-Team für den fachlichen Austausch und die schönen Gruppen-Events. Ein großer Dank gilt meinem Hut-Team für die Unterstützung bei meiner Verteidigung und die tolle Hut-Verleihung!

Danke an Wenzel Plischka, Malte Wehner, Georg Gert und Stephan Zimmer für den Safe Space in eurem Büro und die notwendige Ablenkung vom Alltag durch unzählige witzige Momente. Und sorry, dass ich euch dabei so oft vom Arbeiten abgehalten habe!

Meinen Movie-Night-Boys Jannik Mehlis, Richard Paul und Malte Wehner danke ich für jeden noch so schlechten, aber definitiv horizonterweiternden Film, den ich im Laufe der Jahre schauen musste.

Ein großes Dankeschön geht auch an die BTVler der CVT. Besonders Frederike Schiszler, die das Spinning Lab am Laufen gehalten und mich im-

mer tatkräftig unterstützt hat. Danke, Karin Faensen, für gefühlt eine Million SEM-Bilder! Und danke an Susanne Offermann dafür, dass du die beste Ansprechpartnerin und Seelsorgerin für Probleme jeglicher Art bist.
Meinen Studierenden Tilman Schiffer, Maurits David, Rik Mittelstedt und Kai Blechmann danke ich für ihre großartigen Beiträge zu dieser Dissertation. Mit eurer Kreativität habt ihr dazu beigetragen, dass wir selbst die nervigsten Herausforderungen gemeistert haben, ohne dabei den Spaß an der Sache zu verlieren.
Danke auch an meine Muco: Kerstin Wienkamp, Stefan Herrmann, Tobias Harhues, Matthias Heßelmann und Jan Vehrenberg. Unsere „Arbeits"-Treffen haben sich mit der Zeit immer mehr wie Treffen unter Freunden angefühlt. Danke, dass ihr mich damals aufgenommen habt und für die Unterstützung und vielen Ratschläge.
Der wahrscheinlich größte Dank geht an meine liebste Bürokollegin Maria Restrepo. Du hast alle Höhen und Tiefen dieser Promotion miterlebt und es immer wieder geschafft, mich aus kleinen und großen Krisen herauszuholen. Danke für die unzähligen lustigen, emotionalen und chaotischen Momente. Ohne dich wäre diese Zeit definitiv nicht dieselbe gewesen, und ich bin dankbar, dass ich auch fachlich so viel von dir lernen durfte.
Ebenso danke ich meinen Studienfreunden, dem AK Partyhut & Friends. Danke, dass wir die letzten zehn Jahre gemeinsam überstanden haben und dass ihr mich nach meinem kleinen Aachen-Abenteuer wieder so herzlich in Göttingen aufgenommen habt.
Natürlich danke ich auch meiner Familie für ihre bedingungslose Unterstützung. Besonders hervorheben möchte ich meinen Quonkel Basti. Du warst für mich immer ein Vorbild und hast mir gezeigt, wie viel die Welt zu bieten hat. Danke für dein offenes Ohr, die vielen Feierabendbierchen und unseren kleinen Familien-Außenposten in Aachen.
Zuletzt gilt der größte Dank meiner Mutter. Auch wenn es nicht immer einfach war, hast du mir stets den Rücken freigehalten, an mich geglaubt und versucht, mir alles zu ermöglichen. Ohne deine Unterstützung wäre vieles von dem, was ich erreichen durfte, nicht möglich gewesen. Danke für alles.

„Einfach Schwimmen.“

- Dori

Declaration of planned publications and previous work

The Chapters 4 and 5 are in preparation for publication as research articles.

Some experiments and work of this thesis are based on the following student theses:

Tilman Schiffer, Master thesis, *Analysing the influence of green solvents on phase separation for sustainable polyethersulfone membrane fabrication*, 4th of June 2024

Maurits Benjamin David, Bachelor thesis, *Sustainable fabrication of hollow fiber membranes with green solvents for microfiltration applications*, 25th of September 2024

Artificial Intelligence (AI) Statement

This thesis has been partially rewritten using an artificial intelligence (AI) model to improve readability. All ideas, considerations, and content are original and created by the author. Therefore, AI systems are not concerned with intellectual property. The AI usage rules stipulated by the Faculty of Mechanical Engineering of RWTH Aachen University on July 29, 2025, have been fully satisfied.

Contents

Acknowledgement iii

Artificial Intelligence (AI) Statement ix

Abstract xiii

Zusammenfassung xv

1 Introduction 1

2 Fundamentals 7

2.1 Membrane Processes 7

2.1.1 Definition 7

2.1.2 Membrane classification 8

2.1.3 Membrane applications 9

2.2 Membrane fabrication 11

2.2.1 Thermodynamics of mixtures 11

2.2.2 Ternary phase diagram 15

2.2.3 Structure forming mechanisms 16

2.2.4 Phase separation kinetics 19

2.3 Technical Implementation 21

3 Materials and Methods 25

3.1 Materials 25

3.2 Methods 25

3.2.1 Calculation of Hansen solubility parameters 25

3.2.2 Viscosity 27

3.2.3 Flatsheet membrane casting 27

3.2.4 Hollow fiber fabrication 27

3.2.5 Light transmission measurements 28
3.2.6 Scanning electron microscopy 28
3.2.7 Pure water permeance measurements 29
3.2.8 Retention measurements 29

4 Influence of sustainable solvents and their mixtures on PES membrane fabrication 31
4.1 Introduction 32
4.1.1 Methods 35
4.2 Results and Discussion 37
4.2.1 Influence of solvent type on the polymer solution 37
4.2.2 Phase separation kinetics 40
4.2.3 Porous structure of the membranes 43
4.2.4 Pure Water Permeance and Retention of flat sheet membranes 48
4.2.5 Fabrication of hollow fiber membranes with solvent mixtures 49
4.3 Conclusion 55

5 Tuning the inner and outer coagulation in UF hollow fiber membrane spinning 57
5.1 Introduction 58
5.2 Methods 61
5.2.1 Dope Solution Fabrication 61
5.2.2 Hollow fiber spinning 61
5.3 Results and Discussion 63
5.3.1 Phase Separation Kinetics 63
5.3.2 Influence of Solvent Additives in the Bore Fluid 67
5.3.3 Influence of Coagulation Bath Temperature 75
5.4 Conclusion 80

6 Influencing the pore structure of MF hollow fiber membranes in a combined VIPS-NIPS spinning process 83
6.1 Introduction 84
6.2 Materials and Methods 87
6.2.1 Polymer solution preparation 87
6.2.2 Hollow fiber membrane spinning 87
6.3 Results and Discussion 90
6.3.1 Influence of air gap temperature 90

6.3.2 Influence of air gap length 95
6.3.3 Influence of coagulation bath temperature 96
6.4 Conclusion 101

7 Conclusion and Future Perspectives **103**

Bibliography **107**

List of Abbreviations **121**

Abstract

Polymeric membranes are a key element in modern separation processes. Their characteristics can be tailored to a broad range of applications such as water purification, medical applications, and biopharmaceutical processes. However, the fabrication of polymeric membranes typically relies on toxic, aprotic solvents such as N-methylprrolidone, dimethylacetamide, and dimethylformamide, whose environmental and health impacts motivate the search for sustainable alternatives. Although current research has identified suitable sustainable alternative solvents for polyethersulfone, studies on their application in hollow fiber membrane fabrication are still limited. This thesis will close this gap by investigating the phase separation kinetics of sustainable solvent systems for the fabrication of polyethersulfone (PES) hollow fiber membranes. By systematically using less hazardous solvents like N-butyl-pyrrolidone (NBP), N,N-dimethyllactamid (AMD), 2-pyrrolidone (2P), and triethyl phosphate (TEP) and their mixtures, the study demonstrates that mixed-solvent formulations overcome the limitations of single solvents by shifting solubility parameters, modulating viscosity, and adjusting liquid-liquid demixing rates. Light transmission analysis, scanning electron microscopy, and performance testing reveal that solvent mixtures suppress premature gelation, yield defect-free hollow fibers, and enable precise control of pore connectivity. Furthermore, it was explored whether convenient, well-known strategies for tuning membrane characteristics in the spinning process with common, toxic solvents can also be applied to the sustainable systems. Therefore, process parameters such as bore fluid composition, coagulation bath temperature, and vapor-induced phase separation (VIPS) were systematically varied to influence the inner and outer coagulation of the fibers and broaden the accessible design space from ultrafiltration to microfiltration membranes. The results establish a framework that links solvent thermodynamics and phase separation kinetics to morphology and performance, thereby providing quantitative guidelines for scaling up the sustainable fabrication of hollow fiber membranes. Overall, this work shows that sustainable mixed-solvent systems are not a compromise but a design opportunity, enabling the transition from toxic solvents toward greener membrane manufacturing with industrial relevance.

Zusammenfassung

Polymermembranen sind ein zentrales Element moderner Trennprozesse. Ihre Eigenschaften können gezielt an ein breites Anwendungsspektrum angepasst werden, unter anderem in der Wasseraufbereitung, in medizinischen Anwendungen oder in biopharmazeutischen Prozessen. Die Herstellung von Polymermebranen basiert jedoch in der Regel auf toxischen, aprotischen Lösungsmitteln wie N- Methylpyrrolidon (NMP), Dimethylacetamid (DMAc) und Dimethylformamid (DMF), deren Umwelt- und Gesundheitsrisiken die Suche nach nachhaltigen Alternativen erforderlich machen. Obwohl aktuelle Forschungen bereits geeignete nachhaltige Lösungsmittel für Polyethersulfon (PES) identifiziert hat, sind Studien zu deren Anwendung in der Hohlfasermembranherstellung bislang begrenzt. Diese Arbeit schließt diese Lücke, indem die Phasenseparationskinetik nachhaltiger Lösungsmittelsysteme für die Herstellung von PES Hohlfasermembranen untersucht wird. Durch den systematischen Einsatz weniger gefährlicher Lösungsmittel wie N-Butylpyrrolidon (NBP), N, N-Dimethyllactamid (AMD), 2-Pyrrolidon (2P) und Triethylphosphat (TEP) sowie deren Mischungen wird gezeigt, dass Lösungsmittelmischungen die Grenzen einzelner Lösungsmittel überwinden, indem sie die Löslichkeitsparameter verschieben, die Viskosität modulieren und die Entmischungskinetik anpassen. Messungen der Lichttransmission, Rasterelektronenmikroskopie und Performance-Tests zeigen, dass Lösungsmittelmischungen eine vorzeitige Gelierung unterdrücken, Herstellung von defektfreie Hohlfasern ermöglichen und eine präzise Kontrolle der Porenstrukturen erlauben. Darüber hinaus wurde untersucht, ob bewährte Strategien zur Einstellung der Membraneigenschaften im Spinnprozess mit gängigen, toxischen Lösungsmitteln auch auf nachhaltige Systeme übertragbar sind. Hierzu wurden Prozessparameter wie die Zusammensetzung der Bore-Flüssigkeit, die Temperatur des Fällbades und die dampfinduzierte Phasenseparation (VIPS) systematisch variiert, um die innere und äußere Koagulation der Fasern zu beeinflussen und die Eigenschaften der Membranen von Ultrafiltrations- bis hin zu Mikrofiltrationsmembranen zu erweitern. Die Ergebnisse etablieren ein Rahmenwerk, das die Thermodynamik der Lösung und Kinetik der Phasenseparation mit der Membranmorphologie und -performance verknüpft und damit quantitative Leitlinien für den Scale-up der nachhaltigen Hohlfasermembranherstellung bereitstellt. Insgesamt zeigt diese Arbeit, dass Mischungen von nachhaltigen Lösungsmitteln keinen Kompromiss darstellen, sondern eine zusätzliche Möglichkeit zur Beeinflussung der Membraneigenschaften bieten, die den Übergang von toxischen hin zu umweltfreundlicheren Lösungsmitteln in der Membranherstellung mit industrieller Relevanz ermöglicht.

1 Introduction

In recent decades, growing awareness of man-made environmental damage has led to a rethinking of many industrial processes. Sustainability has become increasingly important, intending to make processes less harmful to both people and the environment [Anas2000; Figo2014; Dume2023]. Under the concept of “green chemistry”, Paul Anastas and John Warner formulated twelve principles for this purpose, which are shown in Figure 1.1 [Anas2000].

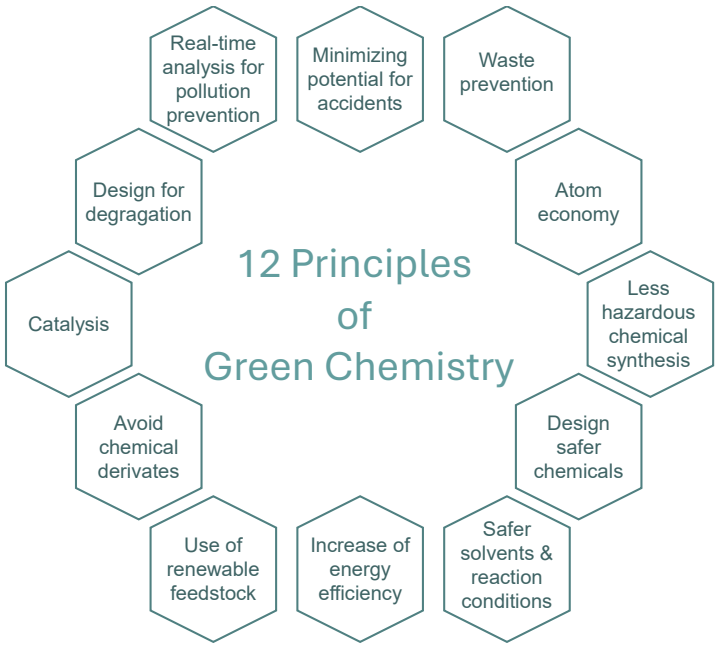


Figure 1.1: The twelve principles of green chemistry according to Anastas and Warner [Anas2000].

Evidence indicates that membrane processes offer increased sustain-

ability compared to their conventional counterparts due to features such as efficiency, flexibility, reduced environmental impact, and lower energy consumption [Bood2013; Osma2024; Drio2012; Mart2017]. Due to their ability to efficiently separate molecular components, polymeric membranes are implemented in various separation processes ranging from reverse osmosis (RO) to nano-, ultra-, and microfiltration [Chun2021; Bake2023]. In many application fields, such as biopharma, hollow fiber membranes are preferred over flat sheet membranes due to their high packing density and low shear forces applied to the target molecules during filtration [Char2012]. However, the fabrication of the membrane itself still has limited sustainability, since it typically involves the use of synthetic polymers and hazardous solvents. For example, the petrochemically produced polymer polyethersulfone (PES) [Kahr2020; Roth2018] is widely used for membrane applications, among other commonly applied polymers like polysulfone (PSf) [Zhan2010; Magg2022], polyvinylidene fluoride (PVDF) [Herr2024; Tepp2022], cellulose acetate (CA) [Nune1996], and polyamide (PA) [Freg2021] [Chun2021; Bake2023]. PES enables fabrication of membranes with an extensive range of different pore sizes while maintaining high mechanical, thermal, and chemical stability [Aume2021; Van 2009]. Non-solvent-induced phase separation (NIPS) is a sufficient technique to fabricate PES membranes with specific morphologies. The polymer solution is immersed in a non-solvent coagulation bath, initiating the exchange of solvent and non-solvent. The NIPS process has been studied extensively by Boom and Smolders *et al.* among others [Boom1992; Boom1994; Smol1992]. They found that the formation of pore structures is based on a complex phase separation process. By precisely controlling the thermodynamic and kinetic aspects of the process, the membrane characteristics, such as porosity, pore size distribution, and the resulting filtration performance, can be tailored to the desired application.

Besides the use of polymers with limited sustainability, the choice of a suitable solvent is also an issue. For example, membranes based on PES are commonly fabricated with polar aprotic solvents like N-methylpyrrolidone

(NMP) [Boom1994; Kim1998], N,N-dimethylacetamide (DMAc) [Thuy2015; Khor2017], and N,N-dimethylformamide (DMF)[Idri2007]. These solvents offer excellent solubility for PES, producing membranes with favorable separation properties, and therefore, have been studied extensively in recent decades. However, they pose significant environmental and health risks due to their toxicity, leading regulatory bodies like the European Chemical Agency (ECHA) to classify them as substances of very high concern (SVHC) [Sher2018; ECHA2018]. Therefore, efforts are being made to find alternative, environmentally friendly solvents for membrane production without compromising performance. This thesis will focus on the use of more sustainable solvents for the fabrication of PES hollow fiber membranes for ultra- and microfiltration applications. More precisely, a complete understanding of the phase separation kinetics and the influence of several process parameters on the membrane morphology and performance will be gained.

Chapter 2 provides a fundamental insight into different membrane types and their application, with a focus on pressure-driven membrane processes. Furthermore, the production of polymeric membranes by means of non-solvent-induced phase separation is explained. First, the thermodynamics of ternary mixtures are introduced, followed by an explanation of the various structure-forming mechanisms during phase separation. In addition, the influence of phase separation kinetics on membrane structures is discussed. Finally, the technical implementation of NIPS in flat and hollow fiber membrane production, as well as the various process parameters influencing the resulting membrane, are presented.

Chapter 3 introduces the fabrication and characterization methods used within this thesis. In detail, the preparation of polymer solutions and their characterization via viscosity measurements is explained. The fabrication of flat and hollow fiber membranes is described, along with their performance characterization, which includes measuring pure water permeance and retention rates, and conducting morphology analysis using scanning electron microscopy. Insights into the phase separation kinetics and ther-

modynamic conditions of polymer solutions were derived by calculating and comparing Hansen solubility parameters and measuring light transmittance during phase separation.

Figure 1.2 shows a graphical outline of the studies presented in the following chapters.

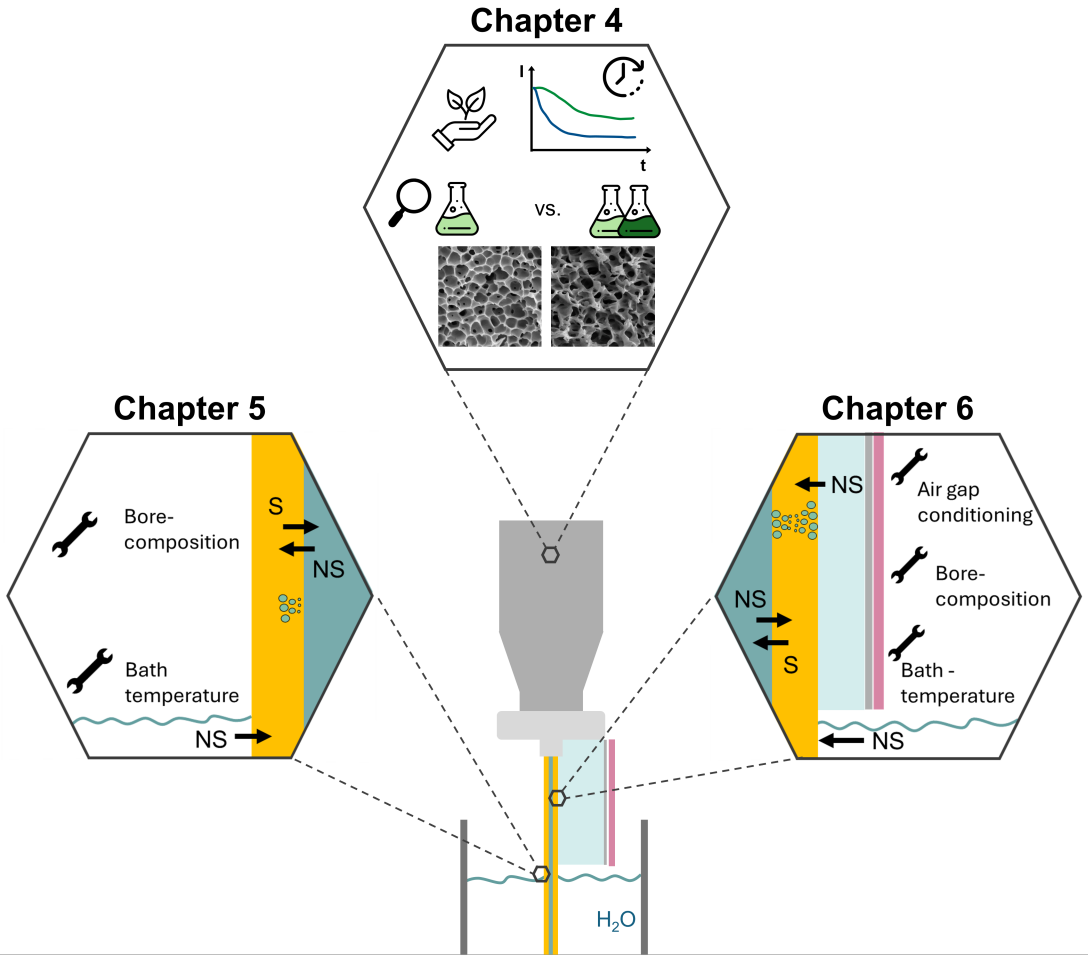


Figure 1.2: Graphical outline of chapter 4, 5 and 6.

Chapter 4 examines how solvent type influences polymer solutions and evaluates their suitability for producing PES hollow fiber membranes. Specifically, phase separation kinetics and the properties of the resulting membranes of the four alternative solvents N-butylpyrrolidone (NBP), Agnique AMD 3L (AMD), 2-Pyrrolidone (2P), and Triethylphosphate (TEP) are analyzed in comparison to NMP-based systems. Mixed solvents are in-

troduced as a method of overcoming the individual disadvantages of each more sustainable alternative solvent by altering the phase separation kinetics. These mixed-solvent systems are then used to produce ultrafiltration hollow fiber membranes, with the solvent ratio acting as an effective lever for adjusting the pore structure and membrane performance.

Chapter 5 addresses the fabrication of ultrafiltration membranes based on the previously developed sustainable mixed-solvent polymer solutions. The influence of process parameters on the internal and external coagulation of the hollow fiber is investigated. By varying the solvent compositions with different non-solvent strengths, the internal phase separation and thus the resulting pore structures are specifically manipulated. This effect is further investigated in advanced phase separation kinetics studies using light transmission measurements. The external phase separation and the resulting pore structure are systematically controlled by varying the coagulation bath temperatures.

Chapter 6 applies systematically acquired knowledge of the phase separation kinetics of mixed-solvent dopes to the production of microfiltration hollow fiber membranes. Furthermore, methods for opening the pore structure on the shell side are investigated. To this end, the existing NIPS spinning setup has been expanded to incorporate a vapor-induced phase separation (VIPS) preconditioning step during the air gap residence time. The influence of the temperature and duration of the VIPS step is examined in more detail, and a broad spectrum of microfiltration cut-offs is fabricated by cleverly combining this with a variation in the bore solution composition and coagulation bath temperature.

Chapter 7 will summarize the key findings of this thesis and provide an outlook on future perspectives.

In general, we hypothesize that greener mixed-solvent systems (NBP/AMD, NBP/2P, NBP/TEP) enable predictable control of hollow-fiber morphology and performance via the three orthogonal levers: bore-fluid

strength (lumen), air-gap conditions (shell), and coagulation-bath temperature (shell), delivering ultra- to microfiltration membranes that achieve similar performance relative to NMP-based processes while reducing solvent hazard and widening the practical spinning window. To prove this hypothesis, we investigate (i) how solvent mixtures shift the onset (t_1) and velocity of phase separation, and how these shifts correlate with shell/lumen morphology (ii) to what extent can bore-fluid choice, air-gap conditions, and bath temperature independently tune lumen vs shell structures? (iii) What reproducible PWP/retention windows are accessible across greener mixtures? Therefore, we map recipes and spinning parameters, demixing kinetics, membrane morphology, and membrane performance to produce actionable design rules for sustainable PES hollow fibers.

2 Fundamentals

2.1 Membrane Processes

2.1.1 Definition

Membranes are defined as semi-permeable structures that control the permeation rate of chemical species in aqueous or gaseous phases. [Bake2023]. In nature, membranes are a crucial component of the metabolism of plants, animals, and humans, as they envelop most cells and only allow substances relevant to metabolism to pass through. Another example is human skin, which allows oxygen to permeate but retains body fluids such as plasma [Meli2007]. Based on natural models, a large number of membrane processes have been developed to date, covering a wide range of applications, including water treatment, the food industry, biopharmaceuticals, and medical applications [Bake2023].

The basic principle of a filtration experiment is represented in Figure 2.1. The membrane separates the different components of the *feed*, as only one component can permeate through the barrier and form the *permeate*. The remaining components of the feed get concentrated in the *retentate*. The selectivity of the membrane is mainly based on steric hindrance, but can also be influenced by electrostatic or chemical interactions [Muld1996]. To separate the components, a driving force must be applied that exceeds the free enthalpy of mixing ΔG_{mix} of the components. The type of driving force depends on the respective separation process and can be either a tempera-

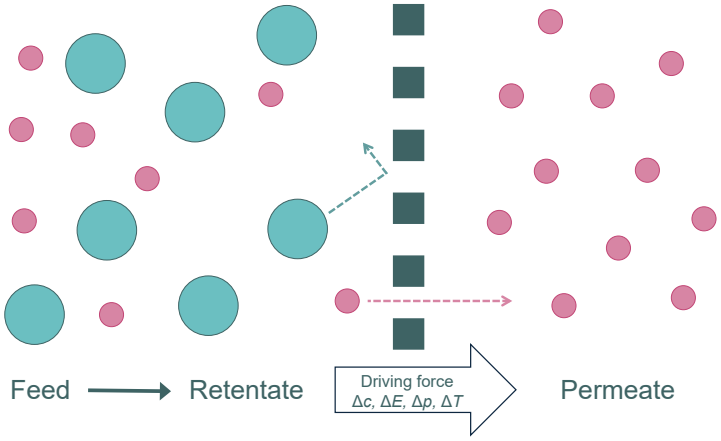


Figure 2.1: Schematic illustration of a basic filtration experiment (adapted from [Muld1996]).

ture difference (ΔT), energy difference (ΔE), concentration difference (Δc), or pressure difference (Δp) [Muld1996]. Within the scope of this thesis, only membranes for pressure-driven processes are investigated.

2.1.2 Membrane classification

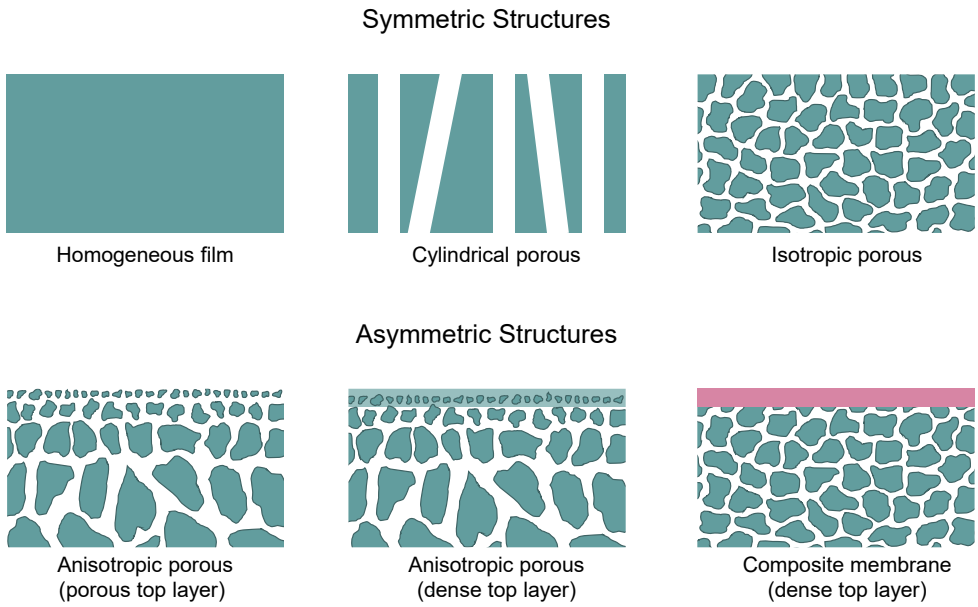


Figure 2.2: Classification of membrane structures(adapted from [Muld1996; Bake2023]).

First and foremost, membranes can be characterized by their nature - bio-

logical or synthetic. Since this thesis focuses on the fabrication of synthetic polymeric membranes, the latter is discussed in more detail below. Synthetic membranes can be further categorized into symmetrical and asymmetrical structures according to their morphology, as shown in Figure 2.2 [Bake2023; Muld1996]. Symmetrical, isotropic membranes exhibit a uniform composition and structure throughout the whole thickness of the membrane. They are either microporous membranes with interconnected or isolated cylindrical pores or nonporous, dense membranes. Microporous membranes typically have pore sizes ranging from 0.01 to 10 µm, which primarily lead to separation through molecular sieving. In contrast, transport in dense membranes occurs via the diffusion of the permeants through the membrane material itself [Muld1996]. Asymmetrical membranes are characterised by multiple layers, each possessing distinct structures and permeabilities. They typically comprise an increase in pore size through the thickness of the membrane, while the top layer is either porous or dense. The denser surface layer is responsible for the separation, while the more open, thicker microporous support layer provides mechanical integrity [Bake2023; Muld1996].

2.1.3 Membrane applications

As mentioned before, the permeation mechanism of a substrate through a membrane is highly dependent on the membrane morphology and can be described by two distinct models. The first, the solution-diffusion model, applies to dense, nonporous membranes typically used in gas separation or reverse osmosis (RO) (see Figure 2.3). The effective "pores" in these dense membranes are considered transient free volume elements, typically less than 5 to 10 Å in diameter, that arise from the thermal motion of polymer chains. In this model, permeants initially dissolve into the membrane material and subsequently diffuse through it along a concentration gradient. The diffusion can be described by Fick's law

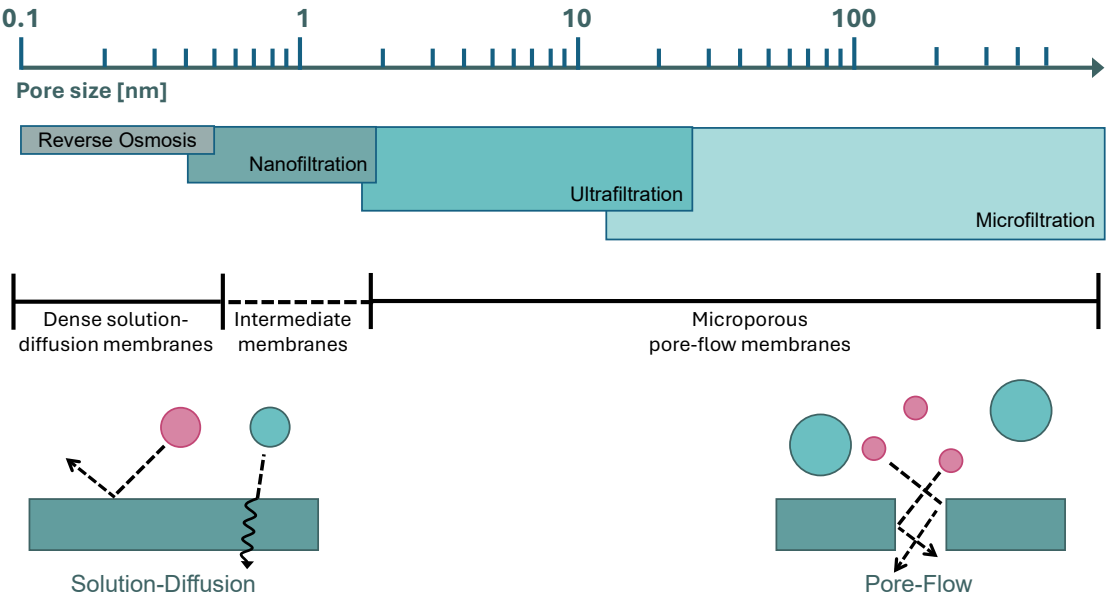


Figure 2.3: Categorization of pressure-driven membrane processes by pore size and transport mechanism (adapted from [Bake2023]).

$$J_i = -D_i \frac{dc_i}{dx} \tag{2.1}$$

where J_i is the transfer rate of a compound i, $\frac{dc_i}{dx}$ is the concentration gradient of compound i, and $-D_i$ is the diffusion coefficient that describes the mobility of compound i. Therefore, the separation efficiency in the solution-diffusion model is determined by the differences in solubility and mobility of the components within the membrane. [Bake2023].

The transport in microporous membranes is described by the pore-flow model. Therefore, compounds are transported by pressure-driven convective flow through fixed, discrete pores, which is fundamentally described by Darcy's law

$$J_i = K' c_i \frac{dp}{dx} \tag{2.2}$$

where $\frac{dp}{dx}$ is the pressure gradient within the porous medium, c_i is the concentration of compound i in the medium and K' is a membrane specific

coefficient [Bake2023]. This model accurately describes transport in microporous membranes used in ultrafiltration (UF) and microfiltration (MF) processes, which feature pores larger than 10 to 15 Å (see Figure 2.3). Notably, a transition region exists for membranes with pore diameters between 5 and 15 Å, such as nanofiltration (NF) membranes, which exhibit characteristics of both pore-flow and solution-diffusion transport mechanisms [Bake2023].

2.2 Membrane fabrication

Selecting the appropriate membrane formation technique is crucial for achieving membrane structures that are well-suited for a specific separation task. Common techniques are sintering, track-etching, vapor deposition, and phase separation [Muld1996]. The most commonly used form of the latter is the non-solvent induced phase separation (NIPS). It involves the dissolution of a membrane-forming polymer in a solvent and subsequent precipitation by contacting it with a non-solvent [Smol1992; Muld1996]. The thermodynamic and kinetic principles of phase separation are explained below. For simplicity, it will be limited to a three-component system consisting of solvent (S), non-solvent (NS), and polymer (P).

2.2.1 Thermodynamics of mixtures

The thermodynamic characterisation of a system is based on equations of state, which determine whether the system is in equilibrium or if spontaneous changes of state can occur. The equilibrium criterion of systems at constant temperature (T) and pressure (p) is given by the free enthalpy (G [J]), which is dependent on the enthalpy (H [J]), temperature [K], and entropy ($S\left[\frac{\mathrm{J}}{\mathrm{K}}\right]$) as shown in equation 2.3 [Muld1996].

$$G = H - T \cdot S \tag{2.3}$$

If the change of free enthalpy ΔG equals zero, the system is in equilib-

rium. In contrast, if at constant pressure and temperature $\Delta G < 0$, spontaneous changes occur [Muld1996]. When considering the mixing of a multicomponent system, as in the case of membrane fabrication via NIPS at constant p and T, the Gibbs free enthalpy of mixing dG_m of a system with the volume V is given by

$$dG_m = V\,dp - S\,dT + \sum \mu_i dn_i \tag{2.4}$$

In addition to single-component systems, a term for the chemical potential μ_i [J/mol] is incorporated, which is defined as the change in the Gibbs free energy of component i at constant p, T, and molar quantity of all other components n:

$$\mu_i = \left(\frac{\delta G}{\delta n_i}\right)_{p,T,n} \tag{2.5}$$

For an ideal solution, the free enthalpy can be simplified to

$$\Delta G_m = RT(x_1 \cdot \ln(x_1) + x_2 \cdot \ln(x_2)) \tag{2.6}$$

with x_i being the mole fraction of the components ($i = 1, 2$) and R the ideal gas constant. Since the result of equation 2.5 is always negative, ideal solutions will always mix spontaneously. However, polymer solutions differ from this behavior as polymeric chains have a significantly lower entropy of mixing than small molecules [Muld1996; Flor1953]. Consequently, a positive mixing enthalpy leads to demixing. Flory and Huggins introduced the Flory-Huggins interaction parameter χ, which is regarded as an excess parameter, encapsulating the non-ideality of the system [Flor1942]. For a ternary system of non-solvent (1), solvent (2) and polymer (3), the Gibbs free enthalpy can be described as

$$\Delta G_m = RT(n_1 \cdot \ln(\phi_1) + (n_2 \cdot \ln(\phi_2) + (n_3 \cdot \ln(\phi_3) + \chi_{12} n_1 \phi_2 + \chi_{13} n_1 \phi_3 + \chi_{23} n_2 \phi_3 \quad (2.7)$$

with the volume fraction ϕ_i and the binary Flory-Huggins interaction parameters χ_{ij} of the component ($i, j = 1, 2$ or 3). To determine the binary interaction parameters, thermodynamic equilibrium data for the binary systems are required. Typically, χ_{13} is determined from the equilibrium sorption amount of the non-solvent in the polymer, χ_{23} from the osmotic pressure or vapour pressure reduction of the corresponding polymer solution, and χ_{12} from vapour-liquid equilibrium (VLE) data of solvent-nonsolvent mixtures [Muld1996]. Those parameters are well known for common membrane-forming systems via the NIPS method. Polymers such as Polyethersulfone (PES) [Kahr2020; Roth2018], polyvinylidene fluoride (PVDF) [Herr2024; Tepp2022], cellulose acetate (CA) [Nune1996; Wijm1983], and polyamide (PA) [Freg2021] are prominent examples for membrane fabrication due to their high mechanical, thermal, and chemical stability. As solvents, typically aprotic, organic solvents such as N-methylpyrrolidone [Boom1994; Kim1998], N, N-dimethylformamide (DMF) [Idri2007], or N, N-dimethylacetamide (DMAc) [Thuy2015; Khor2017] have been widely used in NIPS processes due to their excellent miscibility with the polymers mentioned above.

However, thermodynamic data on alternative, sustainable components, such as less toxic solvents, are limited [Chun2021; Muld1996]. Therefore, interaction parameters are often estimated based on the Hildebrand solubility parameter.

This is defined as

$$\delta = \sqrt{\frac{\Delta E}{V}} \quad (2.8)$$

were V is the molar volume and E is the energy of vaporization [Muld1996]. Hansen [Hans2007] further refined the definition by the contributions from the dispersion forces (δ_d), polar forces (δ_p) and hydrogen bonding (δ_h) as in equation 2.9.

$$\delta_t^2 = \delta_d^2 + \delta_p^2 + \delta_h^2 \tag{2.9}$$

When using a mixture of multiple components (i, l), the solubility parameters of the mixture ($\delta_{x,mix}$ with x= d,p or h) can be estimated for each Hansen Solubility Parameter (HSP) by calculating the weighted average of the HSP of the individual components based on their volume fractions in the mixture as shown in equation 2.10.

$$\delta_{x,mix} = \phi_i \delta_{x,i} + \phi_l \delta_{x,l} \tag{2.10}$$

Those HSP define a three-dimensional space in which δ_t represents the endpoint of the radius vector, which is individual for each component. The distance between the δ_t of two different components (i, j) can therefore be calculated by equation 2.11.

$$\delta_{i,j} = \sqrt{(\delta_{d,i} - \delta_{d,j})^2 + (\delta_{p,i} - \delta_{p,j})^2 + (\delta_{h,i} - \delta_{h,j})^2} \tag{2.11}$$

In general, the smaller the HSP distance between two components, the higher the solubility of the components in each other. The Flory interaction parameters can be estimated with the HSP via equation 2.12.

$$\chi_{ij} = \frac{V_i}{RT} \delta_{ij}^2 \tag{2.12}$$

Due to their independence from the second component in the mixture and their broader applicability, the HSP solubility parameters are tabulated for the majority of substances. However, it is essential to note that differences in concentration and temperature are not taken into account in the solubility parameters. Also, HSP do not include complex aspects like swelling, diffusion, and solvation processes, and therefore cannot be taken as the only

argument for solubility [Venk2019].

2.2.2 Ternary phase diagram

The thermodynamic conditions of a simplified NIPS process can be depicted in a ternary phase diagram as shown in Figure 2.4.

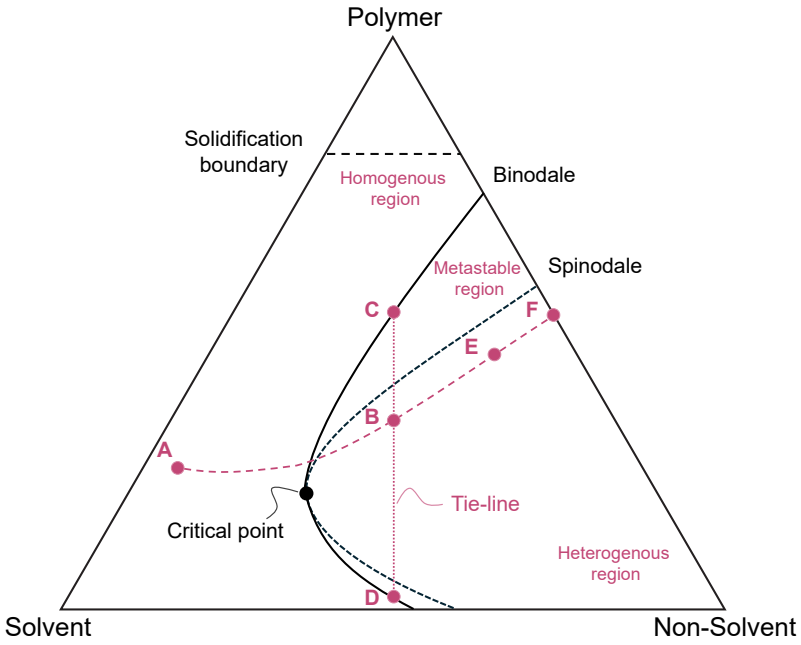


Figure 2.4: Simplified ternary phase diagram of a NIPS process.

The three pure components, polymer, non-solvent, and solvent, are located at the edges of the diagram. The sides of the triangle represent the compositions of the binary mixtures, while every point within the diagram indicates the composition of the ternary system [Bake2023; Muld1996]. The points A-E in Figure 2.4 represent a typical path of the system during phase separation. In general, two main areas are depicted: a homogenous, one-phase area and a heterogeneous, two-phase area where the system is separated into a polymer-lean and a polymer-rich phase. Although the one-phase region is thermodynamically continuous, it can be divided into a liquid and a glassy region, depending on the amount of polymer present in the solution. When the polymer concentration is above the solidification boundary, the solution reaches a critical viscosity and is regarded as a quasi-solid [Chun2021].

Membrane fabrication via NIPS relies on the transfer of a thermodynamically stable, homogenous solution (A) (Figure 2.4 into a thermodynamically unstable area by increasing the amount of non-solvent. Phase separation occurs (B) to compensate for this unstable condition and reach a minimum of the free enthalpy of mixing. Within this heterogeneous area, the free enthalpy of mixing exhibits two minima, which form the end-points of each tie-line and represent the composition of the two formed phases (C, D) at equilibrium [Muld1996; Atki2006]. The connection line between all of the minima is called the binodal or miscibility gap. The two phases that are formed are referred to as the polymer-rich phase (C), which forms the polymer matrix, and the polymer-lean phase (D), which is responsible for the porous network. After complete replacement of the solvent by the non-solvent, the final membrane composition is represented in point (F). The final morphology of the membrane is dependent on the respective pore-forming mechanism and the kinetics during phase separation, which will be explained in the following.

2.2.3 Structure forming mechanisms

Although much research has been conducted in recent decades on the prediction of membrane structures in NIPS processes, this is still only possible to a limited extent, and there are still controversial discussions about specific influences [Guil2011; Nune1996; Wien1996; Tang2020]. However, the following mechanisms are widely accepted. On the one hand, the structure-forming mechanisms rely on the system's entry point into the miscibility gap during phase separation. Figure 2.5 shows the possible paths within the ternary phase diagram during phase separation.

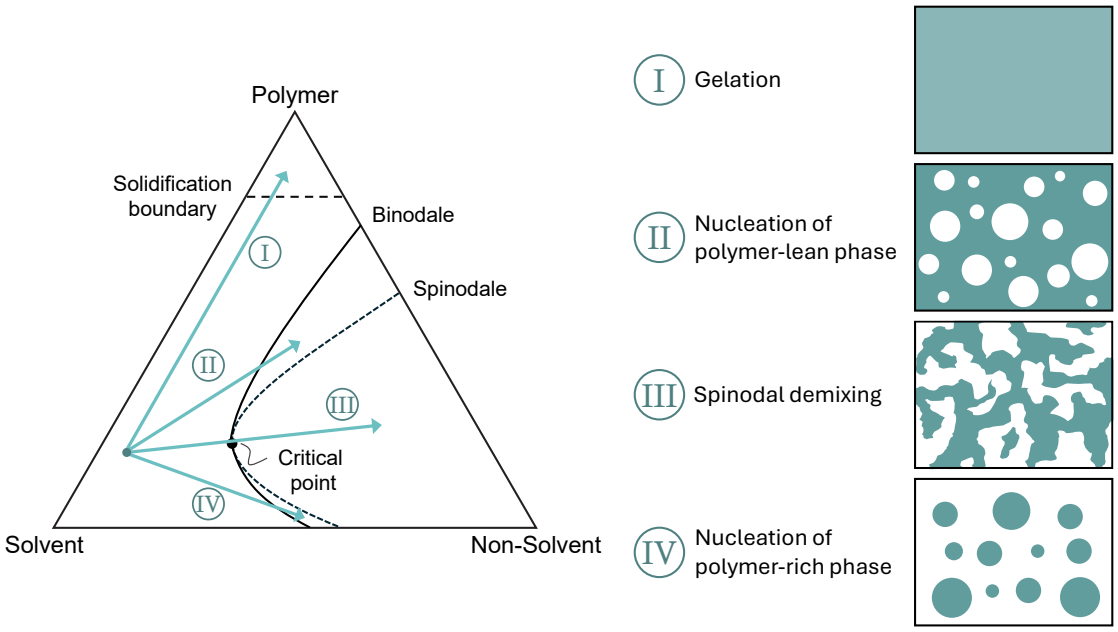


Figure 2.5: Schematic representation of the structure-forming mechanism at different pathways within a ternary phase diagram.

When a polymer solution crosses he solidification boundary without entering the miscibility gap, phase separation does not occur (I). As a result, a dense, non-porous structure is formed. Crossing the binodale as shown in paths (II) to (IV) is necessary for phase-separation, and therefore, pore formation to occur. When the solution enters the metastable area above or below the critical point (II & IV), phase separation based on the nucleation and grow (NG) mechanism will occur [Muld1996]. Since the polymer solution is stable against small fluctuations in composition in the metastable range, phase separation requires a critical radius of the nuclei, which is described by equation 2.13 [Than2014]

$$r_{crit} = -\frac{2\sigma}{\Delta G_v} \tag{2.13}$$

.

and is dependent on the surface energy σ and the free enthalpy per volume ΔG_v. When the solution enters the metastable region at higher polymer concentration above the critical point, nucleation of the polymer-lean

phase will occur (II). In contrast, when the solution enters the metastable area below the critical point at low polymer concentrations (IV), the opposite, nucleation of the polymer-rich phase, occurs [Bake2023; Muld1996]. These nuclei grow in size through further solvent-non-solvent exchange until the structure solidifies. In the first scenario (II), the polymer-rich phase builds a stable membrane backbone. In contrast, the latter scenario (IV) does not lead to stable membrane structures and is therefore undesirable in membrane fabrication processes. When the solution directly enters the unstable region near the critical point without passing the metastable region (III), spinodal demixing (SD) occurs [Muld1996; Nune1996]. Thereby, phase separation occurs spontaneously, and two bicontinous layers are formed. Unless phase separation occurs by NG or SD, structural changes will occur before the membrane finally solidifies in both cases.

The two phenomena most commonly associated with structural changes in phase-separated systems are coalescence and Ostwald ripening [Mats1999]. In coalescence, it is assumed that small nuclei form a larger nucleus on contact to reduce the surface tension between the two phases. This phenomenon can be mathematically described by

$$d^3 = \frac{8\mathrm{k}T\phi_n}{\eta\pi} \cdot t \tag{2.14}$$

with d being the diameter of the nucleus, k the Boltzmann constant, T the temperature, ϕ_n the volume fraction of the nuclei, η the viscosity of the medium and t the time [Mats1999]. The effect of Ostwald ripening is based on the Kelvin effect, where small particles have a higher solubility than large particles [Than2014; Wang2005]. Ostwald ripening states that nuclei below a critical radius shrink, while nuclei above the critical radius grow. Mathematically, the effect can be expressed as

$$d^3 = \frac{64\sigma D_m x_m V_m}{9\mathrm{R}T} \cdot t \tag{2.15}$$

where σ is the interfacial energy, D_m the diffusion coefficient for the

minor phase substance, x_m the molar fraction of the minor phase and V_m the molar volume of the minor phase [Wang2005; Than2014]. During the pore formation in membranes, both effects can occur in parallel, with various influencing factors such as viscosity and the interaction between the two phases, making it impossible to distinguish which pore growth phenomenon predominated.

2.2.4 Phase separation kinetics

While the entry point in the miscibility gap determines which phase separation mechanism occurs, the kinetics of the system influence the mass transfer and, therefore, the compositional changes during the phase separation [Muld1996; Bake2023; Boom1994; Reuv1987b; Stra1975]. Therefore, they significantly influence the structural changes and the resulting membrane structure. In general, a distinction is made between instantaneous and delayed demixing kinetics.

Delayed demixing typically occurs when the exchange of solvent and non-solvent is slow. This is the case when, for example, the system obtains a low affinity between solvent and non-solvent or a high affinity between solvent and polymer [Smol1992; Reuv1987b; Boom1994]. The viscosity of the polymer solution also plays a crucial role in the phase separation kinetics. A higher viscosity slows down the diffusion in the system and, therefore, slows the phase separation [Zhan2010]. This delayed process allows more time for the polymer-poor phase to grow and coalesce before solidification, leading to the formation of a thick, uniform sponge-like structure or closed-cellular pores throughout the membrane cross-section, where the formation of large voids is suppressed [Bake2023; Kahr2020; Magg2022]. In contrast, during instantaneous demixing, the casting solution rapidly crosses the binodal, driven by a rapid solvent-nonsolvent exchange rate [Reuv1987a; Smol1992; Magg2022]. This rapid exchange often results from a high affinity between solvent and non-solvent, and/or a low affinity between solvent and polymer [Smol1992; Reuv1987b; Boom1994].

Also, a low viscosity benefits a fast exchange [Zhan2010]. However, the exchange rates are not equal across the whole membrane cross-section [Muld1996; Stra1977]. Figure 2.6 represents the non-solvent concentration profile within a polymer film at different times. When the phase separation is initiated at the polymer-coagulation bath interface, the solvent/non-solvent exchange rate is high at this location, and a steep concentration gradient is obtained through the membranes' cross-section [Smol1992; Stra1977]. A dense skin layer is formed because of the rapid outflux of solvent and a relatively small penetration of non-solvent, which causes the polymer concentration at the interface to increase rapidly, leading to gelation [Wijm1983]. Due to this rapid precipitation at the surface, the newly formed phases have insufficient time to agglomerate or segregate, resulting in a dense or finely microporous structure [Bake2023; Stra1975; Stra1977]. This skin layer increases the diffusive resistance for further non-solvent inflow and solvent outflow, resulting in these steeper concentration gradients. Consequently, phase separation in the lower layers is delayed, giving the polymer-lean nuclei time to grow and form randomly distributed pores [Stra1977].

Therefore, controlling these kinetic pathways is crucial in determining the macroscopic morphology and microscopic pore architecture, which directly impact the membrane's ultimate separation performance.

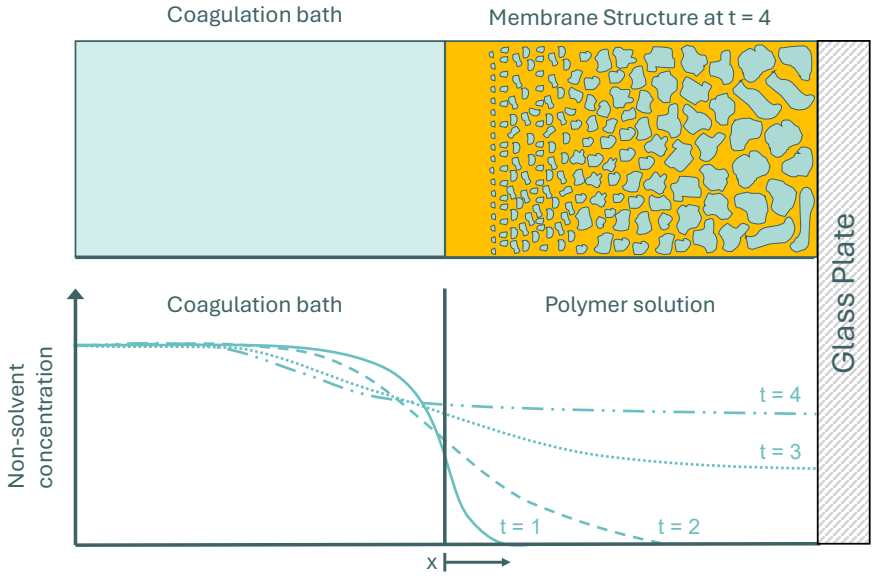


Figure 2.6: Concentration profiles of the non-solvent within the polymer film at different times (adapted from [Stra1977]).

2.3 Technical Implementation

Figure 2.7 schematically shows the fabrication process of a) flat sheet (FS) and b) hollow fiber (HF) membranes via NIPS.

FS membranes are fabricated by applying a polymer solution to an inert support, which is then uniformly spread to a defined thickness using a casting knife (see Figure 2.7 a). This is followed by immersion into a precipitation bath containing a non-solvent medium. Due to the concentration gradient established between the polymer solution and the precipitation medium, the solvent and non-solvent exchange by diffusion, causing phase liquid-liquid separation and subsequent solidification. The relative simplicity of FS membrane fabrication makes it the preferred method for testing new or modified polymer casting solutions on a laboratory scale.

In contrast, HF membrane fabrication requires a more complex spinning line (see Figure 2.7b). Thereby, a polymer solution (dope) is extruded through an annular nozzle, accompanied by a coagulant (bore) fluid co-extruded into the fiber's center to form the hollow interior. Afterwards, the nascent fiber passes through an air gap with a controlled atmosphere, be-

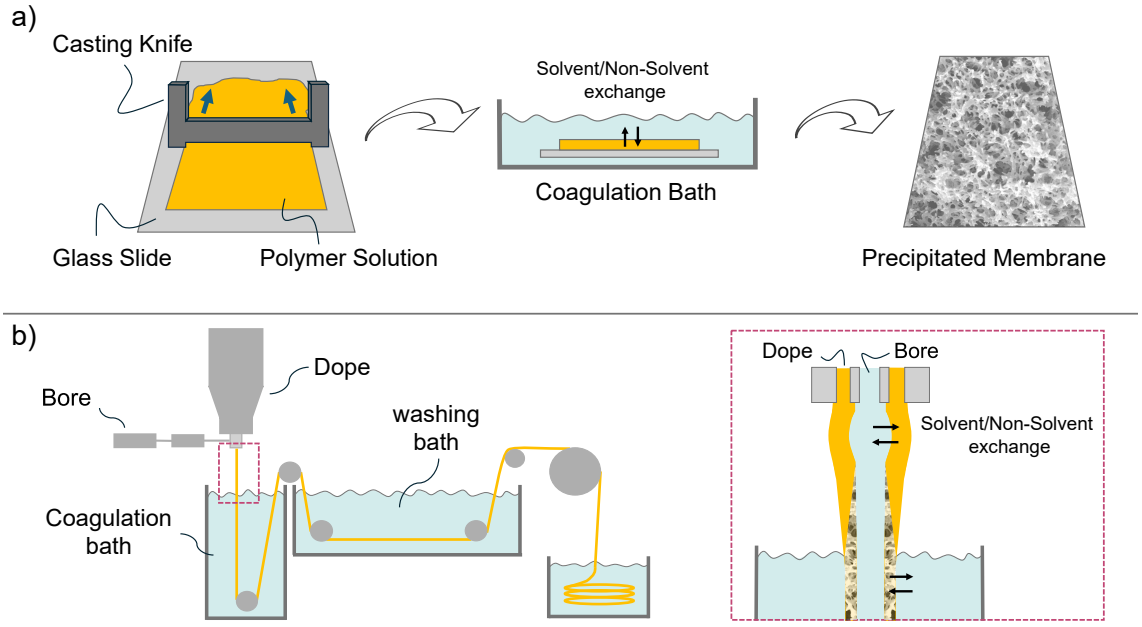


Figure 2.7: Schematic representation of the a) FS and b) HF membrane fabrication process.

fore entering a coagulation bath containing a non-solvent. Within this bath, rapid phase inversion occurs, resulting in polymer precipitation and membrane formation. The fiber is subsequently washed to remove residual solvent and is then wound up.

In this fabrication process, there are several levers to control the thermodynamics and kinetics of the phase separation process. Figure 2.8 summarizes the main parameters in hollow fiber spinning that significantly influence the membrane formation and its final properties. For example, the compositions of dope and bore fluid require a precise adjustment of solvent-polymer-non-solvent affinities to create a platform suitable for the fabrication of the desired membrane structures. The structure-forming mechanism of this platform during phase separation can be further manipulated by adjusting process parameters, such as temperatures, air gap conditions, extrusion rates, and pulling speeds. Among these parameters, there are complex interactions that influence the phase separation kinetics and thermodynamics, and therefore necessitate precise control and optimization. Therefore, a thorough understanding of how these parameters individually and collectively influence membrane properties is required. Within this thesis, various

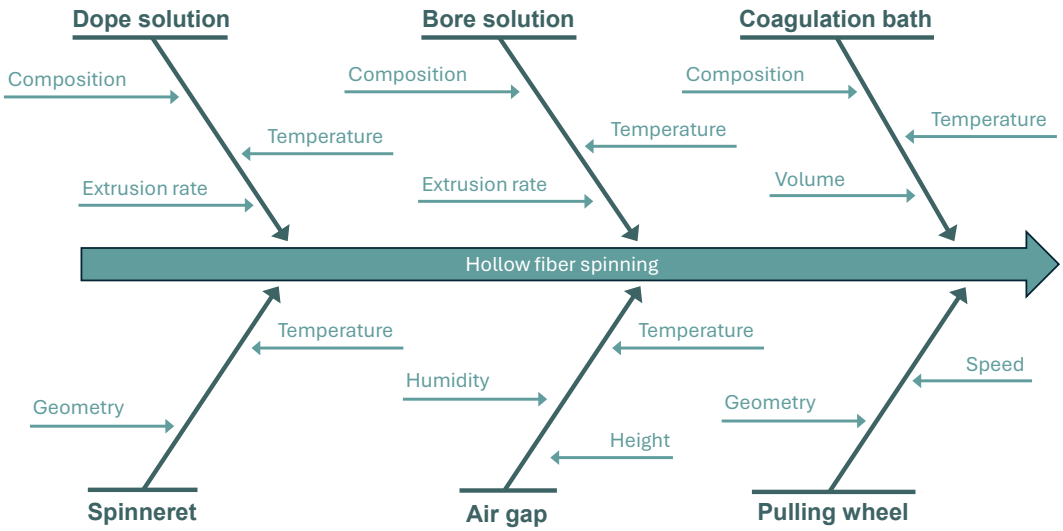


Figure 2.8: Overview of the main process parameters during hollow fiber membrane fabrication (adapted from [Kope2011]).

dope and bore solution compositions are investigated in combination with different air gap lengths and conditions, as well as coagulation bath temperatures.

2

3

Materials and Methods

3.1 Materials

Polyethersulfone Ultrason E6020 P (PES), polyvinylpyrrolidone (PVP) Sokalan® K17 for membrane fabrication and N,N-dimethyllactamid (AMD, Agnique® AMD 3L) were supplied by BASF SE. Polyvinylpyrrolidone K15 (MW = 9000 g/mol) and K30 (MW = 58 000 g/mol) for retention measurements were provided by Ashland™. N-Methylpyrrolidone (NMP) was supplied by Thermo Fisher Scientific Inc., and Triethylphosphate was purchased from sigma aldrich®. N-butylpyrrolidone (NBP,Tamisolve ®NxG) was supplied by Eastman Chemical, and 2-pyrrolidone (2P) by Carl Roth®.

3.2 Methods

3.2.1 Calculation of Hansen solubility parameters

For the comparison of polymer affinities between the investigated solvent systems, the HSP distances were calculated according to equation 2.11. The individual HSP of each component is listed in Table 3.1. The individual HSP for solvent mixtures at different ratios were calculated according to equation 2.10 and listed in Table 3.2.

Table 3.1: Hansen Solubility Parameters for the polymer solution components.

Compound Unit	δ_d $\sqrt{\text{MPa}}$	δ_p $\sqrt{\text{MPa}}$	δ_h $\sqrt{\text{MPa}}$	δ $\sqrt{\text{MPa}}$	Ref
PES	17.6	10.4	7.8	21.9	[Jian2021]
PVP	21.4	11.6	21.6	32.5	[Gron2020]
NMP	18.4	12.3	7.2	23.3	[Jian2021]
NBPsolve	17.2	8.2	5.9	19.9	[Jian2021]
Agnique	18.4	12.9	15.9	27.5	[Gron2020]
2-Pyrrolidone	19.5	17.4	11.3	28.5	[Hans2007]
Triethylphosphate	16.7	11.4	9.2	22.2	[Hans2007]

Table 3.2: Hansen Solubility Parameters of sustainable solvent mixtures in different ratios calculated according to equation 2.10.

Solvents Unit	ratio -	δ_d $\sqrt{\text{MPa}}$	δ_p $\sqrt{\text{MPa}}$	δ_h $\sqrt{\text{MPa}}$	δ $\sqrt{\text{MPa}}$
NBP/AMD	25:75	18.1	11.7	13.3	25.5
NBP/AMD	50:50	17.8	10.5	10.7	23.5
NBP/AMD	75:25	17.5	9.3	8.3	21.7
NBP/2P	25:75	18.9	14.8	9.8	26.4
NBP/2P	50:50	18.3	12.4	8.4	24.3
NBP/2P	75:25	17.8	10.8	7.4	22.1
NBP/TEP	25:75	16.8	10.5	8.3	21.6
NBP/TEP	50:50	17.0	9.7	7.5	21.0
NBP/TEP	75:25	17.1	8.9	6.7	20.5

3.2.2 Viscosity

The viscosity of the polymer solutions was measured with the ViscoQC 300 rotational viscometer (*anton paar GmbH*). 20 mL of the polymer solution was transferred to a beaker. The solution was stirred and heated to 60 °C for 10 minutes to equalize the temperature before the measurement. The viscosity was determined with a RH6 geometry at a shear rate of 100 s^{-1}, and the sample was heated to 60 °C.

3.2.3 Flatsheet membrane casting

For the production of flat sheet membranes, the polymer solution was cast at a uniform speed using a 200 µm casting knife on a glass plate. The glass plate was immediately immersed in a water bath after casting the solution and left to rest until the precipitated polymer film detached from the plate. Afterwards, the membranes were washed for 16 h in water at 60 °C to remove residual additives and solvents. To prohibit pore collapse, the FS membranes were impregnated in a glycerol-water solution (50:50) and dried at room temperature afterwards.

3.2.4 Hollow fiber fabrication

Hollow fiber membranes were produced using a lab-scale spinning line. The polymer solution was heated and co-extruded with a bore solution, facilitating the exchange of solvent and non-solvent at the lumen side of the hollow fiber. After extrusion through the spinneret, the fiber was guided through a 10 or 20 cm air gap into a first coagulation bath containing pure water, and afterwards washed in an additional water bath. In the end it is collected on a winder. The dope-and bore extrusion velocities, as well as the pulling speed were adjusted individually for each system to achieve a fiber wall thickness of approximately 250 µm. To prohibit pore collapse, the HF membranes were impregnated in a glycerol-water solution (50:50) and dried at room temperature afterwards. For further characterization, the hollow fibers were potted in a module equipped with a feed inlet and permeate and reten-

tate outlets. The detailed information on the dope temperature, coagulation bath temperature, bore composition, and extrusion rates is given in the respective chapters.

3.2.5 Light transmission measurements

The light transmission experiments were performed using an adapted setup according to the method described by Reuvers et al. [Reuv1987a]. A light source was positioned above a coagulation bath, and a photodiode was placed below it. The polymer solutions were cast on a glass slide using a 250 µm casting knife and subsequently immersed in the coagulation bath as described above in Section 5.2.2. The decrease in light intensity under the precipitating membrane was detected by the photodiode over time. The time of immersion is referred to as t_0, whereas the onset of demixing is defined as the time t_1 at which the light intensity signals start to decrease. Each measurement was repeated three times, and the results are presented as the mean values with standard deviations.

3.2.6 Scanning electron microscopy

For Scanning Electron Microscopy (SEM) investigations of the cross-sectional porous structure, the membrane samples were fractured in liquid nitrogen, resulting in a straight fracture edge while preserving the pore structure. The samples were then dried under vacuum conditions and sputtered with Quorum platinum 300 TT 100 s. Secondary electron micrographs were taken with a SEM *Hitachi* SU5000 at an acceleration voltage of 5 kV in high vacuum conditions. The obtained SEM images were analyzed with the software *ImageJ*. For the determination of the surface porosity and pore size, a grey-scale threshold was chosen to distinguish between pore and membrane area. The pores were characterized using the built-in "analyze particles" function. Pore-size distributions were characterized by the median (50th percentile) and the quartile range defined by the 25th and 75th percentiles (Q1–Q3). These statistics were selected because the median provides a robust measure of central tendency that is unaffected by extreme

values. At the same time, the Q1–Q3 range describes the variability of the central 50% of observations without being distorted by outliers.

3.2.7 Pure water permeance measurements

Before measuring the pure water permeance (PWP), the membranes were flushed with a 20 wt% aqueous ethanol solution to remove any glycerol from the pores. The permeance was measured using a cross-flow setup in the inside-out direction with a flow rate of 100 mL/min and a transmembrane pressure (TMP) of 0.7 bar. The permeate sample was collected for 60 seconds and then weighed. The membranes´ permeance is described by the Equation 3.1

$$J = \frac{V_P}{\Delta t \cdot \Delta p \cdot A} \tag{3.1}$$

where J is the membrane permeance (LMH/bar)), V_P the volume of the permeate, Δt the duration, Δp the transmembrane pressure, and A the membrane filtration area. Two modules were built per fiber batch, and each was measured four times. The PWP of the respective fiber batch was determined as the mean value with standard deviation from all measurements.

3.2.8 Retention measurements

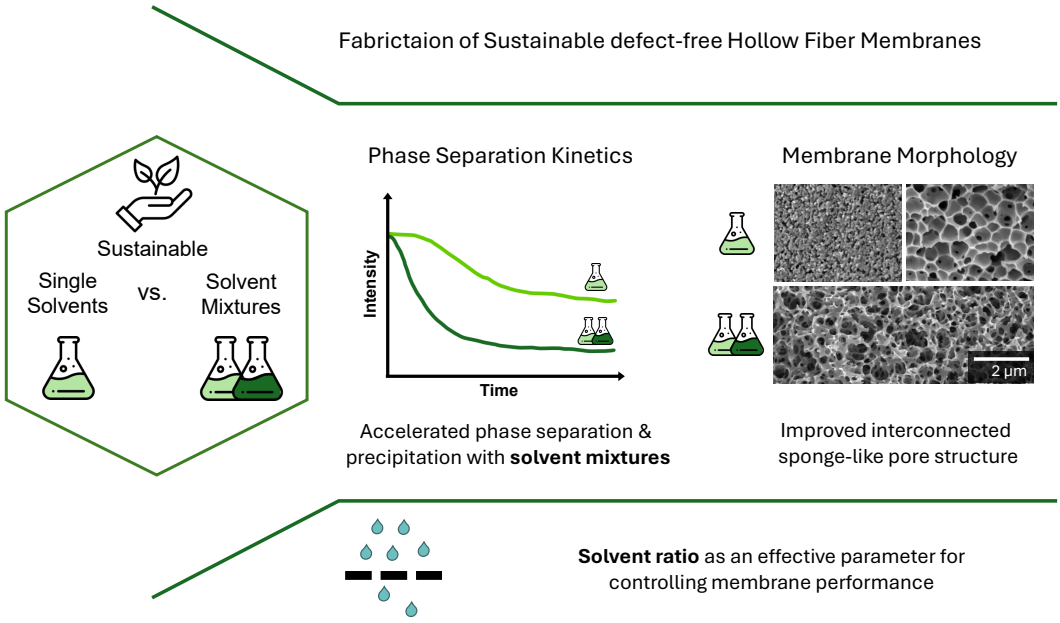
The filtration performance was further evaluated by measuring the retention of PVP K30 (MW 58 kDa). A feed solution containing 0.2 wt% PVP in water was filtered in the inside-out direction through the module in cross-flow mode at a flow rate of 100 mL/min and a TMP of 0.7 bar. After reaching steady state conditions, permeate samples were collected in six aliquots of 2 mL each. The feed c_{feed} and the permeate $c_{permeate}$ concentrations were obtained from their refractive indices, measured with a refractometer (Abbemat 550, Anton Paar), and converted to concentration using a previously established calibration curve. The Retention R was calculated for each sample according to Equation 3.2.

$$R = \left(1 - \frac{c_{permeate}}{c_{feed}}\right) \cdot 100 \tag{3.2}$$

Two modules were built per fiber batch, and four permeate samples were measured for each. The retention of the respective fiber batch was determined as the mean value with standard deviation from all samples.

4

Influence of sustainable solvents and their mixtures on PES membrane fabrication



Parts of this chapter are in preparation for publication:

Lea Greie, Tilman Schiffer, Lara E. Grünig, Kai Blechmann, Frederike Schiszler, Matthias Wessling

Tunable Pore Architecture via Mixed-Solvent Polymer Solutions: Toward Next-Generation Sustainable Hollow Fiber Membranes

4.1 Introduction

Recent research has focussed on the identification of bio-based and less hazardous solvents, including dimethyl sulfoxide [Even2018], N-butylpyrrolidone (TamiSolve® NxG) [Mari2017; Shen2025], Rhodiasolv® PolarClean [Ursi2020], dihydrolevoglycosenone (Cyrene™)[Mari2019], dimethyl isosorbide [Russ2020], triethyl phosphate [Chan2017; Mari2018], 2-pyrrolidone [Kahr2020],γ-valerolactone [Raso2019], and N,N-dimethyllactamid (Agnique® AMD 3L) [Gron2020; Uebe2021; Leop2025]. These alternatives aim to significantly reduce environmental impact and health risks while maintaining or enhancing membrane properties. Kahrs *et al.* showed that the high viscosity of PES dissolved in 2-pyrolidone (2P) was beneficial for suppressing macrovoids in flat sheet membranes. However, no investigation has been conducted on using those high-viscosity solutions in the hollow fiber spinning process to our knowledge. While N-butylpyrrolidone (NBP) was found to be a suitable alternative solvent for the fabrication of PVDF membranes by Russo *et al.*[Russ2021], only a few studies addressed the fabrication of PES membranes. Jiang *et al.* [Jian2021] fabricated thin film composite PES membranes with TamsiSolve® as solvent and found similar results to those fabricated with the toxic solvent NMP. However, it was stated that the polymer and additive concentrations must be balanced precisely to keep the precipitation rate within the desired window. This is particularly important for fabricating hollow fiber membranes, as a slow precipitation lowers the mechanical stability during fiber spinning. Another promising less toxic solvent is triethylphosphate (TEP). It was used by Chang *et al.* to fabricate PVDF hollow fiber membranes for membrane destillation. The membranes exhibited a flux of 20 kg m^{-2} h^{-1} at 60 °C with a NaCl rejection of 99.99% but had low mechanical stability. The investigation of PES membranes fabricated with Triethylphosphate has not yet been reported. Leopold *et al.* [Leop2025] showed that the bio-based solvent Agnique® AMD 3L (AMD) is a promising solvent for the fabrication of PES ultrafiltration hollow fiber membranes. By performing a design of experiments (DoE), the main

influencing factors for the membrane morphology, like the molecular weight of the polymeric additive, could be determined. The promising results of Leopold underlay the need for further investigations in the field of wide cut-off ranges and detailed membrane formation investigation. Although these examples illustrate the potential of more sustainable solvents for the production of PES membranes, the influence of solvents on the kinetics and thermodynamics of phase separation, especially in terms of hollow fiber membrane spinning, has not yet been extensively investigated[Figo2014].

Interactions among solvent, non-solvent, and polymer determine membrane formation pathways, influencing solution viscosity, solvent, and non-solvent exchange rates and, therefore, affecting pore nucleation, growth, and the formation of macrovoid or sponge-like structures[Reuv1987b][Smol1992]. These structural differences play a crucial role in membrane performance for several applications. Replacing NMP with a less toxic alternative solvent is challenging, as the interactions between other solvents and membrane materials are poorly understood. Therefore, thoroughly understanding these interactions is crucial for designing high-performance membranes using environmentally friendly solvents.

Utilizing solvent mixtures has emerged as an effective strategy to address the limitations of individual solvents. By precisely adjusting the solvent ratios, the phase separation behavior can be controlled, enabling the creation of tailored membrane morphologies and improved performance. Li *et al.* [Li2009] produced high-flux porous PVDF membranes by combining DMAc with different alkyl phosphates. The alkyl phosphates increased the solvent power of the mixture for PVDF and accelerated the precipitation. Using different kinds of alkylphosphates in different ratios could alter the membrane characteristics. Solvent mixtures were also used to overcome the limitations of single alternative solvents while maintaining environmental compatibility. Dong *et al.* found that γ-valerolactone as a single solvent was unsuitable for fabricating microporous PSf membranes since nearly impermeable and sticky membranes were obtained. Combining γ-valerolactone with Rhodiasolv® PolarClean leads to an improved polymer solubility and a significant increase in permeance of the membranes. The obtained mem-

brane morphologies are similar to those fabricated with the conventional solvent DMAc [Dong2020].

While current research highlights the potential of solvent mixtures as an effective method to control the solubility of polymers and the membrane formation process, systematic studies on the influence of more sustainable solvents, especially their mixtures, on phase separation remain limited. This chapter addresses this gap by investigating how the alternative solvents NBP, AMD, 2P, and TEP impact the phase separation behavior in PES flat sheet and hollow fiber membrane fabrication. By mixing two solvents, the limitations of the individual solvents were overcome, resulting in improved performance of the membranes. Critical insights into the pore-forming mechanism and the influence of solvent mixtures are provided by measuring light transmission during phase separation and analyzing the morphology and performance of flat sheet and hollow fiber membranes.

4.1.1 Methods

Dope Solution Fabrication

All components were combined in a heated vessel and stirred at 60 °C until a homogeneous solution was obtained. Before the fabrication of either flatsheet (FS) or hollow fiber (HF) membranes, the polymer solution was degassed. The exact compositions of all polymer solutions are given in Table 4.1.

Table 4.1: Composition of the polymer solutions for the flat sheet (FS) and hollow fiber (HF) membrane fabrication.

Code	Ratio Solvent A:B	PES [wt%]	PVP K17 [wt%]	Solvent A [wt%]	Solvent B [wt%]	Water [wt%]
FS-NMP	100:0	18	25	55	-	2
FS-NBP	100:0	18	25	55	-	2
FS-AMD	100:0	18	25	55	-	2
FS-2P	100:0	18	25	55	-	2
FS-TEP	100:0	18	25	55	-	2
FS-NBP/AMD	25:75	18	25	13.75	41.25	2
FS-NBP/2P	25:75	18	25	13.75	41.25	2
FS-NBP/TEP	25:75	18	25	13.75	41.25	2
HF-NBP/AMD-25	25:75	20	20	14.5	43.5	2
HF-NBP/AMD-50	50:50	20	20	29.0	29.0	2
HF-NBP/AMD-75	75:25	20	20	43.5	14.5	2
HF-NBP/2P-25	25:75	20	20	14.5	43.5	2
HF-NBP/2P-50	50:50	20	20	29.0	29.0	2
HF-NBP/2P-75	75:25	20	20	43.5	14.5	2
HF-NBP/TEP-25	25:75	20	20	14.5	43.5	2
HF-NBP/TEP-50	50:50	20	20	29.0	29.0	2
HF-NBP/TEP-75	75:25	20	20	43.5	14.5	2

Membrane fabrication

Flat sheet membranes were fabricated via the process described in Section 3.2.3 using a coagulation bath containing pure water.

The hollow fiber membranes were produced via the procedure described in Section 3.2.4. Within this chapter, the air gap distance was set to 20 cm. The dope temperature and the coagulation bath temperature was kept at

room temperature (25 °C) and the bore solution was composed of water and glycerol (50:50). Table 4.2 summarizes the spinning parameters used for the production of the hollow fiber membranes.

Table 4.2: Spinning parameters for the hollow fiber membrane fabrication.

Solvents	Solvent Ratio A:B	Dope flow [mL/min]	Bore flow [mL/min]	Pulling Speed [m/min]
NBP/AMD	25:75	3.7	2.7	2.2
NBP/AMD	50:50	5.7	3.3	2.7
NBP/AMD	75:25	2.9	2.3	1.5
NBP/2P	25:75	5.8	5.9	2.9
NBP/2P	50:50	5.4	4.7	2.7
NBP/2P	75:25	5.3	3.3	2.4
NBP/TEP	25:75	5.7	4.6	2.4
NBP/TEP	50:50	2.9	2.0	1.4
NBP/TEP	75:25	2.4	1.6	0.9

4.2 Results and Discussion

4.2.1 Influence of solvent type on the polymer solution

The influence of more sustainable solvents AMD, NBP, TEP, and 2P on the characteristics of the polymer solution was investigated by preparing polymer solutions with the same compositions (see Table 4.1). NMP was used as the reference solvent. The solvent power of TEP for PES was insufficient, therefore, preparing a homogenous polymer solution (see Figure 4.1) was not realized. The viscosities of all realizable polymer solutions are given in Figure 4.2.



Figure 4.1: Photograph of the inhomogeneous TEP-PES solution.

The highest viscosity was measured for the solution based on 2P, followed by AMD, NBP, and NMP. In addition to the single solvents, mixtures of NBP with AMD, 2P, and TEP in a 25:75 ratio were also investigated. Notably, the viscosities of the more sustainable solvent solutions are three to five times higher than the viscosity of the NMP solution, which has been observed previously in literature for the solvent AMD and 2P [Kahr2020]. Mixing with NBP led to a decrease in viscosity by 3.5 $Pa \cdot s$ for AMD and 2.0 $Pa \cdot s$ for 2P. In the case of TEP, the solvent power within the NBP/TEP mixture is sufficiently enhanced, enabling the preparation of a homogeneous polymer solution.

The solvent power of the respective solvent influences the viscosity of a polymer solution. In highly concentrated polymer solutions, viscosity in-

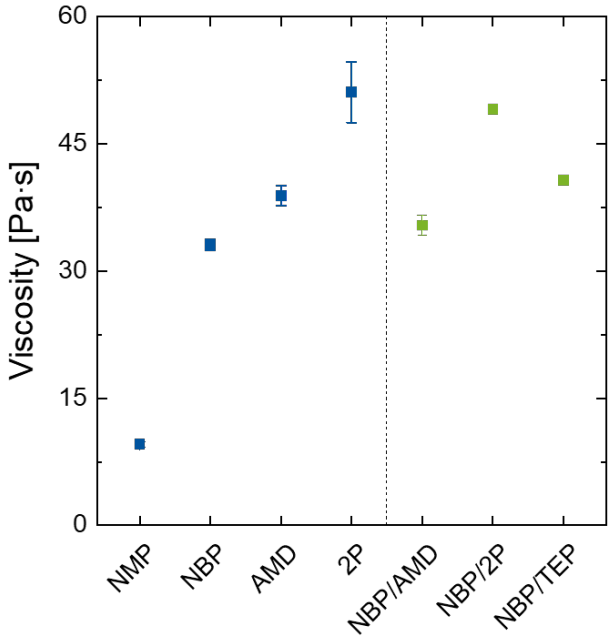


Figure 4.2: Viscosities of polymer solutions (18 wt% PES, 25 wt% PVP K17, 2 wt% water) fabricated with different solvents and solvent mixtures (25:75, NBP:AMD/2P/TEP) at 60 °C and a shear rate of 100 s^{-1}.

creases as solvent power decreases, as a result of aggregation and network formation of the polymer chains [Hoer1974]. A low solvent-polymer interaction also increases the solutionstendency to gel during phase separation [Chun2021]. The solvent power can be estimated by the HSP difference between the solvent and polymer Δ_{S-PES} and Δ_{S-PVP} according to equation 2.11 as listed in Table 4.3 for the single solvent and Table 4.4 for their mixtures at different ratios.

Table 4.3: Hansen Solubility Parameters distances between solvents and polymers.

Compound	Δ_{S-PES} $\sqrt{\text{MPa}}$	Δ_{S-PVP} $\sqrt{\text{MPa}}$
PES	-	14.4
PVP	14.4	-
NMP	2.1	14.7
NBP	2.9	16.6
AMD	8.5	6.6
2P	8.1	12.0
TEP	1.9	13.3

Table 4.4: Hansen Solubility Parameters distances between solvent-mixtures and polymers.

Solvents	ratio -	Δ_{S-PES} $\sqrt{\text{MPa}}$	Δ_{S-PVP} $\sqrt{\text{MPa}}$
NBP/AMD	25:75	5.6	9.0
NBP/AMD	50:50	2.9	11.5
NBP/AMD	75:25	1.2	14.1
NBP/2P	25:75	5.0	12.5
NBP/2P	50:50	2.2	13.6
NBP/2P	75:25	0.6	14.7
NBP/TEP	25:75	0.9	14.1
NBP/TEP	50:50	1.0	14.9
NBP/TEP	75:25	1.9	15.8

A smaller distance Δ between the HSP of the respective compounds indicates a higher affinity. However the HSP is only an estimation, as it does not include complex aspects like swelling, diffusion, and solvation processes [Venk2019]. This is also displayed in the case of TEP. Even though the solvent power of TEP was not sufficient for the present composition, the $\Delta_{s\text{-PES}}$ and $\Delta_{s\text{-PVP}}$ values are even lower than those of NMP. However, for the remaining solvents, the observed viscosities agree with the trends in HSP. 2P has a large distance to PES Δ_{S-PES} and, therefore, a low affinity. This low affinity also correlates with the high viscosity of the solution. Despite the Δ_{S-PES} of AMD being even higher than that of 2P, the Viscosity is lower. The low affinity is mainly due to its higher hydrogen bonding (δ_h) compared to PES. However, this strong hydrogen bonding leads to an HSP distance of AMD to PVP Δ_{S-PVP} that is significantly smaller than that of 2P, increasing its solvent power for the total PES-PVP system and resulting in a lower viscosity [Gron2020]. NBP has a significantly higher affinity to PES and a low affinity to PVP, comparable to NMP. Therefore, mixing AMD, 2P, and TEP with NBP in the ratio of 75:25 leads to a decrease in Δ_{S-PES} and a slight increase in Δ_{S-PVP} for all solvents (see Table 4.4).

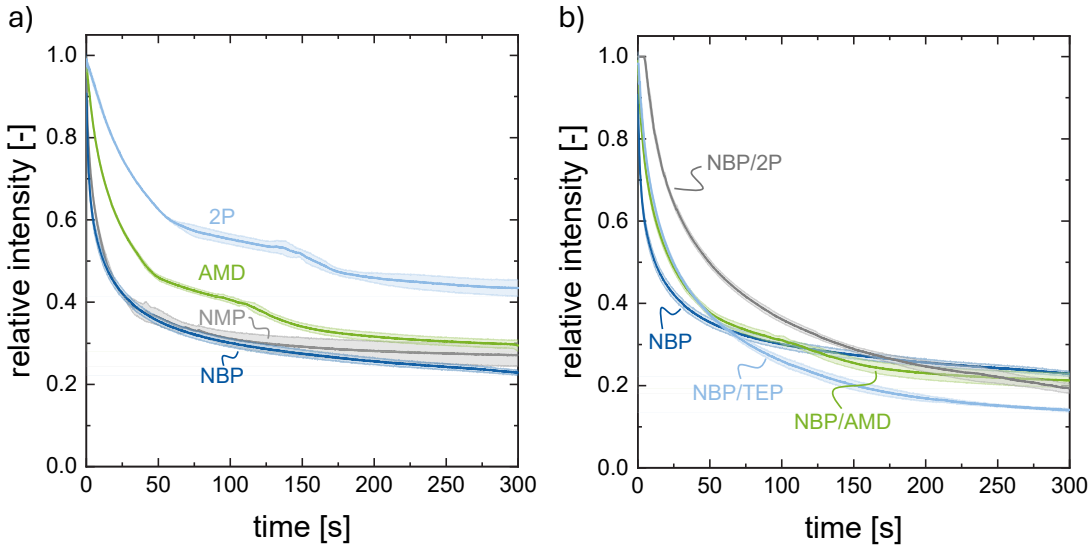


Figure 4.3: Light transmission measurements of polymer solutions with (a) single solvents and (b) mixed solvents (n=3).

4.2.2 Phase separation kinetics

Light transmission measurements were performed as described in Section 3.2.5 to further investigate the influence of the different solvent systems on the phase separation kinetics. In Figure 4.3 a) the light transmissions over the immersion time of the single-solvent polymer films in the water bath are displayed.

Upon liquid-liquid demixing of the polymer solution into polymer-poor and polymer-rich phases, light scattering is caused, and the light transmission during the experiment will be decreased [Reuv1987a]. All polymer solutions caused an instantaneous decrease in light intensity ($t_0 = t_1$) when precipitation in the water bath started. The signals of the NBP and NMP solutions appear similar, while the decrease of light intensity for the AMD and 2P solutions was significantly slower.

The light transmission through the NBP and NMP film dropped significantly during the first 10–25 seconds, followed by a slower rate of decrease. Both solutions show similar behavior within the error bars in the light transmission experiments. However, the experiment provides only limited insights into the lower layers of the film during phase separation. After precipitation for 30 seconds in the coagulation bath, both membranes were

visually compared, and a significant difference between the two membranes was observed (see 4.4). While the NMP membrane is already entirely precipitated, the NBP membrane formed a dense boundary layer on the water interface, but an unprecipitated polymer solution region below.

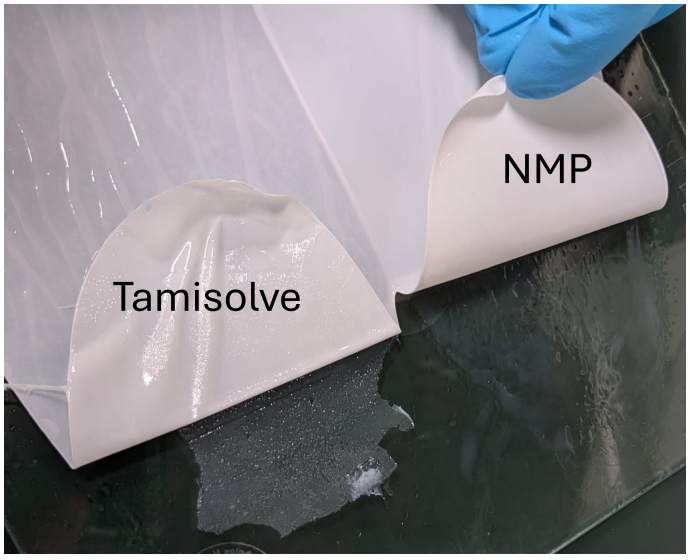


Figure 4.4: Comparison of NBP and NMP membranes after 30 s immersion in water.

The light transmission signals of the AMD and 2P solutions differed not only in the slower decrease but also in the shape of the detected signals. After a first intensity decrease, an intermediate plateau could be detected for ∼50 s. Afterwards, the intensity falls until the final plateau is reached. The final plateau of the 2P solution with an intensity of 0.43 is significantly higher in light intensity than that of the other solutions, at an intensity of 0.23 to 0.30. A lower light transmission indicates a stronger refraction of the light.

Mixing the alternative solvents with NBP significantly influenced the phase separation kinetics of the solution (see Figure 4.3 b). Compared to the single-solvent solutions AMD and 2P, the decrease in light intensity is accelerated. In the NBP/AMD and NBP/TEP solutions, an instantaneous, sharp decrease is observed, while the decrease in the NBP/2P solution is delayed and starts at t_1 = 4 s. The general shape of AMD light intensity curve remains the same in the NBP/AMD mixture but is shifted to lower light intensities. The intermediate plateau is flattened, and the final steady state is

reached after ∼150 s. The shape of the NBP/2P and NBP/TEP curves is similar to that of the single NBP solution, but the intensity decreases more slowly. For the NBP/2P solution, no steady light intensity state was reached within the data collection period.

The kinetics of the liquid-liquid demixing depend on the solvent outflux J_{out} and the non-solvent influx J_{in}. A fast exchange leads to an instantaneous demixing, while a slower exchange results in a delayed onset of phase separation [Smol1992; Reuv1987a; Chun2021]. When the J_{out}/J_{in} ratio is very high, the polymer solution enters the gel state without the occurrence of liquid-liquid demixing. A high affinity of the solvent to the non-solvent can lead to a fast exchange as well as a low affinity to the polymer [Smol1992; Chun2021]. Another critical parameter influencing the phase separation is the diffusivity of the solvent and non-solvent within the polymer solution. The mass transfer is not equal at every position in the polymer film. The increasing coagulation front hinders the mass transfer in the underlying areas. This mass transfer hindrance is also exacerbated by a high viscosity [Zhan2010].

Table 4.5: Octanol-water partition coefficients *log* P_{OW} of the investigated solvents.

Solvent	NMP	NBP	AMD	2P	TEP
log P_{OW}	-0.46 [ECHA2021]	1.27 [ECHA2022]	-0.94 [ECHA2024]	-0.71 [Jain2007]	1.11 [Vers1996]

The affinity of the solvents to non-solvent water can be estimated by the octanol-water partition coefficients *log* P_{OW} listed in Table 4.5. A higher *log* P_{OW} correlates to a higher hydrophobicity of the compound [Mack1980]. NBP is reported to be completely miscible with water [Jian2021; Mari2017]. Nonetheless, the *log* P_{OW} is significantly higher for NBP (1.26) than for NMP (-0.46). This low affinity for water and the significantly higher viscosity compared to the NMP solution align with the slow precipitation observed in the sublayer of the NBP film, as the exchange of solvent and non-solvent is slowed.

AMD and 2P have a lower *log* P_{OW} than NMP and, therefore, a higher

affinity to water, which enables a fast non-solvent influx. However, the significantly higher viscosity of the solutions hinders this influx. Additionally, the low affinity of the solvents for PES enhances the solvent outflux, promoting the gelation of the solution rather than liquid-liquid demixing, which leads to a slow and gradual decrease in light intensity. When mixing the solvents with NBP, the affinity to PES increases, and the tendency to gel decreases. Additionally, the decreased viscosity improves the non-solvent influx, accelerating the liquid-liquid phase separation and, therefore, the decrease in light intensity. In general, the ratio of light scattering depends on the amount and size of the polymer-lean nuclei that are formed during liquid-liquid demixing. Those nuclei form the porous structures of the resulting membranes and can be analyzed by SEM for further insights into the phase separation process.

4.2.3 Porous structure of the membranes

Flat sheet membranes were produced with the polymer solutions of Section 4.2.1, and the morphology was analyzed with scanning electron microscopy. The membrane structure was divided into different layers as demonstrated in Figure 4.5 for a better comparison of the obtained membrane structures. Figure 4.6 shows the SEM images of the membranes fabricated with single solvents, and in Figure 4.7, the membranes fabricated with mixed solvents are displayed. Figure 4.8 shows the SEM images of the polymer-water surface.

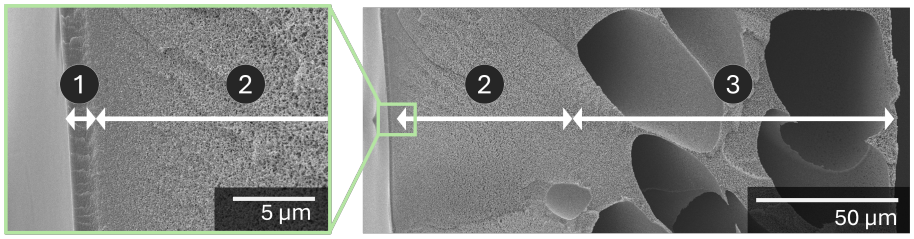


Figure 4.5: Representation of the location of layer 1, 2, and 3 in the FS membranes.

In the membranes fabricated from NMP and NBP, a 1.6- to 1.7 µm dense layer 1 was obtained at the polymer-water interface, with a sponge-like pore

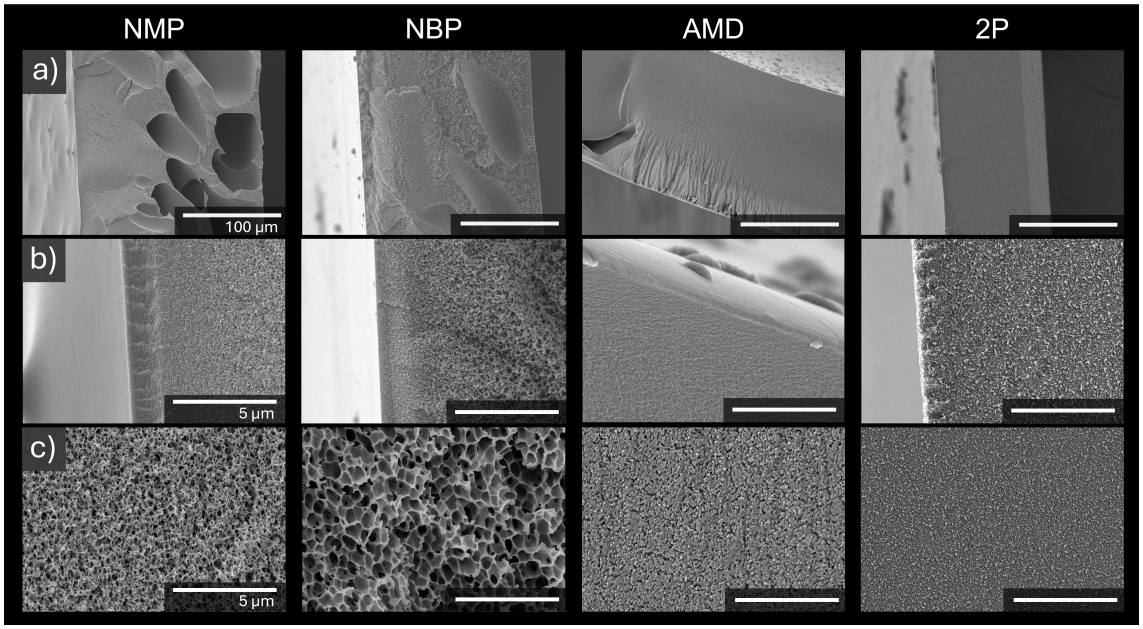


Figure 4.6: SEM images of membranes fabricated with different single solvents. a) Overview cross-section, b) zoom on layer 1, c) zoom on layer 3.

Table 4.6: SEM analysis of the surface porosity, median surface pore size including the quartile range (Q1-Q3), and thickness of layer 1 in the flat sheet membranes.

Membrane	median pore size (Q1-Q3) nm	porosity %	d (layer 1) µm
NMP	41 (33-52)	3.3	1.7
NBP	39 (31-47)	1.2	1.6
AMD	-	-	140
2P	-	-	82
NBP/AMD	34 (30-41)	0.6	6.5
NBP/2P	39 (34-46)	0.9	5
NBP/TEP	34 (29-40)	0.9	9

structure in layer 2 below, and macrovoids in layer 3. While the macrovoids in layer 3 of the NMP membrane are surrounded by a sponge-like pore structure, they are surrounded by closed, cellular pores in the NBP membrane. The size of the surface pores lies in a range of 31 to 52 nm, and the overall surface porosity was 3.3 % at the NMP and 1.2 % at the NBP membrane (see table 4.6). In the case of AMD and 2P, only one layer could be determined over the membrane cross-section. The AMD membrane contains a fine nodular network, whereas in the 2P membranes, no pores are visible (see Figure 4.8). Additionally, both membranes had no visible pores on their surfaces.

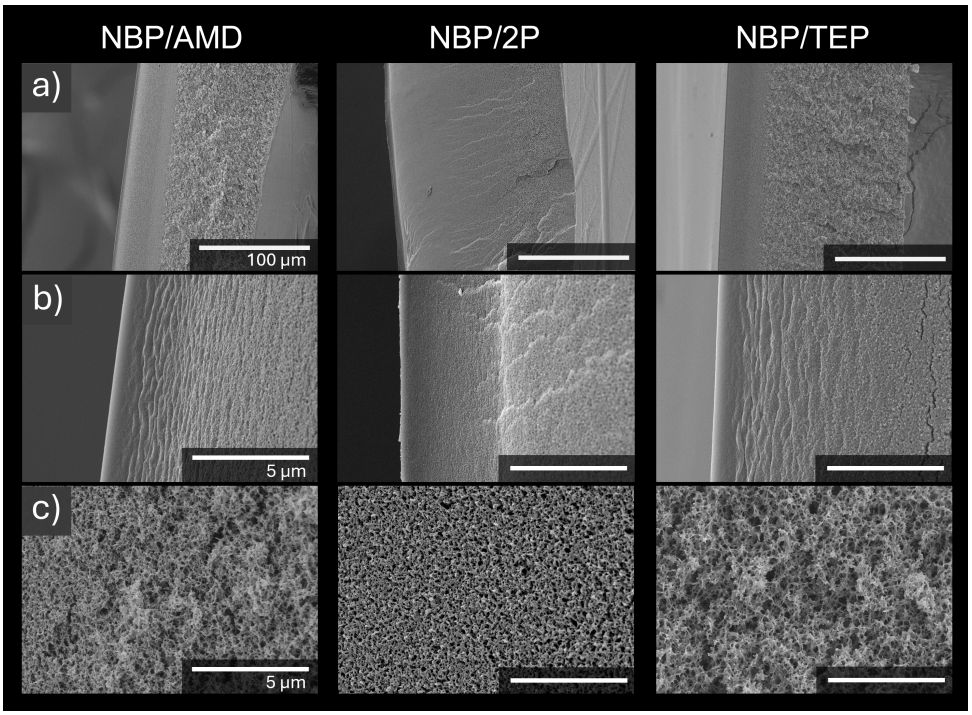


Figure 4.7: SEM images of membranes fabricated with different mixed solvents. a) Overview cross-section, b) zoom on layer 1, c) zoom on layer 3.

The mixed-solvent membranes have an altered structure compared to the pure AMD and 2P membranes. An asymmetric cross-section with three characteristic layers similar to the NBP membrane is obtained for the mixed-solvent membranes. Layer 1 was the thinnest in the NBP/2P membrane, measuring 5 µm, followed by the NBP/AMD membrane with a layer 1 thickness of 6.5 µm and the NBP/TEP membrane with 9 µm. In contrast to the NBP membranes, no macrovoids occur in any of the mixed-solvent membranes. Also, the cellular pore structure observed in layer 3 of the NBP membrane is replaced by a fully sponge-like morphology in all mixtures. The surface porosity is reduced compared to the NBP membrane from 1.6 % to 0.6 % for the NBP/AMD membrane and 0.9 % for the NBP/2P and NBP/TEP membranes. Additionally, the size of the surface pores in the NBP/AMD and NBP/TEP membranes is slightly reduced, ranging from 29 to 41 nm.

During membrane formation by phase inversion, the resulting morphology is critically linked to the kinetics of phase separation. Instantaneous demix-

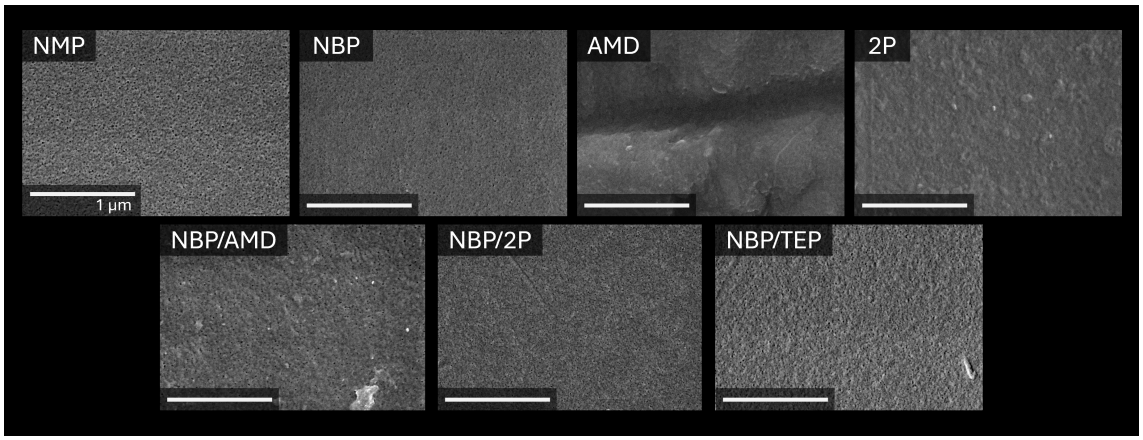


Figure 4.8: SEM images of the polymer-water interface of flat sheet membranes fabricated with single solvents (top) and solvent mixtures (bottom).

ing typically leads to the formation of a dense top layer and macrovoids in the sublayer [Smol1992; Reuv1987a; Chun2021]. Conversely, delayed demixing tends to yield symmetrical, sponge-like membrane structures, while the formation of macrovoids is often suppressed [Smol1992; Stra1975; Magg2022]. The mechanism of pore formation has been extensively discussed in the literature [McKe1996; Smol1992; Boom1992; Reuv1987b; Reuv1987a; Nune1996] and two different mechanisms have been proposed. The first is described by spinodal demixing (SD), and the second is commonly known as Nucleation and growth (NG). During the membrane formation, both mechanisms occur, but depending on the local kinetics, one dominates. Spinodal demixing occurs when the solution demixes in the thermodynamically unstable region, resulting in the formation of bi-continuous pore structures [Hung2016]. Nucleation and growth (NG) occurs when the solution demixes in the metastable region, resulting in the formation of small nuclei of polymer-lean phases[Smol1992; McKe1996]. It has been widely accepted that due to a faster mass transfer, SD is the dominant mechanism at the polymer-water interface. In the sublayer, the time in the metastable region is prolonged due to a slower mass transfer, enabling NG to occur [Su2017]. The final pore structure of the membrane is dependent on the growth and coalescence of the phase-separated domains to lower the interfacial energy between the two phases [Stra1971; Chun2021]. McKelvey & Koros [[McKe1996] stated

that pore formation is influenced by the local rate of solvent-non-solvent exchange and the speed of polymer-rich phase vitrification. If phase separation proceeds very slow, the polymer-rich phase vitrifies before pores interconnect, resulting in a closed-cell morphology. Conversely, rapid phase separation allows pore coalescence and the formation of a more open, sponge-like structure. When the solution enters the gel state without liquid-liquid demixing, dense structures form due to the low fluidity of the polymer-rich phase[Chun2021; Wijm1983].

The occurrence of macrovoids in layer 3 of the NMP and NBP membrane agrees with the previously observed instantaneous and fast phase separation 4.2.2. The observed closed-cellular pore structure in layer 3 of the NBP membrane results from vitrification of the solution before the pores connect. In the NMP solution, this is prohibited due to a faster exchange resulting from a significantly lower viscosity and a higher affinity to the non-solvent.

The symmetrical, dense morphology of the AMD and 2P membrane is in accordance with the significantly slower phase separation. Additionally, the solution's high tendency to gel due to the lower solvent power of AMD and 2P for PES results in denser structures. At positions further away from the interface, the J_{out}/J_{in} ratio is smaller due to a hindered solvent exchange, and liquid-liquid phase separation occurs. However, coarsening of the separated phases is limited due to the high viscosity of the solution. Additionally, the high affinity of the solvent to water facilitates a faster solvent-non-solvent exchange, which turns the polymer-rich phase into the gel phase and locks up the pore structure.

The reduced tendency to gel and lower viscosity in the solvent mixtures lead to a more open pore structure in layer 3. By mixing the solvents with NBP, the affinity to water is decreased, allowing the separated phases to coarsen more before entering the solid state. It was proven that adding a second solvent of lower solubility for PES to NBP diminishes the formation of finger-like marcovoids. Due to the slower phase separation, only sponge-like structures were observed in the membranes' cross-section.

4.2.4 Pure Water Permeance and Retention of flat sheet membranes

To evaluate the effect of the solvent type on the membrane performance, pure water permeance (PWP) and retention of PVP K15 (Mw = 9 kDa) were measured (see Figure 4.9).

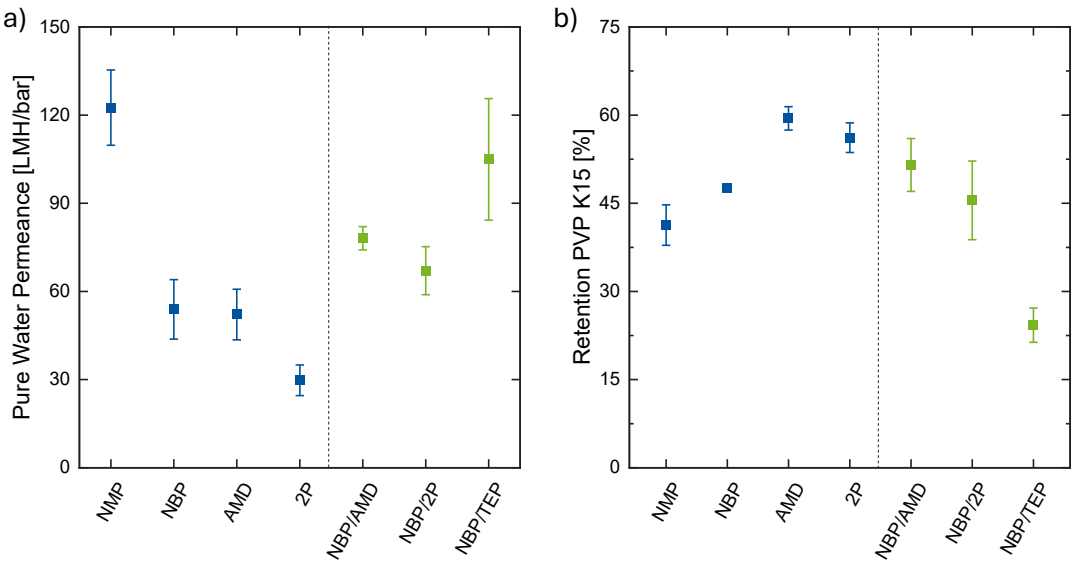


Figure 4.9: a) Pure water permeances (PWP) and b) Retention values of PVP K15 (0.2 wt% in water) of flat-sheet membranes fabricated from single vs. mixed solvents.

The highest PWP of 122 LMH/bar was observed for the membrane fabricated with NMP. The membranes fabricated with the less toxic solvents NBP and AMD reached only about 53 LMH/bar. The lowest PWP of 30 LMH/bar was obtained when using 2P as the solvent. A clear improvement was achieved when using solvent mixtures. The NBP/2P mixture led to an increase in PWP by 100 % compared to 2P. In the case of AMD, it was increased by 50 % when using the NBP/AMD mixture. The NBP/TEP membrane showed, with 105 LMH/bar, the highest permeance within the more sustainable membranes, nearly as high as the permeance of the NMP membrane. When comparing the filtration performance of the single solvent membranes, the AMD and 2P membranes had the highest retention for PVP K15 with 59 and 56 %, followed by the NBP membrane with 48 % and the NMP membrane with 41 % (see Figure 4.9 b). The

retention of the mixed-solvent membranes NBP/AMD and NBP/2P is lower than that of the AMD and 2P membranes, but similar to that of the NBP membrane within the error bars. The retention of the NBP/TEP membrane is 24 %, and therefore, significantly lower than that of the other membranes.

In membrane filtration, there is a trade-off between permeance and solute retention, as larger pores often lead to higher permeance but lower solute retention [Meht2005; Kana2010]. Furthermore, a higher connectivity between the pores lowers the resistance and increases the permeance of the membrane [Wang2011].

The significantly lower PWP of NBP compared to NMP is a results of the reduced number of macrovoids and the lack of interconnectivity of the pores within layer 3 (see Figure 4.6). The size of the surface pores in the NBP membrane is similar to that of the NMP membrane, but the overall surface porosity is only 1.2 %, therefore, the retention value for PVP K15 is slightly higher. Since the AMD and the 2P membrane only consist of one dense layer and have no visible pores via SEM on their surface, their permeance is low, and the retention value for PVP K15 is higher. In mixed-solvent membranes, the decreased thickness of layer 1 and the increased size and connectivity of the pores in layer 3 lead to an increase in PWP compared to single-solvent membranes.

4.2.5 Fabrication of hollow fiber membranes with solvent mixtures

The previous results showed that using the single, less toxic solvents NBP, AMD, 2P, and TEP for fabricating flat sheet membranes has individual disadvantages. The disadvantages can be overcome by mixing NBP with a respective second solvent, whereby precipitation speed, porous structure, and membrane filtration performance can be improved. In the following section, the suitability of using mixed solvent systems for spinning hollow fiber membranes was investigated. Additionally, the ratio of NBP to solvent B was varied to evaluate the influence on pore structure and filtration

performance.

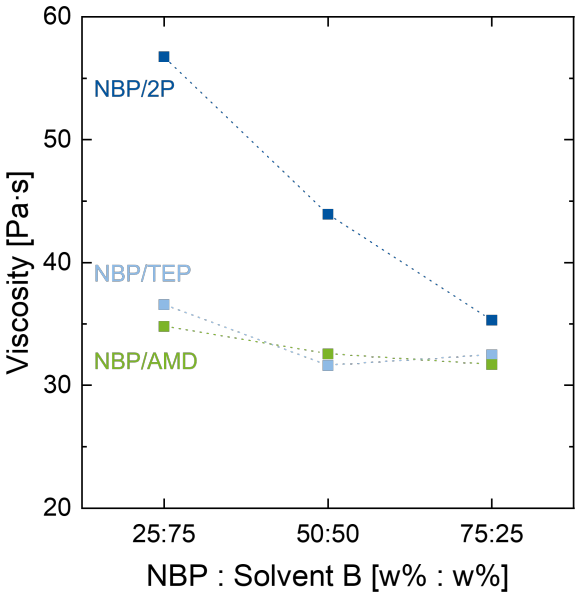


Figure 4.10: Viscosities of polymer solution fabricated with different ratios of solvents mixtures at 60 °C and a shear rate of 100 s^{-1}.

Depending on the solvent B, the viscosity of the solution changes significantly (see Figure 4.10). The NBP/2P solutions obtained the highest viscosity with 35 to 58 Pa · s, while the viscosity of the NBP/AMD and NBP/TEP solutions is in a range of 31 to 37 Pa · s. As the amount of NBP in the solutions increases, the viscosity decreases. Adding higher amounts of NBP to the mixture increases the affinity to PES according to the HSP (see Table 4.4) and, therefore, lowers the viscosity due to less entanglement of the polymer chains.

As shown in Section 4.2.2, at high NBP concentrations, the overall precipitation time increases. Therefore, during HF spinning lower pulling velocities are required for all solvent mixtures with increasing NBP concentration (see Table 4.2). At the same time, this ensured less mechanical stability during spinning and resulted in hollow fibers with a deformed geometry, as shown exemplarily for NBP/AMD in Figure 4.11. At a ratio of 75:25, none of the investigated systems was completely precipitated when collecting the fibers at the end of the spinning line. This effect was already observed in the flat

sheet experiments, where the higher NBP concentration in the solution reduces the mass transfer and solvent-nonsolvent exchange rate below the polymer-water interface (see Figure 4.4).

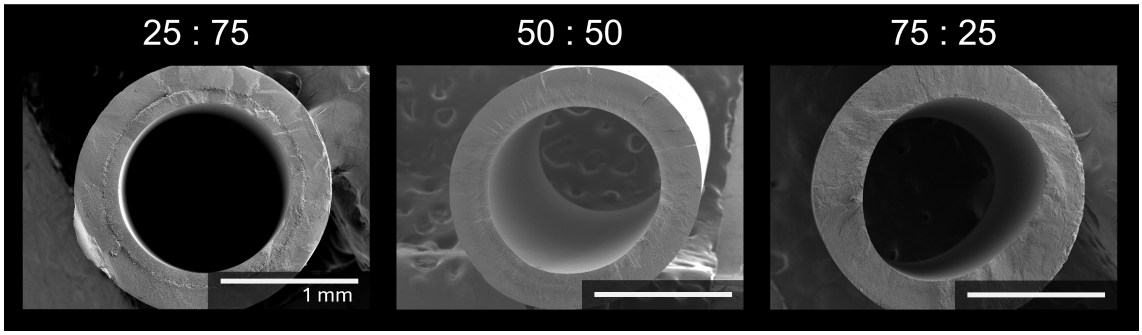


Figure 4.11: SEM images of the cross-section of NBP/AMD hollow fiber membranes spun from different solvent ratios.

To investigate the influence of the solvent ratio on the pore structure, SEM images of the cross-sections (see Figure 4.12) and the lumen surface (see Figure 4.13) were taken. In the cross-section of all three solvent systems, a transition from a sponge-like, interconnected pore structure at a ratio of 25:75 (NBP:Solvent B) to a closed, cellular pore structure at a ratio of 75:25 is observed (see Figure 4.12). A similar pore structure was already observed in layer 3 of the NBP flat sheet membranes (see Section 4.2.3). For the NBP/TEP membranes, this effect is more pronounced, as at a ratio of 50:50 NBP to TEP, the pores are already nearly entirely closed. When comparing the lumen side of the fibers, the NBP/TEP membrane differs significantly from the other membranes (see Figure 4.13). While the NBP/AMD and the NBP/2P membranes have a retentive layer with small, elongated pores, the pores on the lumen of the NBP/TEP membrane resemble a ripped network. The size of the NBP/TEP pores decreases with increasing NBP concentration, from around 1.25 µm to 0.2 µm, and a retentive layer similar to that of the other membranes is obtained. In the NBP/AMD and NBP/2P membranes an increased NBP concentration lead to a slight increase in pore size at the lumen surface by $\sim$ 0.07 µm.

Increasing NBP concentration in the polymer solution lowers the affinity to water and slows the solvent-non-solvent exchange rate. Therefore, the solution vitrifies before the pores can connect. The ripped pore structure of

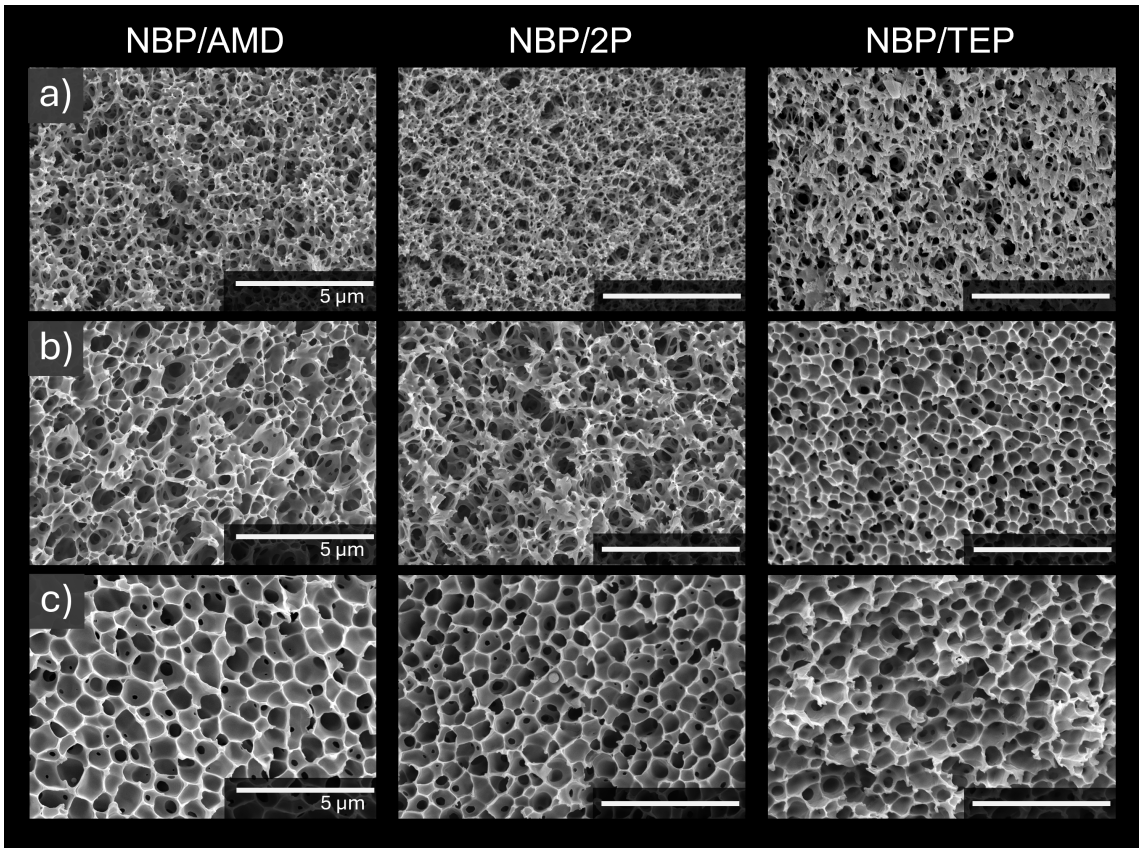


Figure 4.12: SEM images of the inner pore structure of hollow fiber membranes fabricated with a NBP : Solvent B ratio (w%:w%) of a) 25:75, b) 50:50, c) 75:25.

the NBP/TEP membrane results from the stretching of the precipitated layer during the spinning process [Dibr2022]. This effect is more pronounced in the mixtures with a high concentration of TEP because of the previously observed insufficient solvent power of TEP for PES, which leads to faster solidification.

When comparing the pure water permeance of the hollow fiber membranes, all systems show a decreased permeance with increased NBP concentrations (see Figure 4.14a). The decrease is again more pronounced in the NBP/TEP system, as the cellular pores at a 50:50 ratio result in a permeance decrease of 80 %. The permeance loss and the high retention are a results of the closed pore structure with increasing NBP concentration. The filtration performance for PVP K30 of the hollow fiber membranes is presented in Figure 4.14 b. The larger PVP K30 was chosen instead of the PVP K15 used for the FS membranes for better visualisation of the observed

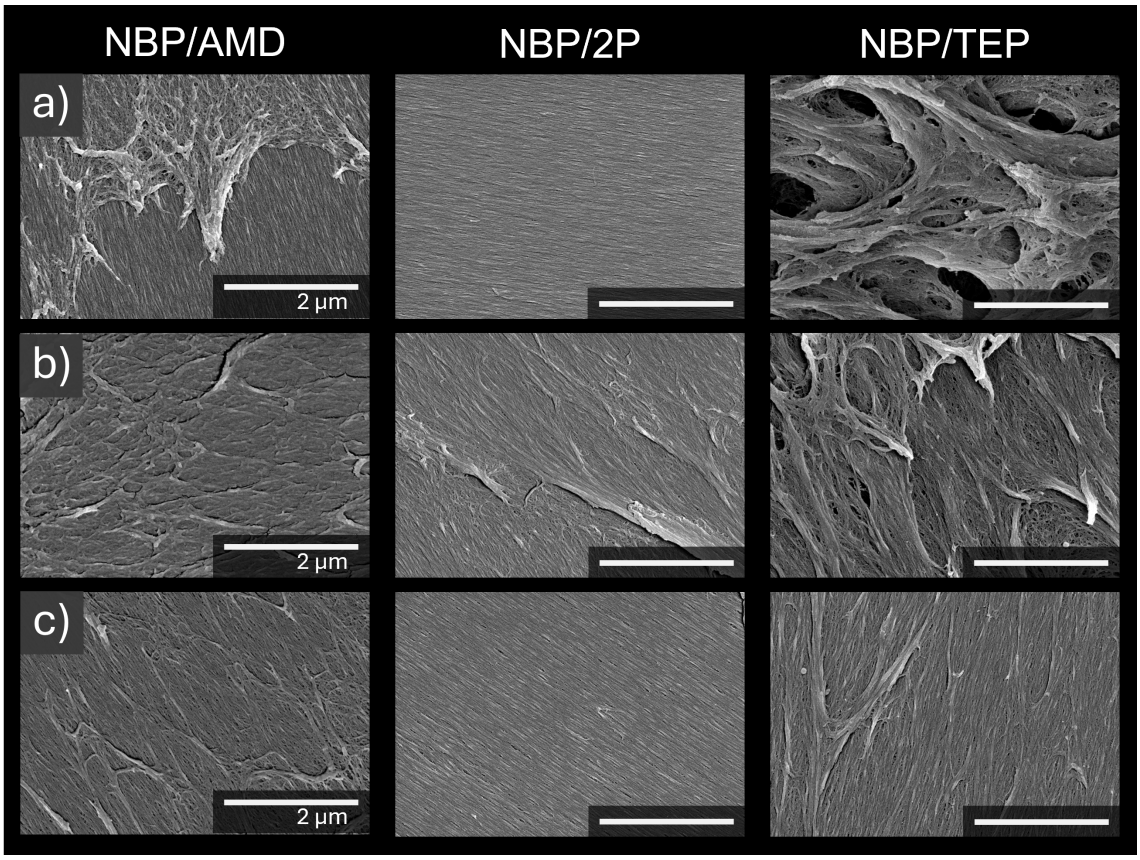


Figure 4.13: SEM images of the lumen surfaces of hollow fiber membranes fabricated with a NBP:Solvent B ratio (w%:w%) of a) 25:75, b) 50:50, c) 75:25.

trend. The results for PVP K15 retention measurements can be taken from table 4.7.

For the NBP/TEP, the retention value increases with decreasing permeance, which is in accordance with the decreasing pore size on the lumen side of the fiber. For the NBP/AMD and NBP/2P fibers, the opposite trend in retention of PVP is observed. With decreasing permeance, the retention also decreases due to the increased pore size in the retentive layer.

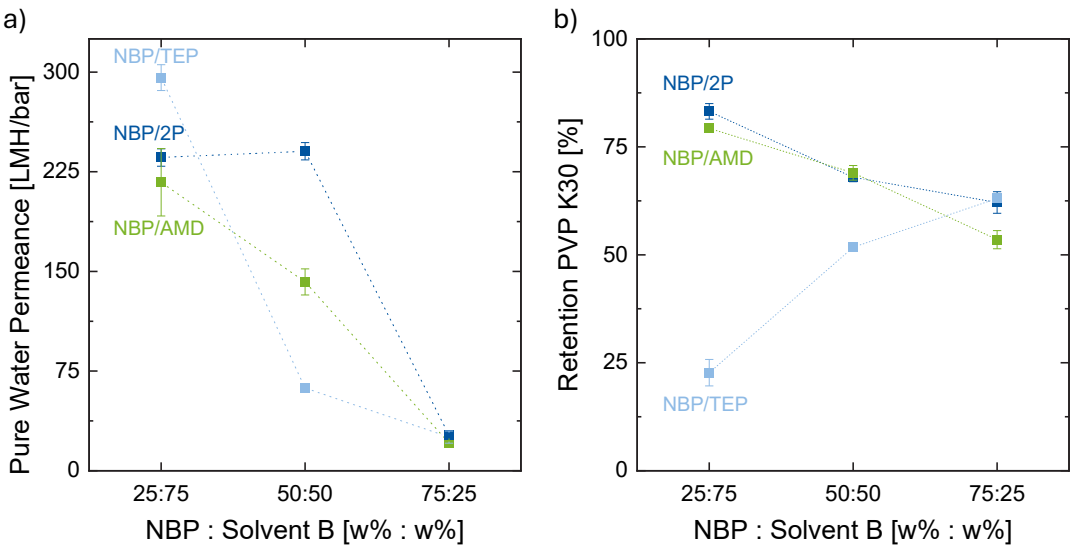


Figure 4.14: PWP and PVP K30 Retention comparison of mixed-solvent Hollow fiber membranes with different solvent ratios (NBP:AMD).

Table 4.7: PVP K15 retention values for hollow fiber membranes fabricated with different mixed-solvent systems in varying ratios.

Solvents	ratio w% : w%	Retention %
NBP/AMD	25:75	24.4 ± 8.5
NBP/AMD	50:50	9.9 ± 1.7
NBP/AMD	75:25	4.3 ± 1.6
NBP/2P	25:75	27.9 ± 3.3
NBP/2P	50:50	11.8 ± 2.5
NBP/2P	75:25	16.4 ± 0.9
NBP/TEP	25:75	0 ± 1.4
NBP/TEP	50:50	2.9 ± 0.8
NBP/TEP	75:25	9.1 ± 1.6

4.3 Conclusion

By systematically combining N-butyl-pyrrolidone (NBP) with the bio-based solvents Agnique® AMD 3L (AMD), 2-pyrrolidone (2P) or triethyl phosphate (TEP), it was demonstrated that mixed-solvent systems can offset the individual drawbacks of each solvent and deliver membranes whose formation kinetics, morphology, and performance rival or even surpass the state-of-the-art NMP systems. Mixing with NBP shifted the Hansen solubility distances toward better PES affinity, making TEP a suitable solvent for PES and accelerating liquid–liquid demixing, as evidenced by light-transmission measurements. Consequently, premature gelation is suppressed, and the formation of macrovoids, which is typical for single NBP solutions, is avoided. Instead, a fully sponge-like cross-sections with reduced dense-layer thicknesses as low as 1.7 µm for NBP/2P, and 8–10 µm for the NBP/AMD and NBP/TEP mixtures compared to over 80 µm for single 2P or AMD systems.

These structural changes translated directly into transport properties. Whereas single less toxic solvents delivered modest pure-water permeances of 30–53 LMH/bar, the NBP/2P and NBP/AMD mixtures increased permeance by 100 % and 50 %, respectively, or even approached the NMP benchmark (NBP/TEP) without sacrificing PVP retention.

Despite the literature showing that improvement of single AMD dope solutions for hollow fiber membrane fabrication is possible [Leop2025], this thesis focused on the positive effects of solvent mixtures and their use as an additional lever for the tuning of pore structures in hollow fiber membranes. All three solvent mixtures could be spun into defect-free hollow fiber membranes. By varying the NBP fraction from 25 % to 75 % the lumen pore size, cross-sectional pore-connectivity, and hence the permeance-retention trade-off were adjusted. The 25:75 NBP/Solvent B recipes produced highly interconnected sponge-like morphologies and the best overall balance of mechanical integrity, pure-water permeance (> 225 LMH/bar), and PVP-K30 rejection (>75 % for NBP/AMD and NBP/2P).

Overall, the study within this chapter confirms that carefully balanced,

less toxic solvent mixtures can overcome the disadvantages of individual solvents, providing a versatile toolbox for membrane engineers. They balance environmental compatibility and processability, allow precise control of phase transformation pathways, and lead to PES flat and hollow fiber membranes whose permeance and selectivity can be adjusted by simple solvent ratio adjustments. These findings pave the way for the industrial replacement of SVHC-class solvents and provide a quantitative framework, based on viscosity, Hansen parameters, and demixing kinetics, for the rational selection of solvents and the scale-up of sustainable hollow fiber membrane production. Based on the established mixed-solvent systems, the following chapters will focus on the influence of several process parameters to develop a broad portfolio of different membrane cut-offs.

5

Tuning the inner and outer coagulation in UF hollow fiber membrane spinning

Parts of this chapter are in preparation for publication:
Lea Greie, Lara E. Grünig, Kai Blechmann, Frederike Schiszler, Matthias Wessling
Influencing the inner and outer phase separation in mixed-solvent ultrafiltration hollow fiber membrane spinning

5.1 Introduction

In Chapter 4, it was demonstrated that sustainable solvent mixtures are an effective strategy for overcoming the limitations of the individual solvents. Mixing N-butyl-pyrrolidone (NBP) with Agnique® AMD 3L (AMD), 2-pyrrolidone (2P) or triethyl phosphate (TEP) alters the affinity between the solvent and the polymer, shifts the demixing kinetics, and prevents premature gelation. This enables the continuous spinning of defect-free PES hollow fibers. Tuning the NBP:Solvent B ratio adjusts pore connectivity and the permeance–retention balance, providing a sustainable platform for membrane design and a path towards industrially relevant performance.

Although adjusting the solvent ratio in the dope solution was effective within a limited PWP and cut-off range, industrial applications require a broader process window of ultrafiltration (UF) membranes to deliver the diverse permeabilities and molecular weight cut-offs demanded by different processes[Meli2007]. For example, in biopharmaceutical processes, UF membranes enable size-based separation of biomolecules. They retain high-molecular-weight species like proteins, viruses, and aggregates, while allowing smaller molecules like salts, solvents, and water to permeate. This is essential for concentration, buffer exchange, and impurity removal [Tutu1983; Ma2024]. UF is also used in clarification steps, for depyrogenation, and sometimes to assist in virus removal or reduction, depending on the membrane cut-off. Their performance depends heavily on membrane material, molecular weight cut-off, operating mode, and fouling behaviour, which must be optimized to ensure yield, purity and scalability of the process [Tutu1983; Ma2024]. The fabrication of hollow fiber membrane via dry-jet wet spinning offers several possibilities to tune the final structure, and therefore, the cut-off of the membrane. It involves a complex membrane formation process, as phase separation is initiated on both the lumen and shell sides [Bake2023]. Therefore, in addition to the solvent ratio, process parameters that directly affect inner and outer coagulation must be systematically investigated.

Previous studies have demonstrated that both the inner and outer fiber

morphology have a strong influence on morphology and transport, particularly when more sustainable solvents are used. Ursino *et al.* [Ursi2020] altered the bore fluid composition in PES hollow fiber spinning with the sustainable solvent PolarClean®. By using mixtures of water and solvent at different concentrations, they were able to adjust the lumen-skin density and affect the PWP. A recent DoE study by Leopold *et al.* [Leop2025] on PES hollow fibre spinning using the more sustainable solvent N,N-dimethyl lactamide (Agnique® AMD 3L) shows that, while the type and concentration of the bore solution have a weak main effect, they become significant in two-factor terms through interaction with the dope solution. In contrast, the study of Bang *et al.* [Bang2020] with the commonly used toxic solvent N-methylpyrrolidone showed a significant influence of the bore solution composition on the membrane characteristics. They used mixtures of water with the solvent NMP, ethylene glycol, or glycerol as a bore fluid to change the filtration characteristics of polysulfone UF membranes. By mixing the strong non-solvent water with a weaker one, the demixing process is slowed, allowing larger pores to develop. With a 50% NMP/water solution as a bore fluid, they produced membranes with a bovine serum albumin rejection rate of more than 97% and a pure water permeance of 167 LMH/bar. These studies emphasises the importance of understanding the interplay between the dope and bore solution compositions during NIPS and indicate the need for targeted studies on bore-fluid compositions when introducing new dope systems, such as those using mixed solvents. The phase separation on the shell side of the fibers can be mainly influenced by the conditions in the coagulation bath [Chun2021; Bake2023]. On the one hand, solvent additives can also influence the coagulation at the outside [Hack2024]. On the other hand, the coagulation can be influenced by varying the temperature of the coagulation bath. Peng et al. [Peng2010] found that small increases in coagulation bath temperature can substantially accelerate solvent/non-solvent exchange, enlarging pores and porosity, and thus increasing permeance. However, sensitive adjustment of inner and outer kinetics is essential to avoid structural stress that may result in delamination.

In this chapter, the hypothesis that (i) using weak (AMD, 2P, TEP) or

strong solvents (NBP) in the bore fluid, at controlled loadings (30–70 wt%), and (ii) increasing the external coagulation-bath temperature (30–50 °C) systematically accelerates phase separation at the lumen and/or shell interfaces in mixed-solvent PES dopes (NBP/AMD, NBP/2P, NBP/TEP) is investigated. This experimental design explicitly explores whether these convenient, well-known strategies for influencing phase separation kinetics can be applied to more complex solvent mixture systems, which is crucial for determining the scalability of the process. It is further hypothesized that these kinetic shifts tune the pore geometry and place the selective layer predominantly on the shell side, increasing PWP with only a moderate loss in PVP retention.

This study extends beyond solvent-ratio optimization, demonstrating how pore geometry and performance in mixed-solvent PES hollow fiber membranes can be tuned by adjusting the bore-solution composition and coagulation bath temperature. It provides practical recipes and mechanistic insight for translating sustainable solvent systems into robust membranes, relevant for biopharmaceutical processes.

5.2 Methods

5.2.1 Dope Solution Fabrication

All components were combined in a heated vessel and stirred at 60 °C until a homogeneous solution was obtained. Before the fabrication of either flatsheet (FS) or hollow fiber (HF) membranes, the solution was degassed. The exact compositions of all polymer solutions are given in Table 5.1.

Table 5.1: Composition of the polymer solutions for hollow fiber (HF) membrane fabrication.

Code	PES [wt%]	PVP K17 [wt%]	NBP [wt%]	AMD [wt%]	2P [wt%]	TEP [wt%]	Water [wt%]
NBP/AMD	18	25	13.75	41.25	-	-	2
NBP/2P	18	25	13.75	-	41.25	-	2
NBP/TEP	18	25	13.75	-	-	41.25	2

5.2.2 Hollow fiber spinning

The Hollow fiber membranes were produced via the procedure described in Section 3.2.4. Within this chapter, the air gap distance was set to 20 cm. The dope temperature was kept at 40 °C and the coagulation bath temperature was varied between 30 to 50 °C. The bore solution was composed of varied amounts of solvent (x = 30, 50, 70 wt%), glycerol (25 wt%), and water (75-x wt%) and is named according to the pattern "solvent concentration - solvent type " (exp. 30% NBP). For a comparison between the individual spinning parameters, the draw ratio was calculated as

$$\text{Draw ratio} = \frac{v_{\text{take-up}}}{(\text{Dope flow}/\ A_{nozzle})} \tag{5.1}$$

were A_{nozzle} = 1.24 mm^2 is the dope extrusion area of the spinning nozzle.

Table 5.2 summarizes the spinning parameters used for the production of the hollow fiber membranes.

Table 5.2: Spinning parameters for the hollow fiber membrane fabrication.

Dope	Bore	Temperature °C	Dope flow [mL/min]	Bore flow [mL/min]	$v_{\text{take-up}}$ [m/min]	Draw ratio
NBP/AMD	30% NBP	30	3.8	3.8	3.8	1.2
NBP/AMD	50% NBP	30	3.7	3.5	3.9	1.3
NBP/AMD	30% AMD	30	3.7	3.5	2.7	0.9
NBP/AMD	50% AMD	30	3.8	3.6	4.1	1.3
NBP/AMD	70% AMD	30	4.4	4.1	8.2	2.3
NBP/AMD	50% AMD	40	3.8	3.4	3.9	1.3
NBP/AMD	50% AMD	50	3.8	3.4	3.8	1.2
NBP/2P	30% NBP	30	3.6	3.5	3.0	1.0
NBP/2P	50% NBP	30	3.5	3.2	3.3	1.2
NBP/2P	70% NBP	30	5.7	3.0	10.9	2.4
NBP/2P	30% 2P	30	3.5	3.1	1.9	0.7
NBP/2P	50% 2P	30	3.6	3.3	2.7	0.9
NBP/2P	70% 2P	30	5.7	4.6	8.2	1.8
NBP/2P	50% 2P	40	3.5	3.3	3.0	1.1
NBP/2P	50% 2P	50	3.5	3.3	2.7	1.0
NBP/TEP	30% NBP	30	3.8	3.5	3.5	1.1
NBP/TEP	50% NBP	30	3.9	3.4	3.5	1.1
NBP/TEP	70% NBP	30	5.7	4.6	12.5	2.7
NBP/TEP	30% TEP	30	3.7	3.4	3.5	1.2
NBP/TEP	50% TEP	30	3.8	3.5	3.5	1.1
NBP/TEP	70% TEP	30	5.7	4.6	6.8	1.5
NBP/TEP	50% TEP	40	3.7	3.4	3.5	1.2
NBP/TEP	50% TEP	50	3.7	3.5	3.5	1.2

5.3 Results and Discussion

5.3.1 Phase Separation Kinetics

Light transmission experiments were conducted to gain quick insights into the influence of varying coagulation conditions on the phase separation kinetics of mixed-solvent polymer solutions. Therefore, different coagulation bath compositions containing either Solvent B/water/glycerol or NBP/water/glycerol mixtures are investigated. The resulting light transmittance curves within the first 50 s are shown in Figure 5.1: panels a), c), and e) present results for Solvent B coagulation bath compositions, while panels b), d), and f) correspond to NBP-based coagulation baths. The onset of light intensity decrease t_1 is summarized in Table 5.3 for each system.

Table 5.3: List of phase separation onsets of different dope solutions in varying coagulation bath compositions.

Dope	Bore	t_1 [s]
NBP/AMD	100% H2O	0.0
NBP/AMD	30% NBP	2.5 ± 0.2
NBP/AMD	50% NBP	2.8 ± 0.2
NBP/AMD	70% NBP	10.9 ± 1.2
NBP/AMD	30% AMD	0.0
NBP/AMD	50% AMD	0.0
NBP/AMD	70% AMD	0.0
NBP/2P	100% H2O	4.8 ± 0.3
NBP/2P	30% NBP	5.1 ± 0.7
NBP/2P	50% NBP	4.7 ± 1.3
NBP/2P	70% NBP	19.5 ± 0.9
NBP/2P	30% 2P	2.0 ± 0.2
NBP/2P	50% 2P	2.1 ± 0.4
NBP/2P	70% 2P	17.2 ± 3.0
NBP/TEP	100% H2O	0.0
NBP/TEP	30% NBP	0.0
NBP/TEP	50% NBP	0.0
NBP/TEP	70% NBP	0.0
NBP/TEP	30% TEP	0.0
NBP/TEP	50% TEP	0.0
NBP/TEP	70% TEP	9.2 ± 0.9

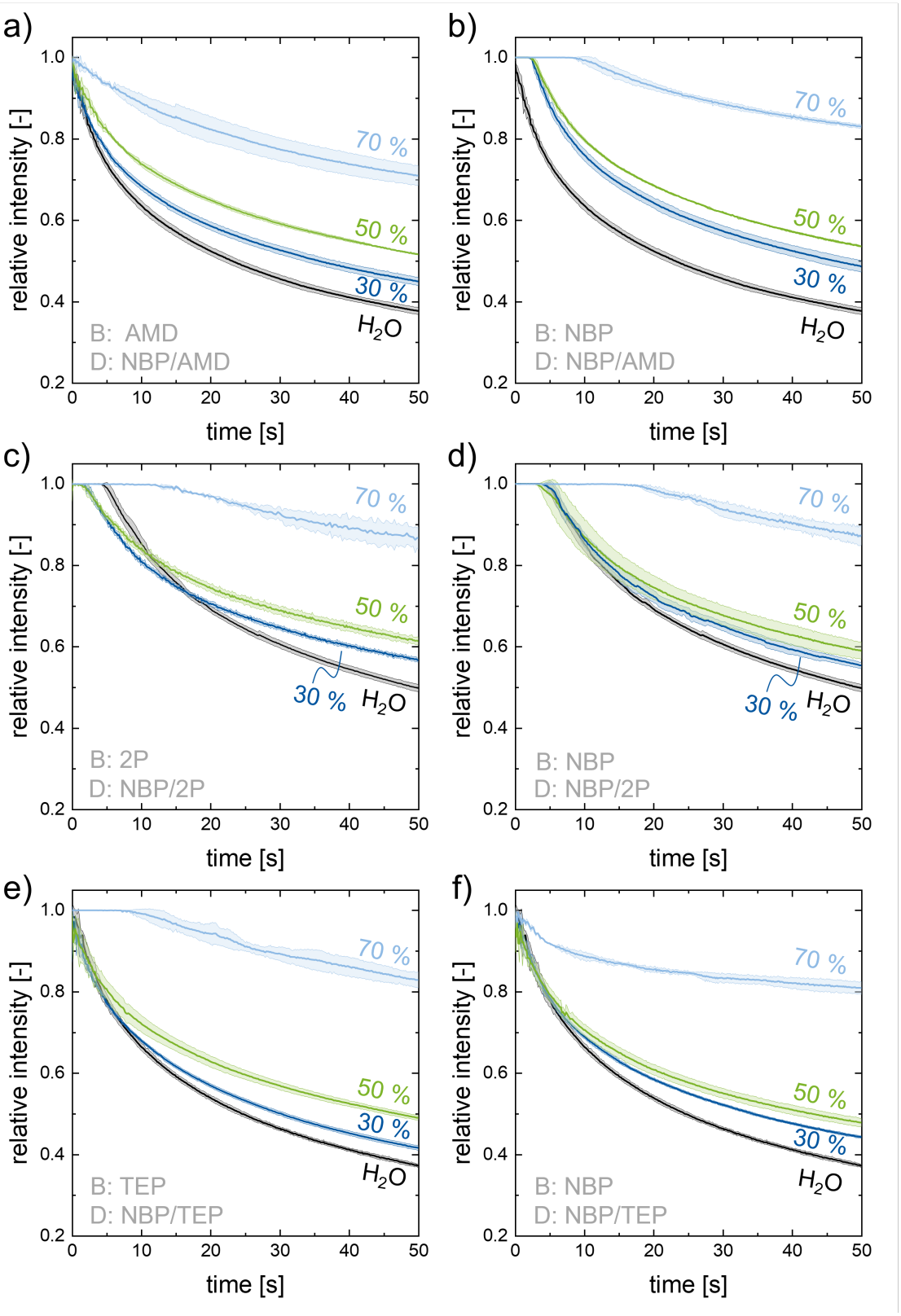


Figure 5.1: Light transmittance curves of mixed-solvent dopes (D) coagulated in coagulation baths with different concentrations of solvent additives (B), compared to a coagulation bath containing pure H_2O.

In all systems, a decrease in light intensity over time is observed, indicating the occurrence of phase separation. Increasing the solvent concentration in the coagulation bath slows down this process compared to coagulation in pure water. The onset of phase separation varies and is listed in Table 5.3 for each specific system.

In the NBP/AMD solution coagulated in AMD-containing baths, phase separation occurs instantaneously across all AMD concentrations (Figure 5.1 a). Replacing AMD with NBP introduces a delay in onset: 2.5 s at 30 %, 2.8 s at 50 % NBP, and $\sim$ 11 s at 70 % NBP (Figure 5.1 b).

For the NBP/2P system, phase separation is already delayed by 4.8 s in pure water. With 30 % and 50 % 2P in the coagulation bath, this delay shortens to approximately 2 s. However, at 70 % 2P, a significant delay of 17.2 $\pm$ 3 s is observed (Figure 5.1 c). Substituting 2P with NBP again extends the delay to approximately 5 s at 30 % and 50 %, and $\sim$ 20 s at 70 %. (Figure 5.1 d).

In the NBP/TEP system, adding 30 % or 50 % TEP to the coagulation bath results in an immediate onset of phase separation, similar to pure water (Figure 5.1 e). At these concentrations, substituting TEP with NBP does not significantly alter the phase separation kinetics (Figure 5.1 f). However, at 70 % TEP, a 9 s delay is observed—an effect not seen in the equivalent NBP-based coagulation bath.

Overall, phase separation becomes progressively slower with increasing solvent concentration across all three systems. Nonetheless, the shift from 30 % to 50 % solvent induces only modest kinetic changes, whereas the increase to 70 % causes a more pronounced effect.

As described by Wijmans *et al.* [Wijm1983], the delay in phase separation arises from complex diffusion processes at the moment of immersion. Solvent tends to accumulate at the polymer–coagulant interface, reducing the influx of non-solvent [Wijm1983; Smol1992]. This effect is more prominent when the solvent exhibits a high affinity for the polymer. A prolonged delay allows more time for coarsening of polymer-lean nuclei, ultimately resulting in larger pore structures. They also noted that above a critical solvent

concentration, phase separation may not occur at all, and instead, the polymer dissolves slowly into the coagulation bath. Additionally, the viscosity of the polymer solution affects diffusion dynamics. Higher viscosity impedes non-solvent influx, further delaying phase separation.

Table 5.4: HSP distances of the solvents to various components.

Compound	$\delta_{s\text{-PES}}$ ($MPa^{1/2}$)	$\delta_{s\text{-}PVP}$ ($MPa^{1/2}$)	$\delta_{s\text{-}H_2O}$ ($MPa^{1/2}$)	$\delta_{s\text{-}gly}$ ($MPa^{1/2}$)	$\delta_{s\text{-}NBP}$ ($MPa^{1/2}$)
NBP	2.9	16.6	37.3	23.7	0
AMD	8.5	6.6	26.7	13.5	11.1
2P	8.1	12.0	31.3	18.9	10.9
TEP	2.0	13.2	33.4	20.1	4.7

The three investigated polymer solutions differed in their viscosity. The NBP/AMD solution exhibited the lowest initial viscosity (34.8 Pa·s), followed by NBP/TEP (36.5 Pa·s) and NBP/2P (38 Pa·s). The NBP/2P solution, which has the highest viscosity among the three, also exhibits the longest phase separation delay. The affinity of the solvent for PES, which is quantified by the Hansen Solubility Parameter (HSP) distance $\delta_{s\text{-PES}}$, plays a key role in determining its accumulation behavior. Lower $\delta_{s\text{-PES}}$ values indicate stronger interactions. Among the solvents studied, AMD and 2P have relatively low affinity for PES (higher HSP distance), while NBP and TEP show significantly higher affinity (see Table 5.4). Consequently, NBP and TEP tend to accumulate more at the film–bath interface, hindering non-solvent influx and delaying phase separation.

With increasing solvent concentration, the accumulation is also increased, enhancing the barrier effect. Additionally, NBP and TEP have lower affinity for water and glycerol, exacerbating this slowdown. In contrast, AMD and 2P, being more miscible with water and glycerol, form weaker barriers, resulting in shorter delays in demixing. However, while this approach explains the observed phase separation delays of the NBP/AMD and NBP/2P solutions, it contradicts the fact that the NBP/TEP solution only shows a delay in a 70 % TEP coagulation bath.

The solvent concentration required to induce a delay depends not only on affinity to the polymer but also on interactions within the dope solution. For

instance, TEP has a higher affinity for NBP than AMD or 2P, enhancing its miscibility and solvent efflux. This may explain why the NBP/TEP system exhibits rapid precipitation despite TEP's higher affinity for PES. Furthermore, in the previous chapter, it was shown that TEP lacks sufficient solvent power to dissolve PES in the present concentrations (see Chapter 4 Figure 4.1), consequently lowering the thermodynamic stability of the mixed-solvent system. This promotes faster phase separation, which requires high TEP concentrations (< 70 %) in the coagulation bath to be delayed.

In summary, the differences in phase separation kinetics can be attributed to variations in solvent–polymer and solvent–non-solvent affinities. AMD and 2P, with their lower affinity to PES and higher miscibility with water/glycerol, allow for quicker non-solvent influx and faster demixing. NBP and TEP, in contrast, accumulate more readily at the interface, creating a stronger barrier and delaying phase separation. Interestingly, despite TEP's favorable miscibility, its poor solvency for PES shifts the system toward rapid precipitation under certain conditions.

The light transmission experiments confirm that higher solvent concentrations in the coagulation bath slow down phase separation, most notably in systems that were coagulated in mixtures containing NBP. Literature suggests that such delays enable prolonged growth and coalescence of polymer-lean nuclei [Wijm1983]. In the following sections, it will be investigated how the slowed phase separation influences the performance and morphology of hollow fiber membranes. Since Solvents B and NBP altered the phase separation kinetics differently, both solvent types will be investigated in the following as a bore fluid additive.

5.3.2 Influence of Solvent Additives in the Bore Fluid

Hollow fiber membranes were spun from the mixed solvent systems NBP/AMD, NBP/2P, and NBP/TEP using three different concentrations of the respective Solvent B (AMD, 2P or TEP) or NBP in the bore fluid to evaluate how the solvent additive influences lumen-side phase separation and, therefore, membrane morphology and performance.

The three dope solutions differ in their initial viscosity, which increased during phase separation until solidification occurred. Among them, the NBP/AMD solution exhibited the lowest initial viscosity (34.8 Pa·s), followed by NBP/TEP (36.5 Pa·s) and NBP/2P (38 Pa·s). When the solvent concentration in the bore fluid was increased during spinning, phase separation on the lumen side was slowed during the residence time in the air gap, resulting in a slower increase in viscosity. To maintain a comparable fiber geometry across the different systems, the draw ratio had to be adjusted individually for each system (see table 5.2). Yet the pulling speed was limited by the mechanical stability of the fibers and could only be increased to the point just before fiber breakage. However, with 70 wt% of Solvent B in the bore solution, the obtained fibers had a significantly thinner wall thickness of 150-180 µm, marking an unfavoured process point as thinner fiber walls tend to decrease the mechanical stability [Zhan2014]. When spinning with 70 % NBP in the bore fluid, the precipitation occurred significantly slower than with Solvent B, as already observed in the light transmission measurements (see section 5.3.1). As a result, significantly higher draw ratios were required (see Table 5.2 and for the NBP/AMD system, no hollow fiber membranes could be spun in a stable process with 70 wt% NBP in the bore.

Membrane Performance

To investigate how the different bore fluid compositions influence the membrane performance, pure water permeance (PWP) and retention measurements with PVP K30 were conducted and summarized in Figure 5.2 for Solvent B containing bore solutions and in Figure 5.3 for the equivalent NBP bore soltuion.

All three systems exhibit an increase in PWP as the concentration of Solvent B in the bore solution increases from 30 % to 50 % and 70 % (see Figure 5.2 a)). The highest relative increase is observed in the NBP/AMD fibers, where the PWP rises by 68 %, from 250 to 420 LMH/bar. Among all systems, the NBP/2P fibers show the lowest PWP, increasing from 155 LMH/bar at 30 % 2P to 235 LMH/bar at 70 % 2P. In contrast, the NBP/TEP system achieves the highest absolute PWP values, starting at

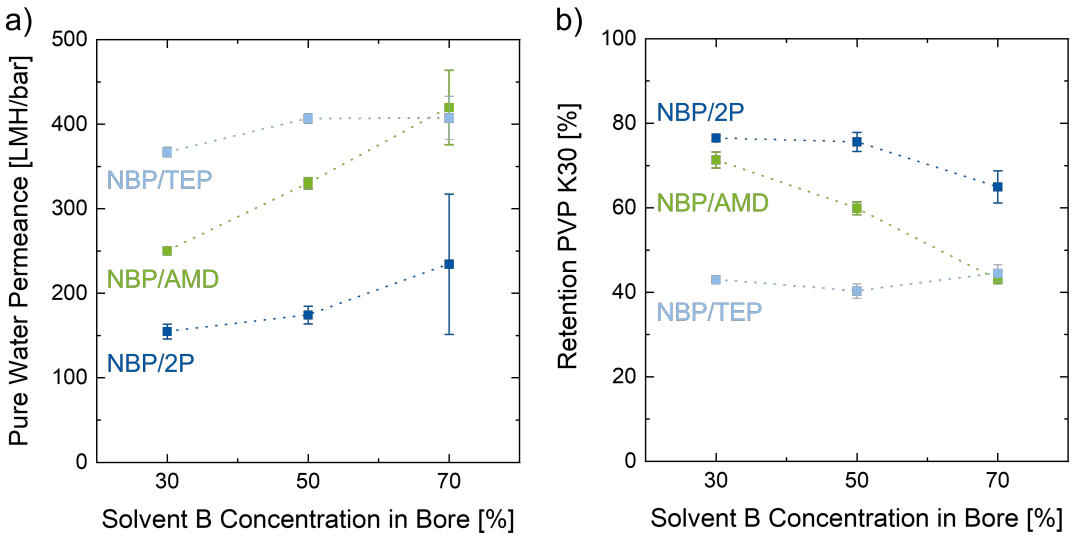


Figure 5.2: PWP (a) and retention (b) of mixed-solvent hollow fiber membranes fabricated with different concentrations of the respective Solvent B (AMD/2P/TEP) in the bore solution at a coagulation bath temperature of 30 °C.

367 LMH/bar with 30 % TEP and rising to 407 LMH/bar at 70 % TEP. This modest increase by 11 % indicates a lower response to solvent concentration than in the other systems. As shown in Figure 5.2 b), an increase in PWP is generally accompanied by a reduction in PVP K30 retention. For the NBP/AMD system, increasing the bore Solvent B concentration from 30 % to 70 % results in a retention drop from 71 % to 43 %. In contrast, the NBP/2P and NBP/TEP systems exhibit minimal changes in retention between 30 % and 50 % solvent concentration. At 70 %, the NBP/TEP fibers show a modest 4 % increase in retention, whereas the NBP/2P fibers experience a 10 % decline.

When substituting the respective Solvent B in the bore solution with NBP, only minor changes in the PWP are observed (see Figure 5.3). The NBP/AMD fibers spun with 30 % and 50 % NBP in the bore show no significant difference in PWP compared to those spun with AMD in the bore solution. In the NBP/TEP system, the PWP is approximately 40 LMH/bar lower when NBP replaces TEP in the bore fluid. The trend of increased PWP with higher solvent concentration (30 to 50 %) remains observable in both cases. For NBP/2P, this influence is more pronounced: increasing NBP from 30 % to 50 % leads to a 50 LMH/bar increase in PWP, compared

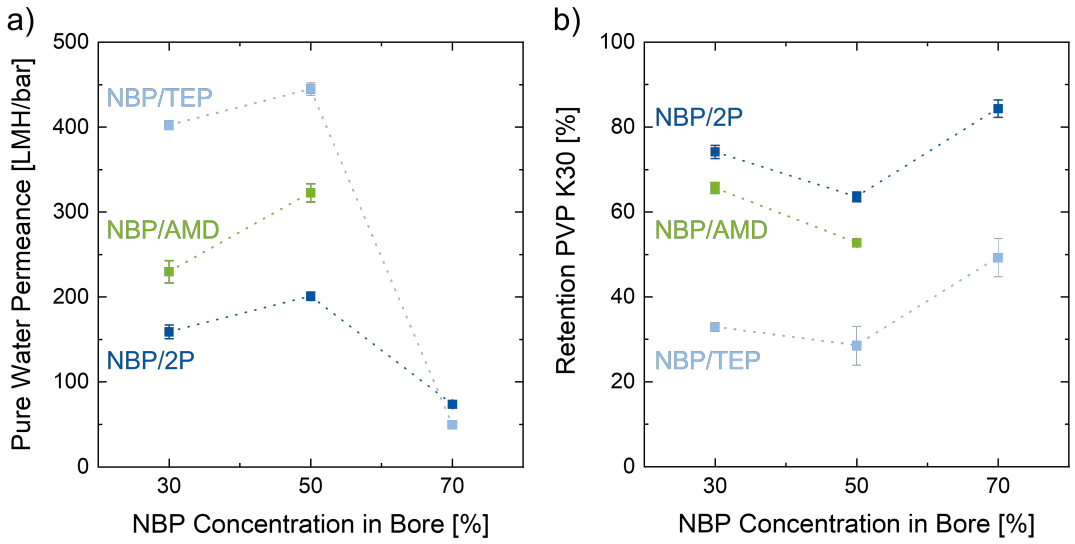


Figure 5.3: PWP (a) and PVP K30 retention (b) of mixed-solvent hollow fiber membranes fabricated with different concentrations of NBP in the bore solution at 30 °C coagulation bath.

to only 25 LMH/bar when using 2P. However, at 70 % NBP, a dramatic decrease in PWP by 89 % for the NBP/TEP fibers and 63 % for the NBP/2P fibers is observed.

Retention measurements for PVP K30, shown in Figure 5.3 b), reveal that retention is generally lower when NBP is used in the bore compared to the respective Solvent B. At 30 % NBP, the retention rates for NBP/AMD and NBP/TEP are 5 % and 10 % lower, respectively. Nonetheless, the increase in retention when raising the NBP concentration from 30 % to 50 % is similar to that observed with Solvent B. In the NBP/2P system, while retention remained constant with 2P concentration rising from 30 % to 50 %, a 10 % decrease is observed when NBP is used instead. Interestingly, at 70 % NBP, the retention increases by 20 % for both NBP/2P and NBP/TEP fibers.

A delayed phase separation due to the higher solvent concentration in the bore fluid leads to a prolonged growing phase of the polymer-lean nuclei [Wijm1983; Bang2020]. As a result, nuclei can coalesce, and the resulting membrane structures are more open and interconnected. Increased porosity and pore size reduce hydraulic resistance of membranes, thereby enhancing PWP while simultaneously lowering solute retention

[Xu2020]. However, exceeding a critical solvent concentration in the coagulant can prevent phase separation, leading instead to polymer dissolution [Wijm1983]. In addition, the polymer-extrusion to pulling-speed ratio has a significant impact on pore structure and, consequently, membrane performance. If pulling speed cannot be sufficiently increased, the resulting low stress on the lumen surface inhibits the formation of the typical elongated pore structure [Dibr2022]. This phenomenon is evident in fibers spun with 70 % NBP in the bore. Although higher solvent concentration typically increases PWP by reducing hydraulic resistance and decreasing retention, this trend breaks at 70 % NBP. For NBP/2P and NBP/TEP fibers, pulling speed could not be increased beyond the critical threshold without fiber breakage. As a result, insufficient stress was applied to form elongated pores, which is confirmed by the SEM images in Figure 5.4. The observed nodular structures on the lumen side also indicate that instead of liquid-liquid phase separation, dissolution of PES in the bore solution was dominant during the spinning. The resulting fibers exhibited significantly lower PWP.

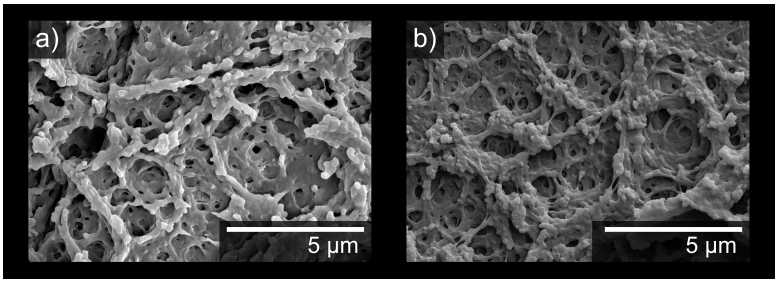


Figure 5.4: SEM images of the lumen surface of (a) NBP/2P and (b) NBP/TEP fibers spun with 70 % NBP in the bore solution.

The generally observed improvement of the PWP with increasing solvent concentration in the bore fits the trends observed in literature [Bang2020]. However, to further confirm the proposed connection between higher and decreased retention to a more open pore structure, the lumen side was investigated with SEM.

Membrane Morphology

SEM images were taken to examine the influence of solvent concentration in the bore fluid on pore morphology. As the spinning process with high NBP concentrations was not stable, but the performance was similar to that spun with solvent B in the bore, only the latter will be examined with SEM. Figure 5.5 shows the lumen side of hollow fibers fabricated with different concentrations of the respective Solvent B in the bore fluid, while the median pore sizes and surface porosities are listed in Table 5.5.

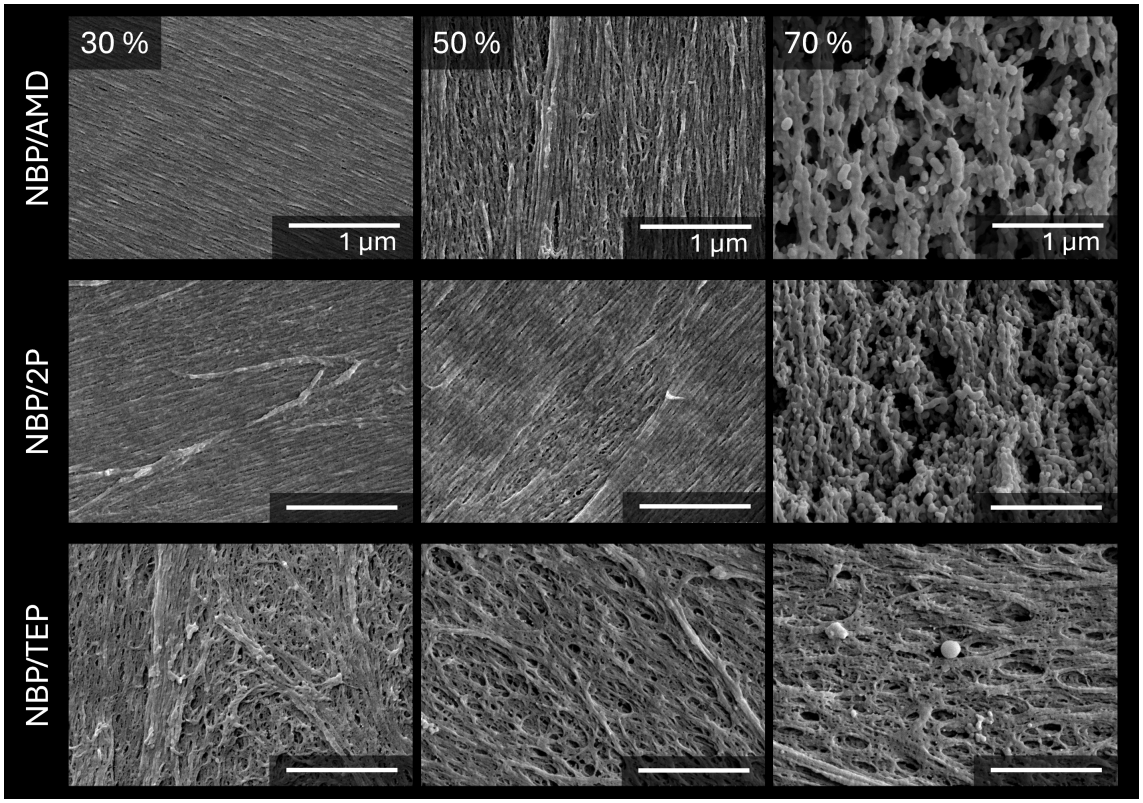


Figure 5.5: SEM images of the lumen side of mixed-solvent hollow fiber membranes fabricated with different concentrations of the respective Solvent B (AMD/2P/TEP) in the bore fluid at 30 °C coagulation bath.

At 30 % Solvent B in the bore solution, the NBP/AMD and NBP/2P fibers exhibit regular lumen surfaces, with surface porosities of 1.6 % and 1.3 %, respectively, and a median pore size of approximately 50 nm (see Table 5.5). The pores display a uniform, elongated shape. In contrast, the NBP/TEP fibers exhibit a more irregular lumen surface, with a higher surface porosity of 4.1 % and a median pore size of 60 nm. The retentive layer appears

Table 5.5: Median pore size including the quartile range (Q1-Q3) and porosity of the lumen of mixed-solvent hollow fibers spun with the respective solvent B in the bore solution.

Solvent	Concentration wt%	Median pore size (Q1–Q3) nm	Porosity %
NBP/AMD	30	51 (41–72)	1.6
	50	63 (46–101)	4.9
	70	143 (68–324)	37.1
NBP/2P	30	49 (39–67)	1.3
	50	41 (31–58)	0.7
	70	96 (55–189)	20.5
NBP/TEP	30	60 (43–93)	4.1
	50	77 (49–135)	9.9
	70	74 (48–127)	10.8

ruptured, exposing a net-like pore structure.

Increasing the solvent concentration to 50 % preserves the general pore shape in all systems, but leads to divergent trends in porosity and pore size. Both increase in the NBP/AMD and NBP/TEP fibers, while they decrease in the NBP/2P fibers. Specifically, surface porosity increases to 4.9 % in NBP/AMD and 9.9 % in NBP/TEP fibers, whereas it decreases to 0.7 % in NBP/2P fibers. At 70 % Solvent B, no further morphological changes are observed in NBP/TEP fibers. However, in NBP/AMD and NBP/2P fibers, the pore structure transitions to an open, nodular network, with surface porosities increasing to 37.1 % and 20.5 % and median pore sizes reaching 143 nm and 96 nm, respectively.

Adding solvent to the bore fluid exerts two opposing effects on phase separation [Chun2021]. On one hand, a higher solvent content reduces the driving force for solvent efflux from the dope solution, delaying phase separation. This delay can lead to the formation of a dense skin layer, which would reduce the PWP and increase the solute retention [Reuv1987a; Smol1992]. On the other hand, due to the delay, the time for growth of the polymer-lean nuclei is prolonged. Also, the added solvent decreases the local polymer concentration at the interface, promoting porosity and thus reducing membrane retention [Wijm1983; Rahb2012; Bang2020].

Dibrov *et al.* demonstrated that the ratio of dope extrusion to fiber take-

up is a critical parameter influencing the shape of the lumen pores in hollow fiber membranes [Dibr2022]. A ratio aligned with the vitrification velocity of the polymer solution yields uniform, elongated pores. Conversely, excessive take-up speed relative to vitrification imposes mechanical stress on the coagulating interface, leading to rupture and rough surface morphologies.

The viscosity of the dope solution also significantly influences surface morphology. Higher viscosity increases diffusion resistance, slowing the growth of polymer-lean nuclei and resulting in smaller pores and lower porosity as seen before in chapter 4.2.3 [Zhan2010].

The observed increases in pore size and porosity with higher Solvent B concentrations support the theory that elevated solvent content lowers the local polymer concentration at the polymer film-coagulation bath interface and promotes the growth of the polymer-lean nuclei. This effect is less pronounced in the highly viscous NBP/2P system due to its greater diffusion resistance compared to the lower-viscosity NBP/AMD and NBP/TEP systems.

The irregular, ripped pore structure on the lumen side of NBP/TEP fibers suggests a rapid fiber take-up rate relative to vitrification. This fits to the fast precipitation of the NBP/TEP solution observed in the light transmission experiments (see section 5.3.1).

However, despite the notable increase in pore size at 70 % solvent B, the corresponding drop in retention is not proportionally significant (see Figure 5.2). One would expect a retention rate of PVP K30 close to zero. This discrepancy could be explained by the location of the selective layer. While changes in bore fluid composition directly affect coagulation on the lumen side, the retentive layer may actually be located on the shell side of the fibers. A comparison of SEM images of the shell and lumen surface, for example, from fibers spun with 70 % Solvent B in the bore (see Figure 5.6) is consistent with this hypothesis. The pore size on the shell is approximately 20 nm, significantly smaller than on the lumen side. In addition, all systems showed a retentive layer with no visible pores in the cross-section located towards the shell side (see Figure 5.6 bottom). Thus, changes to the bore solution may have a limited influence on membrane selectivity. To effectively

tune the cut-off, process parameters affecting outer coagulation must be considered. Therefore, on the one hand, adding solvent additives in the coagulation bath to open the pore structure may be an option. On the other hand, the outer coagulation can be influenced by varying the coagulation bath temperature.

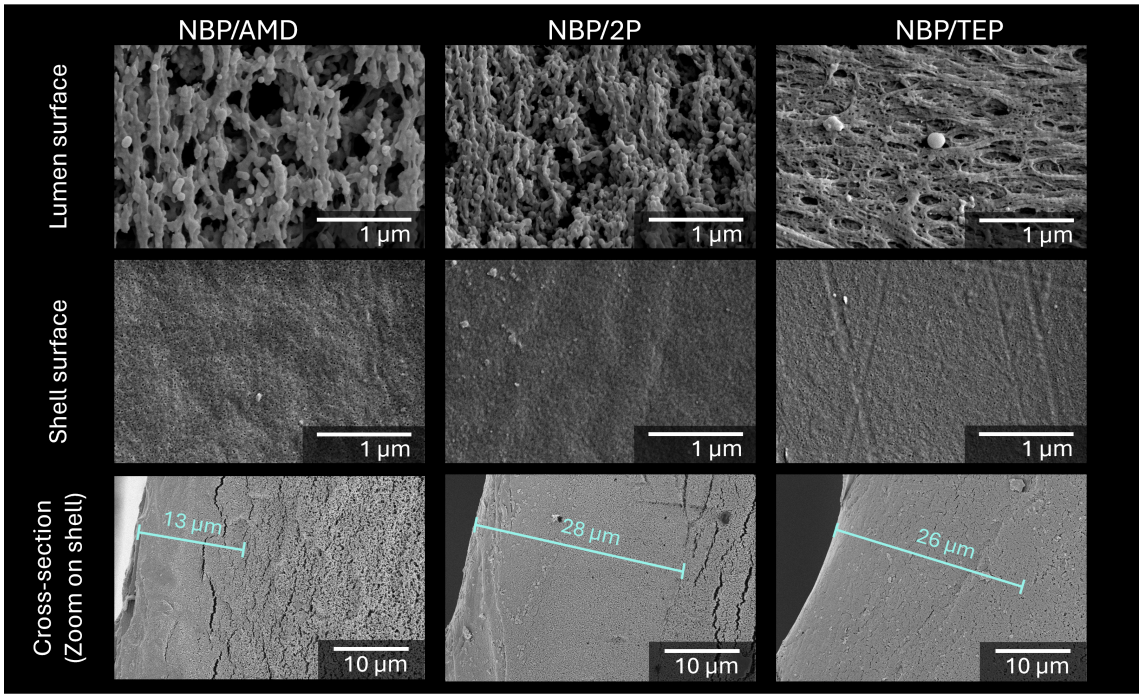


Figure 5.6: SEM image comparison of hollow fiber membranes spun with 70% Solvent B (AMD/2P/TEP) in the bore solution at a coagulation bath temperature of 30 °C. The images show the surface of the lumen shell side, as well as a zoom on the shell side in the fiber cross-section.

5.3.3 Influence of Coagulation Bath Temperature

One way to influence phase separation on the shell side of the hollow fiber is by varying the temperature of the coagulation bath. Figure 5.7 shows SEM images of the shell side of hollow fiber membranes spun with a Solvent B bore solution at different coagulation bath temperatures. The corresponding surface porosities and median pore sizes are summarized in Table 5.6.

An increase in coagulation bath temperature led to a general rise in surface porosity and median pore size on the shell side across all three mixed-

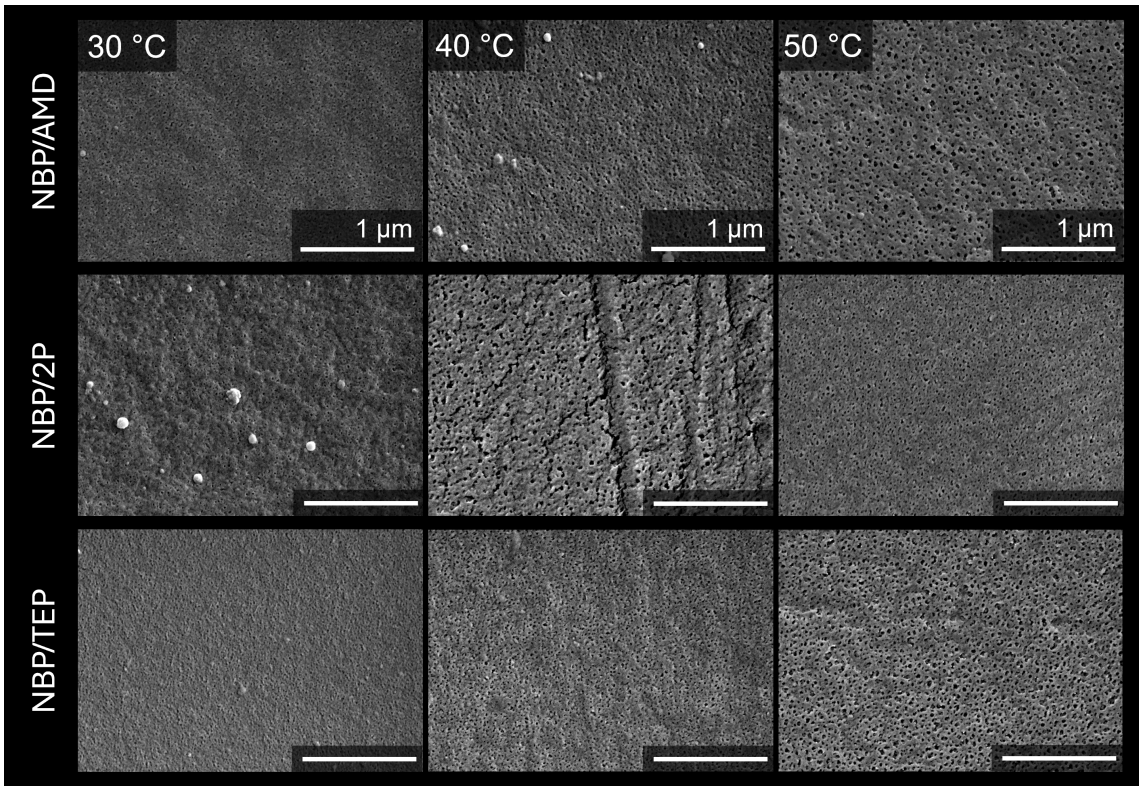


Figure 5.7: SEM images of the outer surface of mixed-solvent hollow fiber membranes spun with 50 % solvent B in the bore at different coagulation bath temperatures.

solvent systems. In the NBP/AMD system, increasing the bath temperature from 30 to 50 °C resulted in a 106 % increase in median pore size, while surface porosity rose from 0.8 % to 6.8 %. For NBP/TEP, the median pore size increased by 64 % and porosity from 0.4 % to 7.8 %. The NBP/2P system exhibited a non-linear trend, with the largest median pore size observed at 40 °C, followed by a 29 % reduction when the temperature was further raised to 50 °C. A similar trend was observed for porosity, which peaked at 4.8 % at 40 °C and declined to 3.1 % at 50 °C. An increase in coagulation bath temperature also led to a decrease in the thickness of the retentive layer, as shown exemplarily for the NBP/AMD fibers in Figure 5.8.

Higher coagulation bath temperatures reduce the viscosity of the dope solution and accelerate the diffusion of solvent and non-solvent [Kahr2019; Zhen2006]. This faster exchange promotes the formation and coarsening of polymer-lean nuclei, resulting in a more open, porous structure [Xu2014; Li2009]. This trend is confirmed by the more porous outer surfaces ob-

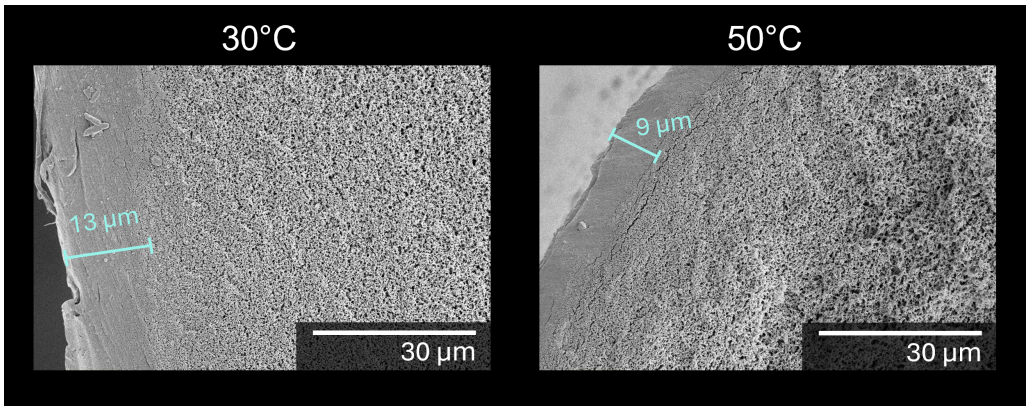


Figure 5.8: SEM image of the cross-section of NBP/AMD fibers spun at different coagulation bath temperatures with zoom on the shell side.

Table 5.6: Median pore size including the quartile range (Q1-Q3), and porosity of the shell side of mixed-solvent hollow fibers spun at different coagulation bath temperatures.

Solvent	Temperature °C	Median pore size (Q1–Q3) nm	Porosity %
NBP/AMD	30	29 (24–36)	0.8
	40	49 (39–63)	3.5
	50	60 (44–86)	6.8
NBP/2P	30	38 (33–43)	0.2
	40	65 (47–86)	4.8
	50	46 (38–58)	3.1
NBP/TEP	30	39 (34–44)	0.4
	40	40 (34–49)	1.8
	50	64 (47–88)	7.8

served in SEM. However, when the temperature exceeds an optimal point, phase separation may occur too quickly, leading to premature solidification before nuclei coarsening can occur [Kahr2019; Kahr2020]. This likely explains the observed drop in pore size and porosity in the NBP/2P system at 50 °C, which has the highest viscosity among the three.

Figure 5.9 presents the PWP and PVP K30 retention of fibers spun at different coagulation bath temperatures using 50 % Solvent B in the bore fluid.

Across all systems, higher coagulation bath temperatures resulted in increased PWP, although the magnitude of this increase varied. From 30 °C to 40 °C, the most significant PWP increase was seen in the NBP/2P sys-

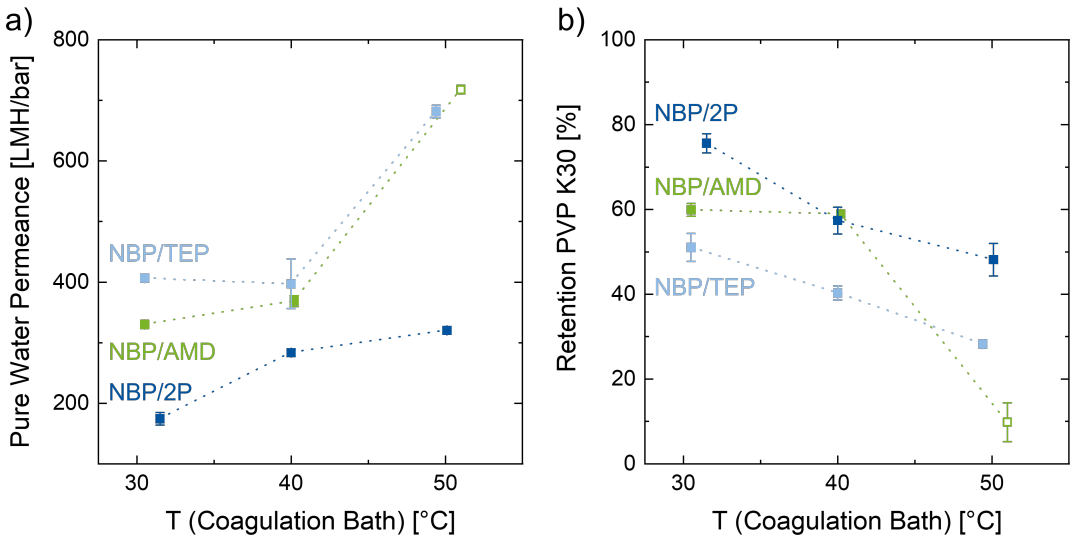


Figure 5.9: PWP (a) and Retention (b) of hollow fiber membranes fabricated with the respective Solvent B (AMD/2P/TEP) in the bore solution at different coagulation bath temperatures. Unfilled squares indicate delaminated fibers.

tem, rising by 63 % from 175 to 285 LMH/bar. A further increase to 50 °C resulted in an additional 12 % gain, reaching 320 LMH/bar. In contrast, the NBP/TEP system showed a slight change from 30 to 40 °C, but heating to 50 °C yielded a sharp 70 % increase to 680 LMH/bar. For the NBP/AMD system, a slight increase of 10 % was observed from 325 to 360 LMH/bar at 40 °C, followed by a significant rise of 93 %, reaching 695 LMH/bar at 50 °C. However, fibers produced under these conditions exhibited delamination between the inner and outer membrane layers (see Figure 5.10).

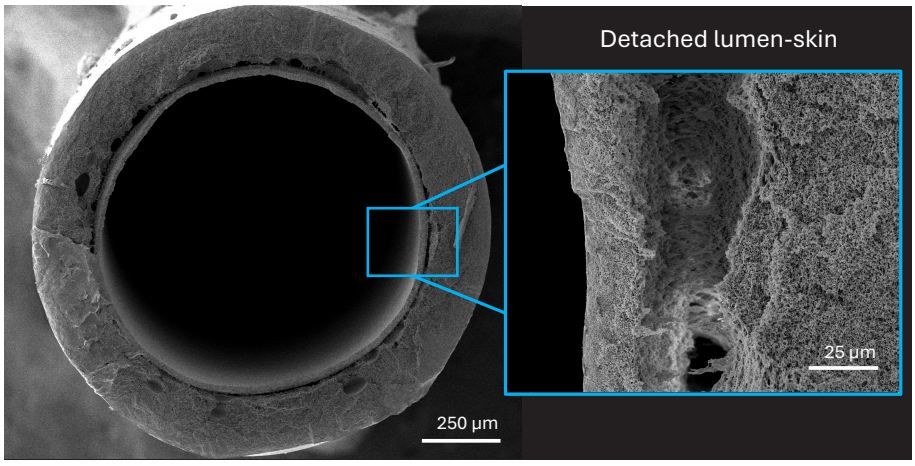


Figure 5.10: Images of the cross-section of a delaminated NBP/AMD fiber, spun with 50 wt% AMD in the bore at 50 °C coagulation bath temperature

Generally, increasing PWP is accompanied by a decrease in solute retention (see Figure 5.9 b). For the NBP/2P and NBP/TEP systems, retention dropped linearly by approximately 25 % from 30 to 50 °C. In contrast, the NBP/AMD system showed no significant change in retention at 40 °C, but a significant decrease from 60 % to 10 % occurred when the temperature was raised to 50 °C.

The increase in porosity and pore size at elevated temperatures reduces hydraulic resistance, thereby enhancing PWP [Xu2020]. However, the occurrence of delamination, particularly in the NBP/AMD system, is attributed to a mismatch in phase separation velocities between the inner and outer coagulation fronts [Feng2021]. The NBP/AMD dope solution, with a viscosity of 34.8 Pa·s (see Table 5.1) and the highest affinity for water (see Table 5.4), promotes rapid solvent–non-solvent exchange. This accelerates outer-layer solidification relative to the inner layer, creating structural stress and ultimately leading to delamination [Zhan2010; Feng2021].

These results demonstrate that coagulation bath temperature is a critical parameter for tuning membrane structure and performance, especially on the shell side.

5.4 Conclusion

This chapter systematically demonstrates how inner and outer coagulation conditions can be tailored to control the structure and performance of mixed-solvent PES ultrafiltration hollow fiber membranes. The choice and concentration of solvent in the bore fluid had a decisive impact on phase separation behavior and the resulting lumen-side pore morphology. The solvents used in the coagulant were either strong (e.g., NBP) or weaker solvents (AMD, 2P, or TEP).

Light transmittance experiments confirmed that increasing the solvent concentration in the coagulant slows phase separation, with the most pronounced effects at 70 wt%. Coagulation baths containing NBP caused significantly more delay than those containing Solvent B, which was attributed to the higher affinity of NBP to PES and the low miscibility with water.

The different phase separation kinetics played a significant role when using either NBP or Solvent B as an additive in the bore solution during hollow fiber spinning. NBP conaining bore solutions lead to less stable spinning processes due to the slow phase separation. Across all systems, increasing the solvent concentration promoted the formation of more porous lumen-side structures and significantly enhanced membrane permeability. Under these conditions, pure water permeance (PWP) increased by up to 350 LMH/bar, while PVP K30 retention decreased moderately by 10–24 %, depending on the dope solution. However, at 70 % NBP in the bore, dissolution of the PES occurred rather than phase separation, leading to dense, nodular pore structures and low PWP.

Despite the fibers spun with 70 % Solvent B in the bore having a high porosity and large pores at the lumen side, the retention of PVP K30 was surprisingly high. SEM images of the cross-section and shell side showed that the retentive layer of the fibers is actually located at the shell side, making further adjustments of the spinning process necessary.

The outer surface morphology was effectively tuned by adjusting the coagulation bath temperature. For all systems, increasing the bath temperature from 30 to 40 °C enlarged pore size and increased PWP, with only

minor losses in retention. The strongest response to the temperature was observed in the NBP/TEP system, in which the PWP was increased by 70 % and the retention rate was reduced by 20%. However, at 50 °C coagulation bath, phase separation in low-viscosity systems such as NBP/AMD occurred too rapidly, leading to delamination and a sharp decrease in retention. These findings underscore the importance of maintaining a balanced control over solvent exchange rates on both the lumen and shell sides to optimize performance.

In conclusion, this work establishes weak solvent-based bore fluids as a promising and sustainable foundation for fabricating high-performance mixed-solvent PES membranes. Importantly, the retentive layer was found to reside on the outer surface, suggesting that parameters affecting outer coagulation are more influential for cut-off tuning in scaled-up processes. The following chapter aims to complement lumen-side tuning with refined control of shell-side porosity. Techniques such as vapor-induced phase separation (VIPS) in the air gap may offer additional strategies to localize the selective layer and broaden the design space for sustainable hollow fiber spinning.

6

Influencing the pore structure of MF hollow fiber membranes in a combined VIPS-NIPS spinning process

6.1 Introduction

Microfiltration (MF) hollow fiber membranes are essential in applications that demand high permeance, gentle hydrodynamics, and mechanically robust modules, such as clarification in bioprocessing, sterile filtration, and pretreatment in water purification [Bake2023; Meli2007]. To align MF manufacturing with green chemistry principles, recent efforts have shifted away from toxic polar aprotic solvents toward safer alternatives that still afford precise control of pore formation and are compatible with process scale-up.

Our previous studies established more sustainable mixed solvent dopes as a practical route to overcome limitations of individual solvents and to achieve robust, macrovoid-free PES hollow fibers. In Chapter 4, mixing the weak solvents AMD, 2P, and TEP each with the strong solvent NBP accelerated demixing, reduced viscosity constraints, and enabled tunable sponge-like structures via adjusting the solvent ratios. Chapter 5 extended the capabilities of this platform beyond solvent ratio control by demonstrating that the composition of the bore solution and coagulation bath temperature can be used to reliably control the morphology of the lumen and shell, respectively. This enables the performance of the membrane to be controlled within ultrafiltration specifications. Together, these results provide a sustainable foundation, yet translating the platform to larger microfiltration cut-offs (0.1 to 10 µm) requires larger, more open pores. Since the pore structures of the ixed-solvent hollow fibers tend to remain dense, particularly on the shell side (see Chapter 5), the classic non-solvent induced phase separation (NIPS) manufacturing process must be adapted.

In the complex spinning process employed for fabricating hollow fiber MF membranes, NIPS is coupled to a vapour-induced phase separation (VIPS) pre-conditioning step in the air gap [Isma2020; Chun2021; Bake2023]. During this pre-conditioning step, the polymer solution is exposed to water vapor, initiating a significantly slower phase separation on the shell side of the fiber. Therefore, polymer-lean nuclei can grow and coalesce before the coagulation bath is reached, resulting in larger pore structures [Chun2021; Isma2020]. Within this coupled process, the precise management of key

process parameters is crucial in determining the resulting membrane structure and performance. Among these, the characteristics of the air gap, bore solution, and external coagulation bath play distinct yet interconnected roles.

The air gap length is a critical parameter, particularly in VIPS, as it determines the exposure time of the nascent fiber to the humid environment before it is immersed in the coagulation bath. Marino *et al.* [Mari2018] showed that the vapor exposure time has a significant influence on the pore size and permeability of polyvinylidene fluoride (PVDF) membranes fabricated with the less toxic solvent TEP. Increasing the vapor exposure time from 0 to 7.5 minutes increased the pore size from 0.1 to 0.45 µm and the permeability from 250 to 8000 LMH/bar. Only a few studies have been done on the influence of the vapor temperature. Bouyer *et al.* [Bouy2010] found that increasing the vapor temperature in VIPS from 25 to 40 °C led to an accelerated mass transfer and the formation of larger pore structures at the upper layer of Polyethyleneimide (PEI) membranes.

The bore solution composition is equally critical, as it directly shapes the lumen skin layer morphology. It influences the thermodynamics and kinetics of the phase inversion process on the lumen side, dictating pore size and porosity. A strong coagulant, such as pure water, typically promotes rapid demixing, leading to a dense inner skin with tiny pores and consequently lower water flux [Wijm1983]. Conversely, introducing solvent additives to the bore fluid decreases its coagulation strength, resulting in delayed demixing, as shown in Chapter 5. This delayed coagulation produces a more porous inner surface with increased pore size and porosity.

In contrast, the temperature of the external coagulation bath directly affects the thermodynamics and kinetics of the phase inversion process on the shell side of the fibers. Increasing the coagulation bath temperature generally accelerates the solvent exchange rate and miscibility, often resulting in larger pores and increased permeability [Chun2021; Bake2023].

Building on mixed-solvent dopes (PES/PVP in NBP/AMD and NBP/2P), this chapter systematically examines air-gap conditioning as a third, shell-focused lever, alongside bore-solution composition and coagulation bath temperature. We hypothesize that by independently tuning (i) bore-fluid co-

agulant strength, (ii) humid air-gap temperature and residence time, and (iii) coagulation-bath temperature, we can orthogonally set the lumen and shell pore architectures of PES fibers and thereby predictably adjust permeance and map process windows that deliver MF-relevant pore architectures with the sustainable mixed-solvent systems NBP/AMD and NBP/2P. We aim to determine whether those parameters can (i) reproducibly shift shell-side porosity and characteristic pore size into the MF range and (ii) provide practically applicable guidelines for tailoring permeance and cut-off. To connect process to structure and performance, we combine scanning electron microscopy (SEM) of shell and lumen surfaces, pure-water permeance (PWP), and a bubble-point–based cut-off determination.

6.2 Materials and Methods

6.2.1 Polymer solution preparation

All components were combined in a heated vessel and stirred at 60 °C until a homogeneous solution was obtained. Before the fabrication of either flatsheet (FS) or hollow fiber (HF) membranes, the solution was degassed. The exact compositions of all polymer solutions are given in Table 6.1.

Table 6.1: Composition of the polymer solutions for MF hollow fiber membrane fabrication.

Code	PES [wt%]	PVP K30 [wt%]	NBP [wt%]	AMD [wt%]	2P [wt%]	Water [wt%]	viscosity [Pa·s]
NBP/AMD	17	25	13.75	41.25	-	4	43.1
NBP/2P	17	25	13.75	-	41.25	4	62.8

6.2.2 Hollow fiber membrane spinning

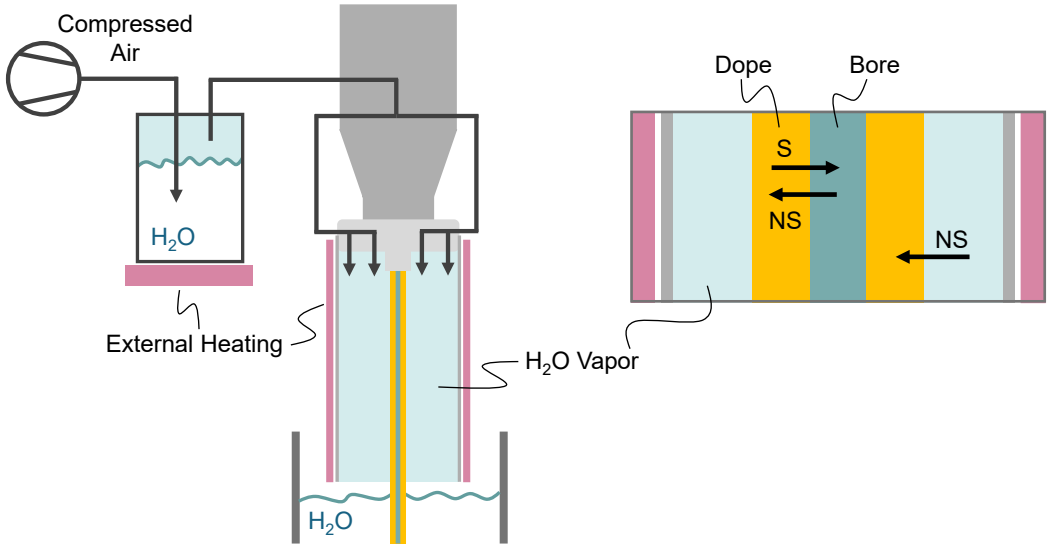


Figure 6.1: Schematic representation of hollow fiber spinning setup with air gap conditioning.

For the spinning of microfiltration hollow fiber membranes, the general setup described in Section 3.2.4 was modified. As shown in Figure 6.1,

the air gap between the nozzle and the coagulation bath was encapsulated within a thermally isolated tube with 6 cm diameter. Compressed air was bubbled through a heated water bath, and the humidified air was then equally distributed at the top of the air gap. The velocity of the humidified air through the air gap chamber was 3 m/min, and the relative humidity was 100% throughout all the experiments. At the bottom of the channel, a 1 cm gap was left open to enable constant airflow. The air gap was heated externally, and the temperature was monitored with a temperature sensor. As a bore fluid, a mixture of 20 w% glycerol, 27 w% water, and 53 w% of the respective solvent (NBP, AMD or 2P) is used. The exact spinning parameters are listed in Table 6.2

Table 6.2: Spinning parameters for microfiltration hollow fiber membrane fabrication.

Dope	Solvent in Bore	l (air gap) cm	T (air gap) °C	T (coagulation bath) °C	Dope flow [mL/min]	Bore flow [mL/min]	Pulling Speed [m/min]
NBP/AMD	NBP	10	62.8	60	4.02	3.67	4.62
NBP/AMD	NBP	10	65.2	60	4.05	3.67	4.62
NBP/AMD	NBP	10	69.3	60	4.05	3.71	4.62
NBP/AMD	AMD	10	60.1	60	3.85	3.93	4.62
NBP/AMD	AMD	10	68.2	60	3.85	3.93	4.62
NBP/AMD	AMD	10	70.2	60	3.85	3.93	4.62
NBP/AMD	NBP	20	60.1	60	4.02	3.58	4.62
NBP/AMD	NBP	20	64.0	60	4.05	3.48	4.62
NBP/AMD	AMD	20	60.1	60	3.79	3.96	4.89
NBP/AMD	AMD	20	64.0	60	3.79	4.03	4.89
NBP/AMD	AMD	20	70.0	60	3.79	4.03	4.89
NBP/AMD	NBP	20	60.4	70	4.02	3.48	4.62
NBP/AMD	NBP	20	60.2	80	4.05	3.67	4.62
NBP/AMD	AMD	20	59.6	70	3.76	3.99	4.62
NBP/AMD	AMD	20	60.2	80	3.73	4.06	4.62
NBP/2P	NBP	10	59.4	60	3.96	3.61	4.62
NBP/2P	NBP	10	64.6	60	3.96	3.61	4.62
NBP/2P	NBP	10	69.5	60	4.08	3.58	4.62
NBP/2P	2P	10	60.0	60	3.82	3.99	4.62
NBP/2P	2P	10	63.1	60	3.82	3.99	4.62
NBP/2P	2P	10	69.1	60	3.82	3.99	4.62
NBP/2P	NBP	20	59.2	60	4.08	3.61	4.62
NBP/2P	NBP	20	64.5	60	4.05	3.61	4.62
NBP/2P	NBP	20	69.3	60	4.08	3.71	3.80
NBP/2P	2P	20	56.2	60	3.93	3.83	4.62
NBP/2P	2P	20	60.0	60	3.88	3.83	4.48
NBP/2P	2P	20	61.2	60	3.99	3.77	4.62
NBP/2P	NBP	20	59.0	70	4.05	3.61	4.62
NBP/2P	NBP	20	60.1	80	4.10	3.51	4.62
NBP/2P	2P	20	59.0	70	3.96	3.93	4.62
NBP/2P	2P	20	59.5	80	3.88	3.90	4.62

Cut-off determination with Bubble-point measurements

A single hollow fiber was potted into a module providing a feed inlet and a retentate outlet on the lumen side and a permeate outlet on the shell side of the fiber. The lumen was filled with a 60% (v/v) isopropanol-water solution. The wetting liquid was pumped from the feed in dead-end mode until all pores and internal module volumes were filled and no air bubbles were visible. The feed line was then connected to a nitrogen supply, and the excess liquid was gently displaced from the lumen while keeping the pores filled with liquid. The measurement of the bubble point was then performed in dead-end mode. The applied nitrogen pressure was increased in increments of 0.1 bar until the first continuous bubble was observed at the shell-side (permeate) of the fiber. This pressure was recorded as the bubble-point pressure p_{BP}.

Assuming cylindrical pores and complete wetting, the maximum effective pore diameter d_{max} was calculated from the Young-Laplace relation,

$$d_{max} = \frac{4\,\sigma\cos(\theta)}{p_{BP}}, \tag{6.1}$$

where σ is the surface tension of the 60% isopropanol–water mixture [Khos2017] at the measurement temperature in N/m and θ is the liquid-solid contact angle, taken as $\cos(\theta) \approx 1$ for full ($\theta \approx 0$ [Pein2023]) wetting. Each fiber batch was measured three times, and the mean value with standard deviation was calculated. The maximum effective pore diameter d_{max} was used in the following as an indication of the microfiltration cut-off of the respective membrane.

6.3 Results and Discussion

6.3.1 Influence of air gap temperature

Hollow fiber membranes were spun through a 10 cm air gap at temperatures between 60 and 70 °C to investigate the influence on the shell-side structure. In addition, two bore solutions, containing either NBP or the respective Solvent B (AMD or 2P), were used to examine their effect on the inner phase separation. SEM images were taken to assess the influence of NIPS and VIPS on the pore structure on both sides of the fibers. Figure 6.2 and Figure 6.3 summarize the SEM images of the fabricated fibers.

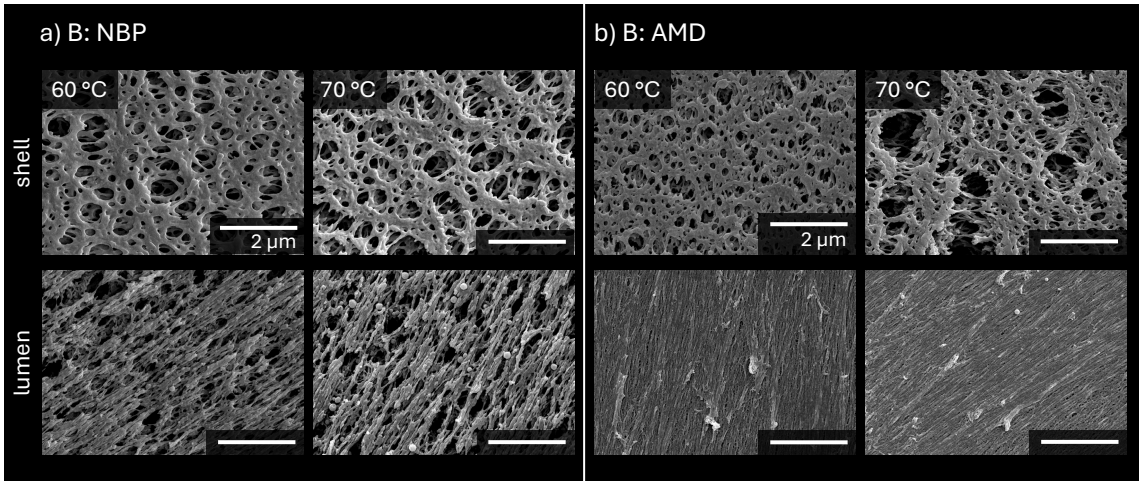


Figure 6.2: SEM images of shell and lumen side of NBP/AMD hollow fibers spun through a 10 cm air gap at 60 and 70 °C with a) NBP and b) AMD in the bore solution.

Pronounced differences in the lumen pore structure are observed for the different bore solutions in both dope systems. With NBP in the bore, an open porous network forms on the lumen side (see Figure 6.2 a) and 6.3 a) with a median pore size of 0.20 µm for both dopes. Upon heating the air gap, pore shape and size are maintained while the porosity increases by about 5 % in both systems (see Table 6.4). In contrast, using AMD or 2P as solvent additives in the bore produces a denser lumen side with elongated pores (median size 70 nm), with no significant size increase upon air-gap

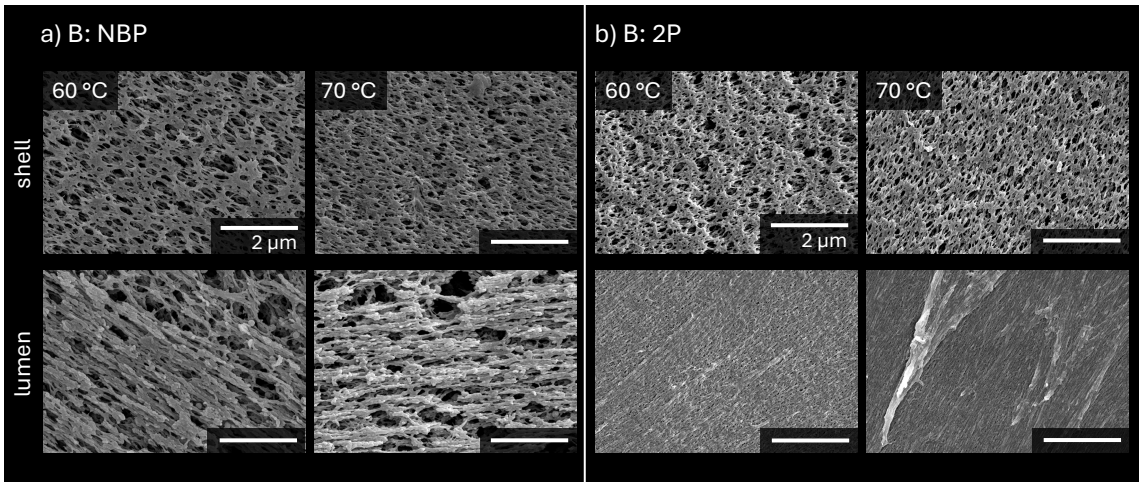


Figure 6.3: SEM images of shell and lumen side of NBP/2P hollow fibers spun through a 10 cm air gap at 60 and 70 °C with a) NBP and b) 2P in the bore solution.

Table 6.3: Shell-side characteristics at different air-gap temperatures.

Dope	Bore	T (air gap) °C	median pore size (Q1–Q3) µm	porosity %
NBP/AMD	NBP	60	0.29 (0.16–0.55)	19.3
NBP/AMD	NBP	70	0.27 (0.14–0.52)	24.8
NBP/AMD	AMD	60	0.21 (0.12–0.39)	18.1
NBP/AMD	AMD	70	0.19 (0.11–0.39)	26.1
NBP/2P	NBP	60	0.25 (0.13–0.52)	29.9
NBP/2P	NBP	70	0.20 (0.11–0.37)	23.3
NBP/2P	2P	60	0.17 (0.10–0.30)	22.8
NBP/2P	2P	70	0.18 (0.11–0.31)	19.2

heating.

On the shell side, a microporous network is observed for both bore solutions. Heating the air gap from 60 to 70 °C decreases the median pore size by 20–50 nm when NBP is in the bore. In NBP/AMD fibers, the presence of Solvent B in the bore also decreases the median pore size by approximately 20 nm upon heating the air gap, whereas in NBP/2P fibers, it increases slightly by about 10 nm. Furthermore, the shell-side porosity of NBP/AMD fibers increases by 5–8 % for both bores at 70 °C, while that of NBP/2P fibers decreases by about 4–7 % (see Table 6.3).

The lumen-side pore structure is primarily governed by internal NIPS induced by the bore solution. Depending on the non-solvent strength, phase

Table 6.4: Lumen-side characteristics at different air-gap temperatures.

Dope	Bore	T (air gap) °C	median pore size (Q1–Q3) µm	porosity %
NBP/AMD	NBP	60	0.20 (0.12–0.43)	35.3
NBP/AMD	NBP	70	0.20 (0.11–0.49)	40.2
NBP/AMD	AMD	60	0.07 (0.05–0.11)	3.8
NBP/AMD	AMD	70	0.08 (0.04–0.08)	2.1
NBP/2P	NBP	60	0.21 (0.11–0.42)	21.3
NBP/2P	NBP	70	0.20 (0.12–0.49)	25.6
NBP/2P	2P	60	0.07 (0.05–0.10)	5.3
NBP/2P	2P	70	0.06 (0.04–0.08)	2.7

separation occurs either rapidly and instantaneously or slowly and delayed. A weak non-solvent causes slow phase separation, where polymer-lean nuclei can grow and coarsen before solidification, yielding a microporous network with larger pores [Wijm1983; Smol1992]. A strong non-solvent causes rapid phase separation and fast solidification as shown in Section 5.3.1. Therefore, polymer-lean nuclei have insufficient time to grow, resulting in a denser pore structure with smaller pores [Wijm1983; Smol1992].

The bore solutions used here differ significantly in their non-solvent power. NBP has a high affinity to PES and thus a low non-solvent strength, whereas AMD and 2P have lower affinity to PES and hence higher non-solvent strength (see Table 6.5). The denser lumen surfaces obtained with AMD or 2P in the bore support the interpretation of instantaneous, fast precipitation.

Table 6.5: HSP distances of the solvents to polyethersulfone.

Solvent	**NBP**	**AMD**	**2P**
$\delta_{s\text{-}PES}$ [MPa$^{1/2}$]	2.9	8.5	8.1

On the shell side, water vapor in the air gap induces phase separation via VIPS, which is significantly slower than NIPS due to slower mass transfer [Isma2020]. A higher air-gap temperature enhances the diffusion and absorption of water vapor into the polymer solution [Bouy2010], which accelerates non-solvent uptake and thereby initiates phase separation while the dope is still in the air gap [Isma2020]. Faster non-solvent uptake gener-

ates a larger number of polymer-lean nuclei, which coarsen and grow until the interfacial polymer concentration becomes too high, leading to solidification [Chae1999; Isma2020; Zhao2018]. Additionally, higher solution viscosity hinders nuclei coarsening by increasing diffusion resistance [Chae1999; Zhan2010].

The differences in shell-side porosity likely arise from the viscosities of the dope. For the lower-viscosity NBP/AMD solution (43.1 Pa·s), higher air-gap temperatures increase porosity, whereas the higher-viscosity NBP/2P solution (62.8 Pa·s) shows a decrease. The higher diffusion resistance in NBP/2P slows pore growth relative to NBP/AMD. Thus, although more nuclei are initiated in both dopes at higher air-gap temperatures, the NBP/2P fibers exhibit a lower surface porosity. When the fiber reaches the coagulation bath, rapid external NIPS causes solidification, preventing further coarsening. Because the residence time in the air gap is short, the nuclei in the NBP/AMD solution do not have time to grow sufficiently. Therefore, the number of shell-side pores increases upon heating the air gap, but the median pore size decreases.

The observed pore structures directly affect membrane performance. Figure 6.4 summarizes the pure water permeance (PWP) and the largest pore size for NBP/2P and NBP/AMD fibers. The largest pore size was calculated using bubble point measurements (see section 6.2.2), assuming complete wetting of the pores, and is used as a cut-off indicator.

The significant differences in lumen structures between bore solutions lead to correspondingly large differences in PWP for both dope systems (Figure 6.4a). With NBP in the bore, PWP is 3–4 times higher than with 2P or AMD at the same air-gap temperature. In the NBP/2P system with NBP in the bore, heating from 60 to 70 °C increases PWP by 26 % (1670 to 2100 LMH/bar). In NBP/AMD, the increase is approximately 50 % (from 2590 to 3880 LMH/bar) when heating from 63 to 70 °C. In contrast, when switching the bore to Solvent B, no significant effect of the air-gap temperature on the PWP is observed. The trends observed for the cut-offs, shown in Figure 6.4b), differ from the PWP trends. In the NBP/2P system, the cut-offs are similar for both bores and increase only slightly upon

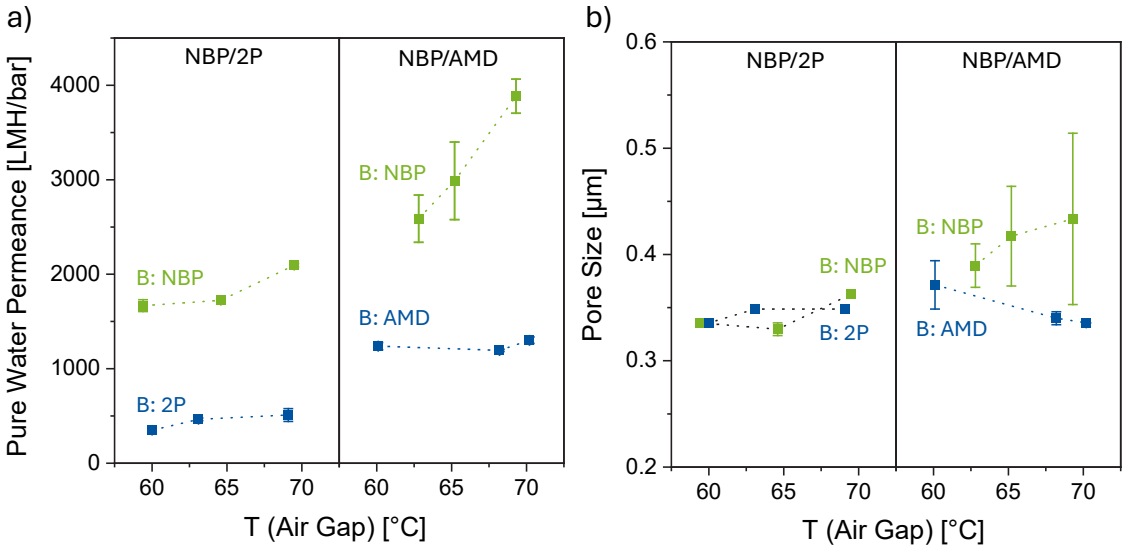


Figure 6.4: a) PWP and b) pore size of NBP/2P and NBP/AMD hollow fiber membranes spun with a 10 cm air gap at different temperatures. The solvents used in the bore fluid are labeled (B: NBP/2P/AMD).

heating from 0.34 to 0.35 µm with the 2P bore and 0.34 to 0.36 µm with the NBP bore. In the NBP/AMD system, the cut-off increases from 0.39 to 0.43 µm with NBP in the bore but decreases from 0.37 to 0.34 µm with AMD in the bore.

6

Increasing porosity and pore size lowers hydraulic resistance in the membrane, thereby raising the PWP [Xu2020]. In NBP/AMD fibers, both shell- and lumen-side porosities increase with air-gap heating, leading to the most substantial PWP increase. In NBP/2P with NBP in the bore, the lumen porosity increases (reducing membrane resistance), but the shell-side porosity and pore size decrease (increasing resistance). The differing air-gap-temperature sensitivities can be rationalized by phase-separation kinetics. With delayed internal phase separation (NBP in bore), the nascent fiber morphology remains responsive to air-gap conditions. In contrast, when internal phase separation is rapid (AMD or 2P in bore), it dominates and masks the slower external VIPS effects. Consequently, PWP is primarily governed by the denser lumen structure. Since the membrane cut-off reflects the largest pore that extends across the cross-section of the membrane, it is limited by the side with the smaller pores. With AMD or 2P in

the bore, the lumen pores are much smaller than shell pores. As their size decreases slightly upon heating, the overall cut-off also decreases. Notably, despite the smaller lumen pores with AMD/2P compared to NBP, the measured cut-offs fall within a similar range. Although the analysis of SEM images gives valuable insights into the median pore size, it only covers a particular area of the membrane surface. Additionally, by calculating the median pore size and the quartile range (see Chapter 3.2.6), larger outlines or defects that would dominate the cut-off are not captured. With NBP in the bore, heating the air gap yields cut-off trends consistent with the PWP response in both dope systems.

6.3.2 Influence of air gap length

The air-gap distance was increased from 10 cm to 20 cm to test whether a longer residence time amplifies the effect of the air gap temperature. Doubling the distance doubles the residence time in the humidified air from 1.3 s to 2.6 s. At higher air-gap temperatures, fibers were more prone to breakage, and the process sometimes became unstable. Consequently, NBP/2P fibers with 2P in the bore could not be spun above 62 °C, and NBP/AMD fibers with NBP in the bore could not be spun above 65 °C. The PWP and largest pore sizes of the remaining fibers are summarized in Figure 6.5.

Increasing the air-gap distance did not improve PWP when AMD or 2P was in the bore (Figure 6.5a). With NBP in the bore, however, PWP increased relative to the 10 cm air gap. For NBP/2P fibers, PWP reached 1750 LMH/bar at 60 °C and 2300 LMH/bar at 70 °C, which is 5–9 % higher than at the same temperatures with a 10 cm air gap. For NBP/AMD, PWP was about 80 % higher (around 5350 LMH/bar) when spun with a 20 cm air gap.

For the cut-off, a clear temperature dependence is observed in all systems, albeit to varying extents. NBP/2P fibers spun at 60–70 °C show cut-offs between 0.29 and 0.38 µm, whereas NBP/AMD fibers range from 0.37 to 0.45 µm. In NBP/2P, the two bore solutions yield similar cut-offs. In NBP/AMD, the cut-off with NBP in the bore is 10–17 % larger than with

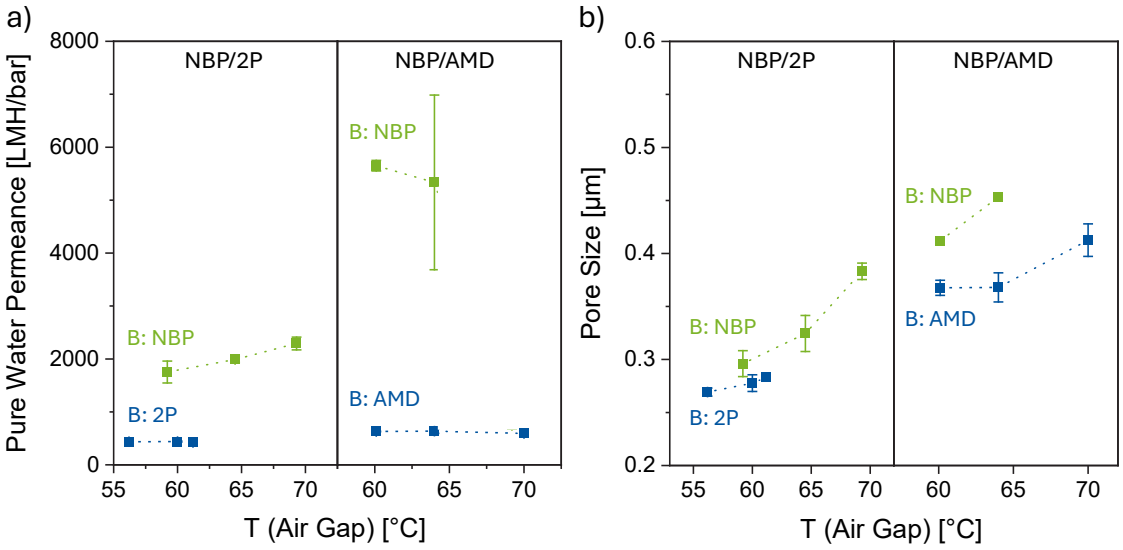


Figure 6.5: a) PWP and b) pore size of NBP/2P and NBP/AMD hollow fiber membranes spun with a 20 cm air gap at different temperatures. The solvents used in the bore fluid are labeled (B: NBP/2P/AMD).

AMD. However, although a significant influence of temperature is observed, the cut-offs are in the same range as with a 10 cm air gap.

With the longer air-gap residence time, exposure to water vapor increases. This extended exposure allows polymer-lean nuclei to grow longer before rapid exchange in the coagulation bath induces solidification. Consequently, the influence of accelerated vapor uptake on pore size is more pronounced at higher air-gap temperatures. Furthermore, due to the decreased resistance of the membrane, the PWP is increased significantly.

6.3.3 Influence of coagulation bath temperature

Another key parameter to tune shell-side phase separation is the coagulation-bath temperature. Figures 6.6 and 6.7 show SEM images of the lumen and shell side of NBP/AMD and NBP/2P fibers spun with 60 and 80 °C coagulation baths. Median pore size and porosity from SEM image analysis are summarized for the lumen in Table 6.7 and for the shell in Table 6.6.

The overall lumen-side appearance remains the same upon heating the bath. NBP in the bore yields an open porous network, whereas AMD or 2P

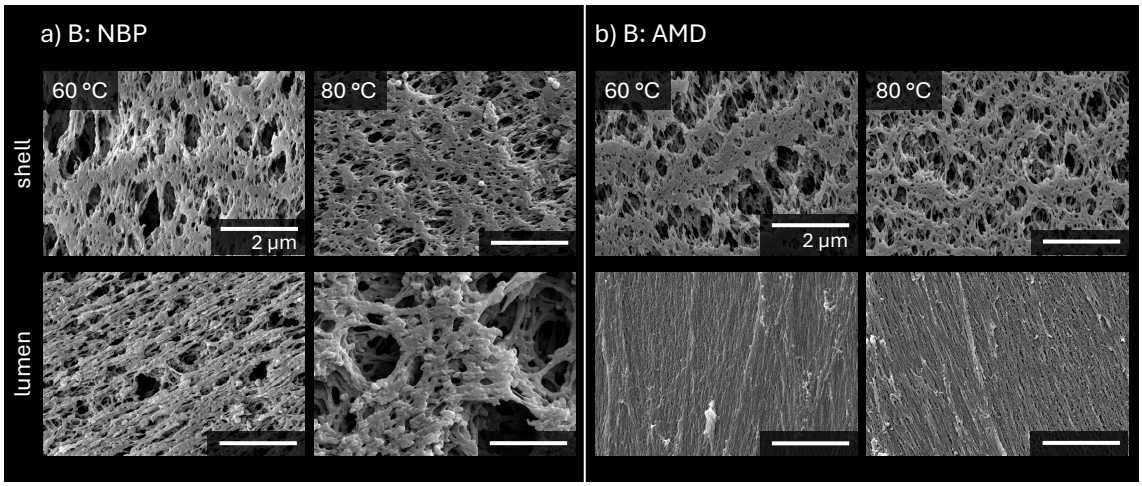


Figure 6.6: SEM images of shell and lumen side of NBP/AMD hollow fibers spun through a 20 cm air gap into 60 and 80 °C coagulation baths with a) NBP and b) AMD in the bore solution.

produces denser, elongated pores. In both dope systems, the lumen median pore size increases by 20–30 nm upon heating, accompanied by a rise in surface porosity by 1–15 %, depending on dope and bore (Table 6.7). On the shell side, the two bores exhibit opposite trends in both dope systems. With AMD or 2P in the bore, the median pore size increases by 30–50 nm and porosity by about 4–7 % when the bath is heated from 60 to 80 °C. In contrast, with NBP in the bore, the median pore size decreases by 20–70 nm and the porosity by 10–17 % (Table 6.6).

Heating the coagulation bath accelerates mass transfer during phase separation, causing the dope to enter the two-phase region more rapidly. The polymer-lean phase therefore has more time to grow before solidification, yielding larger pores [Xu2014; Li2007]. In hollow fibers, solidification is influenced by both outer and inner coagulation. The formation of a dense layer at the lumen increases resistance and slows the further diffusion of the bore solution to deeper layers [Bake2023; Smol1992], thereby delaying inner phase separation and allowing the coagulation bath temperature to have a greater effect.

The lumen-side morphologies of NBP/AMD and NBP/2P fibers are consistent with the expectation that higher coagulation bath temperatures pro-

duce more porous structures. The larger pores and higher porosity obtained with NBP in the bore create less diffusion resistance than the denser lumen structures obtained with AMD or 2P. Consequently, non-solvent influx from the lumen side is less hindered, and overall solidification proceeds faster with the NBP bore than when phase separation is predominantly initiated from only one side. At elevated bath temperatures, non-solvent/solvent diffusion accelerates, generating numerous polymer-lean nuclei whose growth is inhibited by faster solidification.

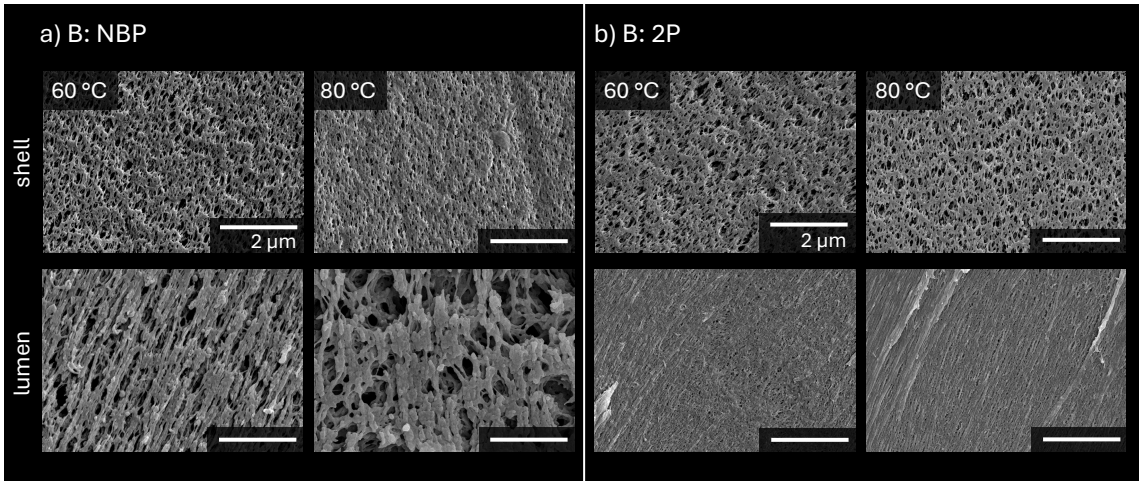


Figure 6.7: SEM images of shell and lumen side of NBP/2P hollow fibers spun through a 20 cm air gap into 60 and 80 °C coagulation baths with a) NBP and b) 2P in the bore solution.

PWP and cut-off of the membranes (Figure 6.8) show a strong dependence on bath temperature. With NBP in the bore, heating from 60 to 80 °C increases PWP by about 2600 LMH/bar for NBP/2P and about 5500 LMH/bar for NBP/AMD. With AMD or 2P in the bore, PWP remains significantly lower. For NBP/2P, it stays near 440 LMH/bar upon heating, while for NBP/AMD, it rises from about 600 to 1400 LMH/bar. The cut-off increases in all systems with bath temperature (Figure 6.8 b). In the NBP/2P system, heating from 60 to 80 °C raises the cut-off by 0.1 µm for both bores, whereby the cut-off with NBP in the bore is 0.04 µm larger than that of the fibers spun with the 2P bore solution. In NBP/AMD, the difference between bores is more pronounced. With NBP in the bore, the cut-off increases

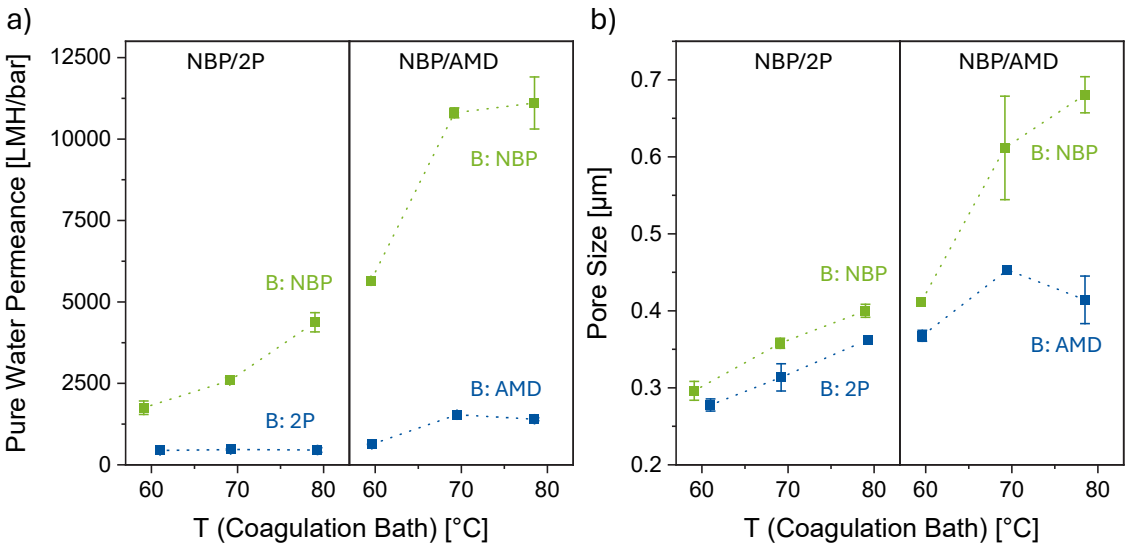


Figure 6.8: a) PWP and b) pore size of NBP/2P and NBP/AMD hollow fiber membranes spun with a 20 cm air gap at different coagulation-bath temperatures. The solvents used in the bore fluid are labeled (B: NBP/2P/AMD).

from 0.41 to 0.68 µm, while with AMD in the bore, it increases from 0.37 to 0.42 µm.

As noted above, higher porosity and larger pores lower hydraulic resistance and increase PWP [Xu2020]. The increase in PWP with NBP in the bore is consistent with the corresponding increases in cut-off. The mismatch between the magnitude of cut-off and PWP changes observed in some cases likely reflects that cut-off is governed by the largest pore, whereas PWP scales with the total effective area. As seen in the SEM images (Figures 6.6 b and 6.7 b), the lumen pores are significantly smaller than the shell pores and therefore dominate hydraulic resistance.

Table 6.6: Shell-side characteristics at different coagulation-bath temperatures.

Dope	Bore	T (coag. bath) °C	median pore size (Q1–Q3) µm	porosity %
NBP/AMD	NBP	60	0.19 (0.12–0.35)	29.0
NBP/AMD	NBP	80	0.17 (0.11–0.35)	18.7
NBP/AMD	AMD	60	0.16 (0.10–0.30)	26.8
NBP/AMD	AMD	80	0.21 (0.12–0.38)	30.6
NBP/2P	NBP	60	0.21 (0.12–0.39)	26.8
NBP/2P	NBP	80	0.14 (0.09–0.21)	9.2
NBP/2P	2P	60	0.15 (0.10–0.27)	17.3
NBP/2P	2P	80	0.18 (0.11–0.32)	24.6

Table 6.7: Lumen-side characteristics at different coagulation-bath temperatures.

Dope	Bore	T (coag. bath) °C	median pore size (Q1–Q3) µm	porosity %
NBP/AMD	NBP	60	0.18 (0.11–0.40)	26.1
NBP/AMD	NBP	80	0.21 (0.11–0.44)	36.1
NBP/AMD	AMD	60	0.06 (0.05–0.09)	2.7
NBP/AMD	AMD	80	0.08 (0.05–0.13)	6.2
NBP/2P	NBP	60	0.20 (0.11–0.43)	23.1
NBP/2P	NBP	80	0.23 (0.12–0.59)	24.2
NBP/2P	2P	60	0.06 (0.05–0.09)	4.6
NBP/2P	2P	80	0.08 (0.05–0.12)	8.2

6.4 Conclusion

This chapter has shown that microfiltration membranes based on the more sustainable mixed solvent dopes NBP/AMD and NBP/2P can be tailored by individually adjusting the inner NIPS and outer VIPS kinetics during hollow fiber spinning. The three process parameters—bore-fluid composition, air-gap conditioning (temperature and residence time), and coagulation-bath temperature afford orthogonal control over lumen and shell morphologies, and consequently, over membranes' permeance and cut-off.

A central outcome is that the type of solvent additive in the bore fluid significantly influences the inner phase separation kinetics and, therefore, both permeance and selectivity. With NBP as a weak non-solvent in the bore, internal phase separation is delayed, resulting in an open, microporous lumen. In contrast, with stronger non-solvents like AMD or2P in the bore, internal phase separation occurs faster, resulting in a denser skin layer with significantly smaller pores. As a consequence, the PWP of membranes spun with NBP bores is four to ten times higher, depending on the dope system, than that of the fibers spun with AMD or 2P in the bore.

Air-gap conditioning provides a shell-focused approach via VIPS. Increasing the air-gap temperature from 60 to 70 °C at an air gap distance of 10 cm increases the number of polymer-lean nuclei and accelerates their growth on the shell side. For the lower-viscosity NBP/AMD dope, this results in higher shell porosity and a slight decrease in median shell pore size. Together with the open lumen obtained with NBP in the bore, this translates into a substantial increase in PWP without affecting the membranes cut-off. For the more viscous NBP/2P dope, the same thermal increment increases the density of the nuclei but hinders coarsening. This results in a modest reduction in shell porosity. Nevertheless, when the lumen remains open, as with the NBP bore, the overall PWP still increases. Increasing the air gap length to 20 cm amplifies these trends by doubling vapour exposure time. This further enhances PWP for NBP-bore fibres and intensifies the increase in cut-off with rising temperatures. However, process stability is limited at the highest temperatures for certain dope/bore combinations.

Furthermore, changing the coagulation bath temperature has been proven to be an effective parameter in influencing the outer coagulation. Elevating the coagulation-bath temperature from 60 to 80 °C accelerates solvent/non-solvent exchange and enables additional growth of the polymer-lean phase before solidification. This universally increases the cut-off and, when paired with an NBP-bore, yields the most significant permeance increments observed in this study. Notably, the magnitude and direction of shell-side changes with bath heating depend on the inner front: when inner precipitation is rapid (AMD or 2P bore), the shell responds with larger pores and higher porosity; when the lumen is already open (NBP bore), faster outer solidification can arrest coarsening, decreasing shell porosity while overall PWP still rises due to lumen dominance.

Within this study, an effective process window for tailoring more sustainable mixed-solvent MF hollow fiber membranes with PWP from 450 to 11000 LMH/bar and cut-offs varying from 0.27 to 0.68 µm is provided.

7

Conclusion and Future Perspectives

This thesis presents a sustainable approach for fabricating polyethersulfone (PES) hollow fiber membranes by combining environmentally friendly solvent–polymer solutions with process levers that independently control inner and outer phase separation. First, the work elucidates how mixed solvents alter the thermodynamics and kinetics of non-solvent-induced phase separation (NIPS). Second, these insights are applied to the fabrication of tunable ultrafiltration (UF) and microfiltration (MF) membranes with performance ranges suitable for scale-up. Throughout the study, Hansen solubility parameter analysis, light transmission measurements, and systematic morphology–performance characterization established a quantitative framework for solvent selection and process design.

In **Chapter 4**, sustainable solvents and their mixtures were systematically investigated to develop suitable dope solutions as alternatives to toxic aprotic systems. While single solvents such as N-butyl pyrrolidone (NBP), N,N-dimethyllactamid (AMD), 2-pyrrolidone (2P), and triethyl phosphate (TEP) each exhibited specific drawbacks, mixing them with NBP compensated for these limitations by shifting polymer affinity, lowering viscosity, and enabling controlled demixing. With this strategy, the low solvent power of TEP could be overcome. Furthermore, the dense membrane structures obtained from AMD and 2P, as well as the encapsulated pore structures of NBP, could be transformed into asymmetric membrane structures with completely sponge-

like pores and no macrovoids.

These structural changes translate directly into transport characteristics. In flat sheet membranes, the PWP of the mixed-solvent membranes is significantly higher than in the single-solvent systems, while the retention is only moderately decreased. All three mixed solvent systems could be spun into defect-free hollow fiber membranes across broad composition ranges. Adjusting the NBP concentration within the dope solution tuned the pore morphology. Membranes with a high amount of NBP (75 w%:25 w% NBP:Solvent B) exhibit an encapsulated pore structure, resulting in a low PWP of around 50 LMH/bar for all systems. In contrast, membranes spun from a dope solution with a low NBP concentration (25 w%:75 w% NBP:Solvent B) exhibit an open, interconnected pore structure and high PWP from 220-300 LMH/bar across the systems.

Building on this platform, **Chapter 5** showed that inner and outer coagulation can be independently tuned to tailor the selective layer and set the membrane cut-off. On the lumen side, increasing solvent concentration in the bore fluid (30–70%) delayed phase separation, enlarged pores, and boosted PWP by up to $\sim$350 LMH/bar with moderate retention of PVP K30 losses (10–24%). High solvent concentrations (> 70 %) in the bore solution risk dissolution of the polymer instead of liquid-liquid phase separation and, therefore, mark an operational limit. Using strong non-solvents such as AMD, 2P, or TEP in the bore improved mechanical stability during spinning compared to weaker NBP bores. On the shell side, raising the coagulation-bath temperature from 30 to 50 °C generally enlarged pores and increased PWP, with the strongest response in NBP/TEP. Excessively high bath temperatures (50 °C), however, caused delamination in low-viscosity dopes such as NBP/AMD. Together, these findings established weak solvent-based bore fluids as a promising, sustainable foundation for PES ultrafiltration hollow fiber membranes, while highlighting that both inner and outer coagulation must be considered when tailoring performance.

To extend the cut-off into the MF range, **Chapter 6** coupled vapour-induced phase separation (VIPS) with NIPS by conditioning the air gap with

heated, humid air (100 % humidity). Slow VIPS on the shell side generated open structures, whereas the bore fluid had a critical influence on lumen formation. In contrast to UF spinning, AMD- and 2P-based bores produced dense retentive lumen layers, whereas NBP bores generated large pores. Increasing the air gap temperature (60 to 70 °C, 10 cm gap) enhanced shell porosity, with effects that depended on the dope viscosity and synergized with lumen-side structures. Fibers with dense lumens exhibited only modest increases in PWP. In contrast, fibers with an open porous lumen responded strongly to the air gap temperature. Extending the air gap to 20 cm amplified these effects but narrowed the stable process window. At higher air-gap temperatures, fibers were more prone to breakage, and the process sometimes became unstable. Consequently, NBP/2P fibers with 2P in the bore could not be spun above 62 °C air gap temperature, and NBP/AMD fibers with NBP in the bore could not be spun above 65 °C. Raising the coagulation bath temperature (60–80 °C) further coarsened structures, universally shifting cut-offs and—when paired with NBP bores—yielding the most significant PWP increments. Across these parameters, MF windows were achieved with PWP ranging from 450 to 11,000 LMH/bar and cut-offs from 0.27 to 0.68 µm, consistent with the interplay of VIPS-driven shell porosity and bore-controlled lumen precipitation.

Overall, this thesis demonstrates that sustainable mixed-solvent systems are not a compromise but a design opportunity. By adjusting solvent power and affinity to the coagulant, demixing kinetics can be precisely controlled, quantified by HSP distances, viscosity, and light transmission. Moreover, manipulating both inner and outer coagulation enables the reproducible tuning of pore structures, achieving UF and MF performance windows comparable to those of conventional toxic-solvent processes.

Looking forward, the complex interplay of process parameters should be examined statistically. A formal design-of-experiments (DoE) across solvent ratios, bore compositions, VIPS conditions, and bath temperatures would enable systematic mapping of response surfaces for permeance, cut-off, and mechanical stability. These empirical models could be coupled with physics-informed surrogate models to reduce experimental effort and guide

process optimization. Further improvements in spinning stability are possible, for example, in the fabrication of MF membranes with a 20 cm air gap. Tuning the polymer concentration or dope temperature can adjust the viscosity of the dope solution, thereby broadening the process window toward higher air gap temperatures. Additionally, varying the humidity within the air gap might also be a valuable parameter for producing different cut-off membranes.

Sustainability assessments will also become increasingly important. Solvent-management strategies and life-cycle assessments (LCA) should be integrated to quantify environmental benefits relative to NMP-based processes. Approaches such as wastewater recycling for use in coagulation baths could further reduce resource consumption. Finally, the concept of mixed sustainable solvents is not restricted to NBP, AMD, 2P, and TEP. Extending this approach to other solvent systems and applying it to polymers such as PVDF or polyamides could open pathways toward applications beyond biopharmaceutical processes, including gas separation.

Bibliography

[Anas2000] P. T. Anastas and J. C. Warner. *Green Chemistry: Theory and Practice*. Oxford University Press, May 2000. ISBN: 9780198506980.DOI: 10.1093/oso/9780198506980.001.0001 (cit. on p. 1).

[Atki2006] P. Atkins, J. De Paula, J. de Paula, M. Bär, A. Schleitzer, and C. Heinisch. *Physikalische Chemie*. Wiley, 2006. ISBN: 9783527315468. (Cit. on p. 16).

[Aume2021] B. M. Aumeier, F. Vollmer, S. Lenfers, S. Yüce, and M. Wessling. "Polymeric membranes with sufficient thermo-mechanical stability to deploy temperature enhanced backwash". *Chemie Ingenieur Technik*, vol. 93, no. 9. 2021. DOI: https://doi.org/10.1002/cite.202100020 (cit. on p. 2).

[Bake2023] R. W. Baker. *Membrane Technology and Applications*. 4th ed. Hoboken, NJ: John Wiley & Sons, 2023. ISBN: 978-1-119-68598-2. (Cit. on pp. 2, 7–11, 15, 18–20, 58, 59, 84, 85, 97).

[Bang2020] Y. Bang, M. Obaid, M. Jang, J. Lee, J. Lim, and I. S. Kim. "Influence of bore fluid composition on the physiochemical properties and performance of hollow fiber membranes for ultrafiltration". *Chemosphere*, vol. 259. 2020. DOI: https://doi.org/10.1016/j.chemosphere.2020.127467 (cit. on pp. 59, 70, 71, 73).

[Bood2013] K. Boodhoo and A. Harvey. *Process Intensification Technologies for Green Chemistry: Engineering Solutions for Sustainable Chemical Processing*. Wiley, 2013. ISBN: 9781118498538. (Cit. on p. 2).

[Boom1992] R. Boom, I. Wienk, T. van den Boomgaard, and C. Smolders. “Microstructures in phase inversion membranes. part 2. the role of a polymeric additive”. *Journal of Membrane Science*, vol. 73, no. 2. 1992. DOI: https://doi.org/10.1016/0376-7388(92)80135-7 (cit. on pp. 2, 46).

[Boom1994] R. Boom, T. van den Boomgaard, and C. Smolders. “Mass transfer and thermodynamics during immersion precipitation for a two-polymer system: Evaluation with the system pes—pvp—nmp—water”. *Journal of Membrane Science*, vol. 90, no. 3. 1994. DOI: https://doi.org/10.1016/0376-7388(94)80074-X (cit. on pp. 2, 3, 13, 19).

[Bouy2010] D. Bouyer, W. Werapun, C. Pochat-Bohatier, and A. Deratani. “Morphological properties of membranes fabricated by vips process using pei/nmp/water system: Sem analysis and mass transfer modelling”. *Journal of Membrane Science*, vol. 349, no. 1. 2010. DOI: https://doi.org/10.1016/j.memsci.2009.11.036 (cit. on pp. 85, 92).

[Chae1999] H. Chae Park, Y. Po Kim, H. Yong Kim, and Y. Soo Kang. “Membrane formation by water vapor induced phase inversion”. *Journal of Membrane Science*, vol. 156, no. 2. 1999. DOI: https://doi.org/10.1016/S0376-7388(98)00359-7 (cit. on p. 93).

[Chan2017] J. Chang, J. Zuo, L. Zhang, G. S. O’Brien, and T.-S. Chung. “Using green solvent, triethyl phosphate (tep), to fabricate highly porous pvdf hollow fiber membranes for membrane distillation”. *Journal of Membrane Science*, vol. 539. 2017. DOI: https://doi.org/10.1016/j.memsci.2017.06.002 (cit. on p. 32).

[Char2012] C. Charcosset. *Membrane Processes in Biotechnology and Pharmaceutics*. Elsevier Science, 2012. ISBN: 9780444563347. (Cit. on p. 2).

[Chun2021] T.-S. Chung and Y. Feng. *Hollow Fiber Membranes - Fabrication and Applcations*. 1st Edition. Radarweg 29, PO Box 211, 1000 AE Amsterdam, Netherlands: ELsevier Inc., 2021. (Cit. on pp. 2, 13, 15, 38, 42, 46, 47, 59, 73, 84, 85).

[Dibr2022] G. Dibrov, G. Kagramanov, V. Sudin, S. Molchanov, E. Grushevenko, A. Yushkin, and V. Volkov. “Influence of draw ratio and take-up velocity on properties of ultrafiltration hollow fiber membranes from polyethersulfone”. *Fibers*, vol. 10, no. 3. 2022. DOI: https://doi.org/10.3390/fib10030029 (cit. on pp. 52, 71, 74).

[Dong2020] X. Dong, T. J. Jeong, E. Kline, L. Banks, E. Grulke, T. Harris, and I. C. Escobar. “Eco-friendly solvents and their mixture for the fabrication of polysulfone ultrafiltration membranes: An investigation of doctor blade and slot die casting methods”. *Journal of Membrane Science*, vol. 614. 2020. DOI: https://doi.org/10.1016/j.memsci.2020.118510 (cit. on p. 34).

[Drio2012] E. Drioli and E. Fontananova. “Membrane materials for addressing energy and environmental challenges”. *Annual Review of Chemical and Biomolecular Engineering*, vol. 3, no. Volume 3, 2012. 2012. DOI: https://doi.org/10.1146/annurev-chembioeng-062011-081027 (cit. on p. 2).

[Dume2023] L. Dumee, M. Sadrzadeh, and M. Shirazi. *Green Membrane Technologies towards Environmental Sustainability*. Elsevier, 2023. ISBN: 9780323951661. (Cit. on p. 1).

[ECHA2018] E. C. A. ECHA, *Registry of restriction intentions*, Accessed: 20. Mai 2025, 2018. [Online]. Available: https://echa.europa.eu/de/registry-of-restriction-intentions/-/dislist/details/0b0236e1806abf64 (cit. on p. 3).

[ECHA2021] E. c. d. ECHACHEM, *1-methyl-2-pyrrolidone echa dossier*, Accessed: 02 June 2025, 2021. [Online]. Available: https://chem.echa.europa.eu/100.011.662/dossier-view/c6ec0d64-26ed-4e3f-9e47-3e6595a6f200/be7ec1a3-a544-4d10-9e0d-5fc7509d5546_be7ec1a3-a544-4d10-9e0d-5fc7509d5546?searchText=N-Methylpyrolidone (cit. on p. 42).

[ECHA2022] E. c. d. ECHACHEM, *1-butylpyrrolidin-2-one echa dossier*, Accessed: 02 June 2025, 2022. [Online]. Available: https://chem.echa.europa.eu/100.020.399/dossier-view/ba4f7bc3-93ab-4984-a043-34769eca79f9/IUC5-1dcd41c5-d311-457d-bff9-2bd7f97effa2_bfaca997-025a-49c2-9f3d-5d5b4a99de86?searchText=3470-98-2 (cit. on p. 42).

[ECHA2024] E. c. d. ECHACHEM, *2-hydroxy-n,n-dimethyl-propanamide echa dossier*, Accessed: 02 June 2025, 2024. [Online]. Available: https://chem.echa.europa.eu/100.132.568/dossier-view/9737b974-eae7-44c3-8402-27f647560d66/c791a1de-09ed-4f3c-ab06-b3f559531285_c791a1de-09ed-4f3c-ab06-b3f559531285?searchText=35123-06-9 (cit. on p. 42).

[Even2018] N. Evenepoel, S. Wen, M. Tilahun Tsehaye, and B. Van der Bruggen. "Potential of dmso as greener solvent for pes ultra- and nanofiltration membrane preparation". *Journal of Applied Polymer Science*, vol. 135, no. 28. 2018. DOI: https://doi.org/10.1002/app.46494 (cit. on p. 32).

[Feng2021] Y. Feng, M. Weber, C. Maletzko, and T.-S. Chung. "Delamination of single layer hollow fiber membranes induced by bi-directional phase separation". *Journal of Membrane Science*, vol. 622. 2021. DOI: https://doi.org/10.1016/j.memsci.2020.118992 (cit. on p. 79).

[Figo2014] A. Figoli, T. Marino, S. Simone, E. Di Nicolò, X.-M. Li, T. He, S. Tornaghi, and E. Drioli. "Towards non-toxic solvents for membrane preparation: A review". *Green Chemistry*, vol. 16, no. 9. 2014. DOI: https://doi.org/10.1039/C4GC00613E (cit. on pp. 1, 33).

[Flor1942] P. J. Flory. "Thermodynamics of high polymer solutions". *The Journal of Chemical Physics*, vol. 10, no. 1. Jan. 1942. DOI: https://doi.org/10.1063/1.1723621 (cit. on p. 12).

[Flor1953] P. Flory. *Principles of Polymer Chemistry*. (Baker lectures 1948). Cornell University Press, 1953. ISBN: 9780801401343. (Cit. on p. 12).

[Freg2021] V. Freger and G. Z. Ramon. "Polyamide desalination membranes: Formation, structure, and properties". *Progress in Polymer Science*, vol. 122. 2021. DOI: https://doi.org/10.1016/j.progpolymsci.2021.101451 (cit. on pp. 2, 13).

[Gron2020] O. Gronwald and M. Weber. "Agnique amd 3l as green solvent for polyethersulfone ultrafiltration membrane preparation". *Journal of Applied Polymer Science*, vol. 137, no. 9. 2020. DOI: https://doi.org/10.1002/app.48419 (cit. on pp. 26, 32, 39).

[Guil2011] G. R. Guillen, Y. Pan, M. Li, and E. M. V. Hoek. “Preparation and characterization of membranes formed by nonsolvent induced phase separation: A review”. *Industrial & Engineering Chemistry Research*, vol. 50, no. 7. 2011. DOI: https://doi.org/10.1021/ie101928r (cit. on p. 16).

[Hack2024] C. Hackett, D. Hale, B. Bair, G.-D. Manson-Endeboh, X. Hao, X. Qian, S. Ranil Wickramasinghe, and A. Thompson. “Polysulfone ultrafiltration membranes fabricated from green solvents: Significance of coagulation bath composition”. *Separation and Purification Technology*, vol. 332. 2024. DOI: https://doi.org/10.1016/j.seppur.2023.125752 (cit. on p. 59).

[Hans2007] C. M. Hansen. *Hansen solubility parameters: a user’s handbook*. CRC press, 2007. (Cit. on pp. 13, 26).

[Herr2024] S. Herrmann, F. Ullrich, M. Tepper, and M. Wessling. “On the geometry and material stability of tubular pvdf-tio2 static mixer membrane contactors for photocatalytic ozonation of micropollutants”. *Journal of Membrane Science*, vol. 702. 2024. DOI: https://doi.org/10.1016/j.memsci.2024.122753 (cit. on pp. 2, 13).

[Hoer1974] D. Hoernschemeyer. “The influence of solvent type on the viscosity of concentrated polymer solutions”. *Journal of Applied Polymer Science*, vol. 18, no. 1. 1974. DOI: https://doi.org/10.1002/app.1974.070180105 (cit. on p. 38).

[Hung2016] W.-L. Hung, D.-M. Wang, J.-Y. Lai, and S.-C. Chou. “On the initiation of macrovoids in polymeric membranes – effect of polymer chain entanglement”. *Journal of Membrane Science*, vol. 505. 2016. DOI: https://doi.org/10.1016/j.memsci.2016.01.021 (cit. on p. 46).

[Idri2007] A. Idris, N. Mat Zain, and M. Noordin. “Synthesis, characterization and performance of asymmetric polyethersulfone (pes) ultrafiltration membranes with polyethylene glycol of different molecular weights as additives”. *Desalination*, vol. 207, no. 1. 2007. DOI: https://doi.org/10.1016/j.desal.2006.08.008 (cit. on pp. 3, 13).

[Isma2020] N. Ismail, A. Venault, J.-P. Mikkola, D. Bouyer, E. Drioli, and N. Tavajohi Hassan Kiadeh. “Investigating the potential of membranes formed by the vapor induced phase separation process”. *Journal of*

Membrane Science, vol. 597. 2020. DOI: https://doi.org/10.1016/j.memsci.2019.117601 (cit. on pp. 84, 92, 93).

[Jain2007] P. Jain and S. H. Yalkowsky. "Solubilization of poorly soluble compounds using 2-pyrrolidone". *International Journal of Pharmaceutics*, vol. 342, no. 1. 2007. DOI: https://doi.org/10.1016/j.ijpharm.2007.03.056 (cit. on p. 42).

[Jian2021] X. Jiang, W. F. Yong, J. Gao, D.-D. Shao, and S.-P. Sun. "Understanding the role of substrates on thin film composite membranes: A green solvent approach with tamisolve® nxg". *Journal of Membrane Science*, vol. 635. 2021. DOI: https://doi.org/10.1016/j.memsci.2021.119530 (cit. on pp. 26, 32, 42).

[Kahr2019] C. Kahrs, T. Gühlstorf, and J. Schwellenbach. "Influences of different preparation variables on polymeric membrane formation via nonsolvent induced phase separation". *Journal of Applied Polymer Science*, vol. 137, no. 28. 2019. DOI: https://doi.org/10.1002/app.48852 (cit. on pp. 76, 77).

[Kahr2020] C. Kahrs and J. Schwellenbach. "Membrane formation via nonsolvent induced phase separation using sustainable solvents: A comparative study". *Polymer*, vol. 186. 2020. DOI: https://doi.org/10.1016/j.polymer.2019.122071 (cit. on pp. 2, 13, 19, 32, 37, 77).

[Kana2010] D. M. Kanani, W. H. Fissell, S. Roy, A. Dubnisheva, A. Fleischman, and A. L. Zydney. "Permeability–selectivity analysis for ultrafiltration: Effect of pore geometry". *Journal of Membrane Science*, vol. 349, no. 1. 2010. DOI: https://doi.org/10.1016/j.memsci.2009.12.003 (cit. on p. 49).

[Khor2017] M. Khorsand-Ghayeni, J. Barzin, M. Zandi, and M. Kowsari. "Fabrication of asymmetric and symmetric membranes based on pes/peg/dmac". *Polymer Bulletin*, vol. 74, no. 6. 2017. DOI: https://doi.org/10.1007/s00289-016-1823-z (cit. on pp. 3, 13).

[Khos2017] S. Khosharay, S. Tourang, and F. Tajfar. "Modeling surface tension and interface of (water+methanol), (water+ethanol), (water+1-propanol), and (water+meg) mixtures". *Fluid Phase Equilibria*, vol. 454. 2017. DOI: https://doi.org/10.1016/j.fluid.2017.09.017 (cit. on p. 89).

[Kim1998] J.-H. Kim and K.-H. Lee. “Effect of peg additive on membrane formation by phase inversion”. *Journal of Membrane Science*, vol. 138, no. 2. 1998. DOI: https://doi.org/10.1016/S0376-7388(97)00224-X (cit. on pp. 3, 13).

[Kope2011] K. K. Kopec, “Charged porous membrane structures for separation of biomolecules”, Dissertation, University of Twente, Enschede, 2011. DOI: 10.3990/1.9789036531467 (cit. on p. 23).

[Leop2025] K. H. Leopold, D. Breite, M. Schmidt, A. Prager, M. Went, M. Kühnert, D. Enke, and A. Schulze. “Design of sponge-like pes hollow fiber membranes using the environmentally friendly solvent n,n-dimethyl lactamide”. *Separation and Purification Technology*, vol. 365. 2025. DOI: https://doi.org/10.1016/j.seppur.2025.132625 (cit. on pp. 32, 55, 59).

[Li2007] J.-F. Li, Z.-L. Xu, and H. Yang. “Microporous polyethersulfone membranes prepared under the combined precipitation conditions with non-solvent additives”. *Polymers for Advanced Technologies*, vol. 19, no. 4. 2007. DOI: https://doi.org/10.1002/pat.982 (cit. on p. 97).

[Li2009] Q. Li, Z.-L. Xu, and L.-Y. Yu. “Effects of mixed solvents and pvdf types on performances of pvdf microporous membranes”. *Journal of Applied Polymer Science*, vol. 115, no. 4. 2009. DOI: https://doi.org/10.1002/app.31324 (cit. on pp. 33, 76).

[Ma2024] R. Ma, J. Li, P. Zeng, L. Duan, J. Dong, Y. Ma, and L. Yang. “The application of membrane separation technology in the pharmaceutical industry”. *Membranes*, vol. 14, no. 1. 2024. DOI: https://doi.org/10.3390/membranes14010024 (cit. on p. 58).

[Mack1980] D. Mackay, A. Bobra, W. Shiu, and S. Yalkowsky. “Relationships between aqueous solubility and octanol-water partition coefficients”. *Chemosphere*, vol. 9, no. 11. 1980. DOI: https://doi.org/10.1016/0045-6535(80)90122-8 (cit. on p. 42).

[Magg2022] I. V. Maggay, M.-L. Yu, D.-M. Wang, C.-H. Chiang, Y. Chang, and A. Venault. “Strategy to prepare skin-free and macrovoid-free polysulfone membranes via the nips process”. *Journal of Membrane Science*, vol. 655. 2022. DOI: https://doi.org/10.1016/j.memsci.2022.120597 (cit. on pp. 2, 19, 46).

[Mari2017] T. Marino, F. Russo, A. Criscuoli, and A. Figoli. “Tamisolve® nxg as novel solvent for polymeric membrane preparation”. *Journal of Membrane Science*, vol. 542. 2017. DOI: https://doi.org/10.1016/j.memsci.2017.08.038 (cit. on pp. 32, 42).

[Mari2018] T. Marino, F. Russo, and A. Figoli. “The formation of polyvinylidene fluoride membranes with tailored properties via vapour/non-solvent induced phase separation”. *Membranes*, vol. 8, no. 3. 2018. DOI: https://doi.org/10.3390/membranes8030071 (cit. on pp. 32, 85).

[Mari2019] T. Marino, F. Galiano, A. Molino, and A. Figoli. “New frontiers in sustainable membrane preparation: Cyrene™ as green bioderived solvent”. *Journal of Membrane Science*, vol. 580. 2019. DOI: https://doi.org/10.1016/j.memsci.2019.03.034 (cit. on p. 32).

[Mart2017] A. A. Martins, N. S. Caetano, and T. M. Mata. “Lca for membrane processes”, in: *Sustainable Membrane Technology for Water and Wastewater Treatment*. Ser. Green Chemistry and Sustainable Technology, A. Figoli and A. Criscuoli, Eds., Singapore: Springer Singapore, 2017. ISBN: 978-981-10-5623-9.DOI: https://doi.org/10.1007/978-981-10-5623-9_2 (cit. on p. 2).

[Mats1999] H. Matsuyama, M. Teramoto, T. Uesaka, M. Goto, and F. Nakashio. “Kinetics of droplet growth in the metastable region in cellulose acetate/acetone/nonsolvent system”. *Journal of Membrane Science*, vol. 152, no. 2. 1999. DOI: https://doi.org/10.1016/S0376-7388(98)00226-9 (cit. on p. 18).

[McKe1996] S. A. McKelvey and W. J. Koros. “Phase separation, vitrification, and the manifestation of macrovoids in polymeric asymmetric membranes”. *Journal of Membrane Science*, vol. 112, no. 1. 1996. DOI: https://doi.org/10.1016/0376-7388(95)00197-2 (cit. on p. 46).

[Meht2005] A. Mehta and A. L. Zydney. “Permeability and selectivity analysis for ultrafiltration membranes”. *Journal of Membrane Science*, vol. 249, no. 1. 2005. DOI: https://doi.org/10.1016/j.memsci.2004.09.040 (cit. on p. 49).

[Meli2007] T. Melin and R. Rautenbach. *Membranverfahren: Grundlagen der Modul- und Anlagenauslegung*. 3rd ed. Berlin Heidelberg: Springer-Verlag, 2007. ISBN: 9783540343288. (Cit. on pp. 7, 58, 84).

[Muld1996] M. Mulder. *Basic Principles of Membrane Technology*. 2nd ed. Dordrecht: Kluwer Academic Publishers, 1996. ISBN: 978-94-009-1766-8.DOI: 10.1007/978-94-009-1766-8 (cit. on pp. 7–9, 11–13, 15–20).

[Nune1996] S. P. Nunes and T. Inoue. "Evidence for spinodal decomposition and nucleation and growth mechanisms during membrane formation". *Journal of Membrane Science*, vol. 111, no. 1. 1996. DOI: https://doi.org/10.1016/0376-7388(95)00281-2 (cit. on pp. 2, 13, 16, 18, 46).

[Osma2024] A. I. Osman, Z. Chen, A. M. Elgarahy, M. Farghali, I. M. A. Mohamed, A. Priya, H. B. Hawash, and P.-S. Yap. "Membrane technology for energy saving: Principles, techniques, applications, challenges, and prospects". *Advanced Energy and Sustainability Research*, vol. 5, no. 5. 2024. DOI: https://doi.org/10.1002/aesr.202400011 (cit. on p. 2).

[Pein2023] R. I. Peinador, D. Darbouret, C. Paragot, and J. I. Calvo. "Automated liquid–liquid displacement porometry (lldp) for the non-destructive characterization of ultrapure water purification filtration devices". *Membranes*, vol. 13, no. 7. 2023. DOI: https://doi.org/10.3390/membranes13070660 (cit. on p. 89).

[Peng2010] J. Peng, Y. Su, W. Chen, Q. Shi, and Z. Jiang. "Effects of coagulation bath temperature on the separation performance and antifouling property of poly(ether sulfone) ultrafiltration membranes". *Industrial & Engineering Chemistry Research*, vol. 49, no. 10. 2010. DOI: https://doi.org/10.1021/ie9018963 (cit. on p. 59).

[Rahb2012] M. Rahbari-sisakht, A. Ismail, and T. Matsuura. "Effect of bore fluid composition on structure and performance of asymmetric polysulfone hollow fiber membrane contactor for co2 absorption". *Separation and Purification Technology*, vol. 88. 2012. DOI: https://doi.org/10.1016/j.seppur.2011.12.012 (cit. on p. 73).

[Raso2019] M. A. Rasool and I. F. J. Vankelecom. "Use of y-valerolactone and glycerol derivatives as bio-based renewable solvents for membrane preparation". *Green Chemistry*, vol. 21, no. 5. 2019. DOI: https://doi.org/10.1039/C8GC03652G (cit. on p. 32).

[Reuv1987a] A. Reuvers and C. Smolders. “Formation of membranes by means of immersion precipitation: Part ii. the mechanism of formation of membranes prepared from the system cellulose acetate-acetone-water”. *Journal of Membrane Science*, vol. 34, no. 1. 1987. DOI: https://doi.org/10.1016/S0376-7388(00)80021-6 (cit. on pp. 19, 28, 40, 42, 46, 73).

[Reuv1987b] A. Reuvers, J. van den Berg, and C. Smolders. “Formation of membranes by means of immersion precipitation: Part i. a model to describe mass transfer during immersion precipitation”. *Journal of Membrane Science*, vol. 34, no. 1. 1987. DOI: https://doi.org/10.1016/S0376-7388(00)80020-4 (cit. on pp. 19, 33, 46).

[Roth2018] H. Roth, T. Luelf, A. Koppelmann, M. Abel, and M. Wessling. “Chemistry in a spinneret – composite hollow fiber membranes in a single step process”. *Journal of Membrane Science*, vol. 554. 2018. DOI: https://doi.org/10.1016/j.memsci.2018.02.051 (cit. on pp. 2, 13).

[Russ2020] F. Russo, F. Galiano, F. Pedace, F. Aricò, and A. Figoli. “Dimethyl isosorbide as a green solvent for sustainable ultrafiltration and microfiltration membrane preparation”. *ACS Sustainable Chemistry & Engineering*, vol. 8, no. 1. 2020. DOI: https://doi.org/10.1021/acssuschemeng.9b06496 (cit. on p. 32).

[Russ2021] F. Russo, T. Marino, F. Galiano, L. Gzara, A. Gordano, H. Organji, and A. Figoli. “Tamisolve® nxg as an alternative non-toxic solvent for the preparation of porous poly (vinylidene fluoride) membranes”. *Polymers*, vol. 13, no. 15. 2021. DOI: https://doi.org/10.3390/polym13152579 (cit. on p. 32).

[Shen2025] A. M. Shenoy, R. Thür, B. van Duffel, and I. F. Vankelecom. “Use of green polar aprotic solvents tamisolve® nxg, dmso and methyl-thf for the synthesis of asymmetric polyimide-based biogas purification membranes”. *Journal of Membrane Science*, vol. 717. 2025. DOI: https://doi.org/10.1016/j.memsci.2024.123573 (cit. on p. 32).

[Sher2018] J. Sherwood, T. J. Farmer, and J. H. Clark. “Catalyst: Possible consequences of the n-methyl pyrrolidone reach restriction”. *Chem*, vol. 4, no. 9. 2018. DOI: https://doi.org/10.1016/j.chempr.2018.08.035 (cit. on p. 3).

[Smol1992] C. Smolders, A. Reuvers, R. Boom, and I. Wienk. “Microstructures in phase-inversion membranes. part 1. formation of macrovoids”. *Journal of Membrane Science*, vol. 73, no. 2. 1992. DOI: https://doi.org/10.1016/0376-7388(92)80134-6 (cit. on pp. 2, 11, 19, 20, 33, 42, 46, 65, 73, 92, 97).

[Stra1971] H. Strathmann, P. Scheible, and R. Baker. “A rationale for the preparation of loeb-sourirajan-type cellulose acetate membranes”. *Journal of Applied Polymer Science*, vol. 15, no. 4. 1971. DOI: https://doi.org/10.1002/app.1971.070150404 (cit. on p. 46).

[Stra1975] H. Strathmann, K. Kock, P. Amar, and R. Baker. “The formation mechanism of asymmetric membranes”. *Desalination*, vol. 16, no. 2. 1975. DOI: https://doi.org/10.1016/S0011-9164(00)82092-5 (cit. on pp. 19, 20, 46).

[Stra1977] H. Strathmann and K. Kock. “The formation mechanism of phase inversion membranes”. *Desalination*, vol. 21, no. 3. 1977. DOI: https://doi.org/10.1016/S0011-9164(00)88244-2 (cit. on pp. 20, 21).

[Su2017] S.-L. Su, D.-M. Wang, and J.-Y. Lai. “Critical residence time in metastable region – a time scale determining the demixing mechanism of nonsolvent induced phase separation”. *Journal of Membrane Science*, vol. 529. 2017. DOI: https://doi.org/10.1016/j.memsci.2017.01.059 (cit. on p. 46).

[Tang2020] Y.-h. Tang, E. Ledieu, M. R. Cervellere, P. C. Millett, D. M. Ford, and X. Qian. “Formation of polyethersulfone membranes via nonsolvent induced phase separation process from dissipative particle dynamics simulations”. *Journal of Membrane Science*, vol. 599. 2020. DOI: https://doi.org/10.1016/j.memsci.2020.117826 (cit. on p. 16).

[Tepp2022] M. Tepper, Y. Eminoglu, N. Mehling, J. Walorski, H. Roth, and M. Wessling. “Rotation-in-a-spinneret integrates static mixers inside hollow fiber membranes”. *Journal of Membrane Science*, vol. 656. 2022. DOI: https://doi.org/10.1016/j.memsci.2022.120599 (cit. on pp. 2, 13).

[Than2014] N. T. K. Thanh, N. Maclean, and S. Mahiddine. “Mechanisms of nucleation and growth of nanoparticles in solution”. *Chemical Reviews*, vol. 114, no. 15. 2014. DOI: https://doi.org/10.1021/cr400544s (cit. on pp. 17–19).

[Thuy2015] Y. L. Thuyavan, N. Anantharaman, G. Arthanareeswaran, and A. F. Ismail. “Impact of solvents and process conditions on the formation of polyethersulfone membranes and its fouling behavior in lake water filtration”. *Journal of Chemical Technology & Biotechnology*, vol. 91, no. 10. 2015. DOI: https://doi.org/10.1002/jctb.4846 (cit. on pp. 3, 13).

[Tutu1983] R. S. Tutunjian. “Ultrafiltration processes in biotechnology”. *Annals of the New York Academy of Sciences*, vol. 413, no. 1. 1983. DOI: https://doi.org/10.1111/j.1749-6632.1983.tb47897.x (cit. on p. 58).

[Uebe2021] S. Uebele, K. S. Johann, T. Goetz, O. Gronwald, M. Ulbricht, and T. Schiestel. “Poly(ether sulfone) hollow fiber membranes prepared via nonsolvent-induced phase separation using the green solvent agnique® amd 3 l”. *Journal of Applied Polymer Science*, vol. 138, no. 37. 2021. DOI: https://doi.org/10.1002/app.50935 (cit. on p. 32).

[Ursi2020] C. Ursino, F. Russo, R. Ferrari, M. De Santo, E. Di Nicolò, T. He, F. Galiano, and A. Figoli. “Polyethersulfone hollow fiber membranes prepared with polarclean® as a more sustainable solvent”. *Journal of Membrane Science*, vol. 608. 2020. DOI: https://doi.org/10.1016/j.memsci.2020.118216 (cit. on pp. 32, 59).

[Van 2009] B. Van der Bruggen. “Chemical modification of polyethersulfone nanofiltration membranes: A review”. *Journal of Applied Polymer Science*, vol. 114, no. 1. 2009. DOI: https://doi.org/10.1002/app.30578 (cit. on p. 2).

[Venk2019] S. Venkatram, C. Kim, A. Chandrasekaran, and R. Ramprasad. “Critical assessment of the hildebrand and hansen solubility parameters for polymers”. *Journal of Chemical Information and Modeling*, vol. 59, no. 10. 2019. DOI: https://doi.org/10.1021/acs.jcim.9b00656 (cit. on pp. 15, 39).

[Vers1996] K. Verschueren. *Handbook of Environmental Data on Organic Chemicals*. 3rd ed. New York: Van Nostrand Reinhold, 1996. ISBN: 0-442-01916-5. (Cit. on p. 42).

[Wang2005] Q.-b. Wang, R. Finsy, H.-b. Xu, and L. Xi. “On the critical radius in generalized ostwald ripening”. *Journal of Zhejiang University Science B*, vol. 6, no. 8. Aug. 2005. DOI: https://doi.org/10.1007/BF02842426 (cit. on pp. 18, 19).

[Wang2011] Z. Wang, J. Ma, and Q. Liu. “Pure sponge-like membranes bearing both high water permeability and high retention capacity”. *Desalination*, vol. 278, no. 1. 2011. DOI: https://doi.org/10.1016/j.desal.2011.05.023 (cit. on p. 49).

[Wien1996] I. Wienk, R. Boom, M. Beerlage, A. Bulte, C. Smolders, and H. Strathmann. “Recent advances in the formation of phase inversion membranes made from amorphous or semi-crystalline polymers”. *Journal of Membrane Science*, vol. 113, no. 2. 1996. DOI: https://doi.org/10.1016/0376-7388(95)00256-1 (cit. on p. 16).

[Wijm1983] J. Wijmans, J. Baaij, and C. Smolders. “The mechanism of formation of microporous or skinned membranes produced by immersion precipitation”. *Journal of Membrane Science*, vol. 14, no. 3. 1983. DOI: https://doi.org/10.1016/0376-7388(83)80005-2 (cit. on pp. 13, 20, 47, 65, 67, 70, 71, 73, 85, 92).

[Xu2014] J. Xu, Y. Tang, Y. Wang, B. Shan, L. Yu, and C. Gao. “Effect of coagulation bath conditions on the morphology and performance of psf membrane blended with a capsaicin-mimic copolymer”. *Journal of Membrane Science*, vol. 455. 2014. DOI: https://doi.org/10.1016/j.memsci.2013.12.076 (cit. on pp. 76, 97).

[Xu2020] M.-H. Xu, R. Xie, X.-J. Ju, W. Wang, Z. Liu, and L.-Y. Chu. “Antifouling membranes with bi-continuous porous structures and high fluxes prepared by vapor-induced phase separation”. *Journal of Membrane Science*, vol. 611. 2020. DOI: https://doi.org/10.1016/j.memsci.2020.118256 (cit. on pp. 71, 79, 94, 99).

[Zhan2010] Z. Zhang, Q. An, Y. Ji, J. Qian, and C. Gao. “Effect of zero shear viscosity of the casting solution on the morphology and permeability of polysulfone membrane prepared via the phase-inversion process”. *Desalination*, vol. 260, no. 1. 2010. DOI: https://doi.org/10.1016/j.desal.2010.05.002 (cit. on pp. 2, 19, 20, 42, 74, 79, 93).

[Zhan2014] S. Zhang, P. Sukitpaneenit, and T.-S. Chung. “Design of robust hollow fiber membranes with high power density for osmotic energy production”. *Chemical Engineering Journal*, vol. 241. 2014. DOI: https://doi.org/10.1016/j.cej.2013.10.063 (cit. on p. 68).

[Zhao2018] Q. Zhao, R. Xie, F. Luo, Y. Faraj, Z. Liu, X.-J. Ju, W. Wang, and L.-Y. Chu. “Preparation of high strength poly(vinylidene fluoride) porous membranes with cellular structure via vapor-induced phase separation”. *Journal of Membrane Science*, vol. 549. 2018. DOI: https://doi.org/10.1016/j.memsci.2017.10.068 (cit. on p. 93).

[Zhen2006] Q.-Z. Zheng, P. Wang, and Y.-N. Yang. “Rheological and thermodynamic variation in polysulfone solution by peg introduction and its effect on kinetics of membrane formation via phase-inversion process”. *Journal of Membrane Science*, vol. 279, no. 1. 2006. DOI: https://doi.org/10.1016/j.memsci.2005.12.009 (cit. on p. 76).

List of Abbreviations

2P 2-pyrrolidone

AMD Agnique AMD 3L

FS flat sheet

HF hollow fiber

HSP Hansen Solubility Parameter

LMH/bar $L^{-1}m^{-2}h^{-1}bar^{-1}$

MF microfiltration

NBP N-butylpyrrolidone

NF nanofiltration

NIPS non-solvent-induced phase separation

NMP N-methylpyrrolidone

PES polyethersulfone

PVP polyvinylpyrrolidone

PWP pure water permeance

RO reverse osmosis

SEM Scanning Electron Microscopy

TEP Triethylphosphate

UF ultrafiltration